U.PORTO
FACULDADE DE CIÊNCIAS
UNIVERSIDADE DO PORTO

PhD

Analysis of Plasmonics Based Fiber Optic Sensing Structures

Hamed Moayyed

Thesis Submitted to Faculdade de Ciências da Universidade do Porto in partial fulfillment of the requirements for the degree of Ph. D. in Physics

2016

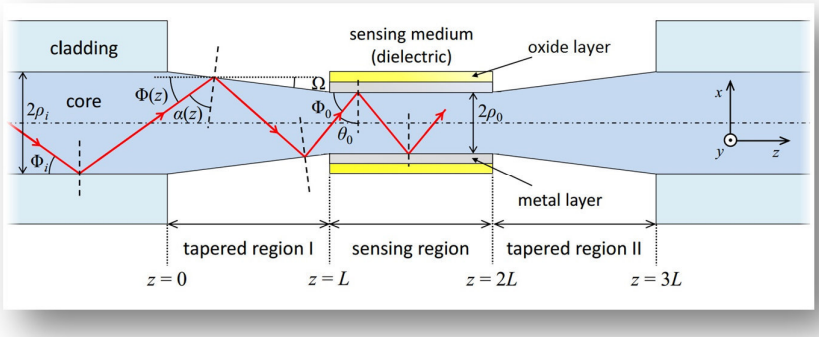

Analysis of Plasmonics Based Fiber Optic Sensing Structures

Hamed Moayyed

Physics
Departmento de Física e Astronomia

Supervisor
José Luís Campos de Oliveira Santos, Full Professor
Faculdade de Ciências da Universidade do Porto
Co-supervisor
Diana Catarino das Neves Viegas, Research Fellow
International Iberian Nanotechnology Laboratory

"Nothing in life is to be feared, it is only to be understood.
Now is the time to understand more, so that we may fear less."

Marie Curie

Acknowledgements

Firstly, I would like to express my sincere gratitude to my advisor Prof. José Luís Santos for the continuous support of my Ph.D study and related research, for his patience, motivation, and immense knowledge. His guidance helped me in all the time of research and writing of this thesis. His words can always inspire me and bring me to a higher level of thinking. What I learn from him is not just how to do the studies to meet the graduation requirements, but how to view this world from a new perspective.

I especially want to thank Prof. Faramarz Farahi for introducing me to my advisor, and providing me this special opportunity to pursue my academic goals.

My co-advisor, Dr. Diana Viegas, has been always willing to listen to me and give me advices. I am deeply grateful to her for her supports that helped me sort out the technical details of my work. A special thanks to other members of our research team Dr. Luis Coelho and Ivo Leite, for their many valuable discussions, constant caring and support.

To all my colleagues and friends from UOSE, namely, Luísa Mendonça, Dr. Pedro Jorge, Dr. Orlando Frazão, Dr. Susana Silva, Dr. Marta Ferreira, Dr. Ivo Nascimento, Dr. Joel Carvalho, Dr. Paulo Caldas, Rita Ribeiro, Dr. Carlos Gouveia and Hamid Hosseiny that somehow contributed for the great experience and my profound joy that it is working in this group.

To INESC TEC for providing the facilities without which my research work would not be possible. A word of recognition to Dr. Paulo Marques and Dr. Ireneu Dias for their support whenever it was needed.

Heartfelt thanks goes to my family for their unconditional support; to my parents, without whom I would not have gotten here, to my lovely wife Parisa for her endless patience, encouragement and constant support, and to my beloved daughter Hana, who her beautiful smile has been a source of strength and inspiration.

Sumário

Plasmónica é hoje em dia uma palavra da *moda* no domínio da Ciência e na Tecnologia tantas vezes é ela pronunciada e escrita. Frequentemente uma situação deste tipo não tem justificação objectiva, mas tal não é o caso. O volume de ciência e de tecnologia de qualidade que resulta da investigação e desenvolvimento em Plasmónica é enorme e cresce a ritmo acelerado. Na realidade esta realidade não é de todo surpreendente caso se compreenda o que efectivamente significa a plasmónica, a interacção coerente em ambiente controlado de um electrão e de um fotão, constituindo-se uma nova entidade designada de plasmon, sendo esta não mais um fotão ou um electrão, mas sim uma entidade hibrida que evidencia características de ambos. É esta mistura que possibilita, por exemplo, conseguir-se imagem óptica com resolução bem superior à determinada pelo convencional limite de difracção, isto porque neste caso o que domina é a propriedade do electrão de evidenciar um comportamento ondulatório determinado pelo seu comprimento de onda de DeBroglie, o qual é ordens de grandeza inferior ao comprimento de onda associado ao fotão. É certo que a área da Plasmónica não é nova, antes pelo contrário já que existe há mais de 100 anos, mas de facto foi só recentemente que o desenvolvimento da Nanociência e da Nanotecnologia possibilitou a construção de condições que permitem a geração de plasmões em ambiente controlado. Foi este progresso que originou o enorme desenvolvimento da Plasmónica nas componentes de estudos fundamentais e de desenvolvimentos tecnológicos, sendo reconhecido que se está apenas no início.

Na perspectiva histórica, uma das primeiras aplicações da Plasmónica foi na sensorização óptica, primeiro com suporte em plataformas construídas pela assemblagem de componentes ópticos discretos, mais tarde tirando partido da fibra óptica, um progresso que se poderá qualificar de elevado alcance e que originou o aparecimento de uma nova área no domínio da sensorização óptica, de modo sucinto identificada de *sensores SPR em fibra óptica*. O programa de investigação que deu origem a esta tese situa-se nesta área, mais precisamente na análise teórica e computacional de estruturas várias em fibra óptica que incorporam ressonância plasmónica orientada para se conseguir uma determinada funcionalidade de sensorização. Essas estruturas diferenciam-se pelo tipo de metal ou camada hibrida que se considera para suporte da ressonância plasmónica, ou então pela geometria adoptada para a fibra óptica. Os resultados que se obtêm a partir desse estudo e que se apresentam nesta tese têm valor pela compreensão que possibilitam dos princípios físicos envolvidos, assim como no que respeita à identificação das suas características de sensorização, mas também porque permitem orientar a fabricação dessas estruturas, muito em particular quando esta necessita de ser sintonizada no sentido de satisfazer especificações que decorrem da aplicação a que se destinam.

Esta tese está organizada em sete capítulos. No ***Capítulo 1*** começa-se por localizar historicamente a investigação do fenómeno da ressonância plasmónica no domínio óptico e de como pode ser utilizado para se conseguir funcionalidades de sensorização, primeiro em plataformas construídas pela assemblagem de componentes ópticos discretos, mais tarde pela utilização da fibra óptica. De seguida, avança-se para a contextualização desta abordagem de sensorização no âmbito da actual e dinâmica actividade de I&D em Plasmónica. No ***Capítulo 2*** são apresentados os conceitos centrais que permitem a compreensão do fenómeno da ressonância plasmónica, assim como a identificação das condições que possibilitam a sua existência em guias de onda planos. É também analisada a propagação do campo electromagnético em estruturas multicamada. No ***Capítulo 3*** apresenta-se a revisão das várias técnicas que têm sido utilizadas na interrogação de sensores baseados em plasmónica, sendo analisado o nível de desempenho passível de ser conseguido quando se considera as abordagens de interrogação que têm sido descritas na literatura, nomeadamente interrogação angular, no domínio espectral, em intensidade e em fase. O ***Capítulo 4*** desenvolve o estudo de sensores SPR em fibra óptica em configurações que integram uma camada metálica única ou uma camada mista (metal + óxido) na perspectiva da interrogação em fase. Os metais considerados são a prata, o ouro, o cobre e o alumínio no contexto da utilização da fibra óptica com a geometria habitual, em *taper* e quando se considera a configuração em optrodo. No ***Capítulo 5*** expõe-se um estudo sobre as características de sensores em fibra óptica baseados em plasmónica nos quais se considera uma camada interna de metal (prata) coberta por uma outra com propriedades dieléctricas (óxido). Pretende-se com esta abordagem deslocar o comprimento de onda de ressonância plasmónica para a região espectral utilizada pelos sistemas de comunicação por fibra óptica, significando com isto a possibilidade de incorporar nos elementos sensores componentes e dispositivos de elevado desempenho e relativamente baixo custo como consequência da sua utilização massiva nos sistemas de comunicação óptica. Diferentes óxidos serão considerados para a camada externa, como o dióxido de titânio, o dióxido de silício e o óxido de alumínio, pretendendo-se com este estudo aferir como melhorar a sensibilidade destas estruturas de sensorização a variações do índice de refracção do meio envolvente. O ***Capítulo 6*** trata o problema da integração de redes em fibra óptica (redes de Bragg e redes de período longo) com estruturas convencionais de sensorização em fibra utilizando ressonância plasmónica, sendo o objectivo tornar estas estruturas compatíveis com o domínio da tecnologia da fibra monomodo onde se situam os sistemas de comunicação por fibra óptica, resultando daí as vantagens acima já identificadas. Em particular, procurar-se-á estudar uma configuração de sensorização de elevado potencial, nomeadamente a que resulta do acoplamento de redes de período longo às estruturas convencionais de sensorização SPR em fibra. Finalmente, no ***Capítulo 7*** apresentam-se notas finais relativas ao trabalho desenvolvido e projectam-se caminhos para investigação futura.

Abstract

Plasmonics is nowadays a fancy word in the world of Science and Technology so many times it is pronounced or so often it is written. It frequently happens such a situation represents a momentary fashion, but it will be fair to emphasize this is not the case. The amount of good science and technology that derives from R&D in Plasmonics is huge and is growing at an accelerated pace. As a matter of fact, such reality is not at all surprising if one understands what plasmonics means, a coherent interaction of an electron and a photon in a controlled environment generating a new entity, named *plasmon*, which is no more a photon or an electron, but a hybrid entity which shows flavours of both. It is this mix of flavours that enables, for example, optical imaging well below the standard diffraction limit because, in such case, dominates the electron flavour which has a wave behaviour determined by its DeBroglie wavelength with a value orders of magnitude smaller than the optical wavelength. It is true the field of Plasmonics is not new, is over 100 years old, but it was only recently that the Nanoscience and the Nanotechnology developed to a point that enabled to build up environments where plasmons could be generated in controlled conditions. It was such possibility that induced the burst of activity in Plasmonics, both at a fundamental level and at technological developments, being well present the perception this is just the beginning.

Historically, one of the first applications of Plasmonics was optical sensing, first supported in bulk platforms and latter in optical fibers, a development that was truly a breakthrough, introducing a new branch in the field of optical fiber sensing shortly identified as *SPR optical fiber sensors*. The research programme that originated this thesis is anchored in this optical sensing approach, mostly focused on the theoretical and computational analysis of several fiber optic structures incorporating plasmonic resonance behaviour and oriented to the sensing functionality. Such structures differentiate on the type of metal or hybrid layer considered to support plasmonic resonance, or on the geometry of the optical fiber. Their research and the results obtained reported in this thesis are relevant by itself in what concerns the understanding of the basic working principles and identification of their sensing characteristics, but also to guide the implementation of these sensing devices particularly when they need to be tailored to fit the demands of a specific application.

The thesis is organized in seven chapters. ***Chapter 1*** starts by locating historically the research on the phenomenon of plasmonic resonance in the optical domain and how it can be applied to achieve sensing functionalities, first in bulk optics platforms and later associated with the utilization of optical fibers. Then, it proceeds to contextualize this sensing approach within the actual and rather active field of R&D in Plasmonics. ***Chapter 2*** delivers the basic concepts that permit the understanding of the phenomenon of plasmonic resonance and the conditions for its existence on dielectric-metal-dielectric slabs. The propagation of an electromagnetic field in a

multilayer structure will also be discussed. ***Chapter 3*** presents a worked review of the different techniques to interrogate plasmonic based sensors, addressing in particular the performance level that can be achieved with each of the interrogation approaches analysed, namely angular interrogation, spectral interrogation, intensity interrogation and phase interrogation. ***Chapter 4*** develops the study of SPR based optical fiber sensing configurations integrating a single metal or a bimetallic layer and, with the focus on phase interrogation, it is analysed the performance associated with the utilization of different metals, namely silver, gold, copper, and aluminium when the tapered and the tip (optrode) optical fibers geometric layouts are addressed. ***Chapter 5*** presents a theoretical investigation of optical fiber plasmonic based sensors incorporating an internal metallic layer of silver covered with an oxide layer. The objective is to shift the resonance condition to longer wavelengths, therefore more suited to benefit from a broad range of optical fiber technologies developed along the years within the context of optical fiber communications systems. Different oxide materials like titanium dioxide, silicon dioxide and aluminium oxide are considered aiming to achieve enhanced sensitivity to refractive index variations of the external medium, particularly when addressing phase interrogation. ***Chapter 6*** deals with the integration of fiber gratings with standard fiber optic SPR sensing technology to bring it to the singlemode domain, therefore turning it compatible with the vast field of fiber optic communication systems with its large portfolio of advanced and cost effective components and devices. In particular, emphasis is allocated on the theoretical analysis of long period grating (LPG) assisted optical fiber sensing structures supported by Plasmonics. Finally, ***Chapter 7*** presents some final notes relative to the research performed and are outlined some paths for future work.

Table of Contents

List of Figures

List of Tables

1

Historical Overview of Plasmonics

Summary: *This Chapter starts to locate historically the research on the phenomenon of plasmonic resonance in the optical domain and its support to achieve sensing functionalities, first in bulk optics platforms and later associated with the utilization of optical fibers. This sensing approach is contextualized within the actual and rather active field of R&D in Plasmonics which is continuously opening new horizons in science and in technology.*

1.1 First Descriptions

Plasmonics has been studied since the beginning of the 20th century, although the great developments on SPR were achieved in the late 60s with bulk configurations. Surface plasmons are electromagnetic excitations that propagate in wave like form along the planar interface between a metal and a dielectric medium. The plasmon excitation produces a minimum in the spectral transmittance for certain wavelength and refractive index values.

Between 1902 and 1912 *R.M. Wood* at *John Hopkins University (Baltimore, USA)* [1] (figure 1.1) noticed that, when he shone polarized light on a metal backed diffraction grating, a pattern of unusual dark and light bands appeared in the reflected light. Although he speculated about how the light, gratings and metal interacted a clear answer to the phenomenon was not provided.

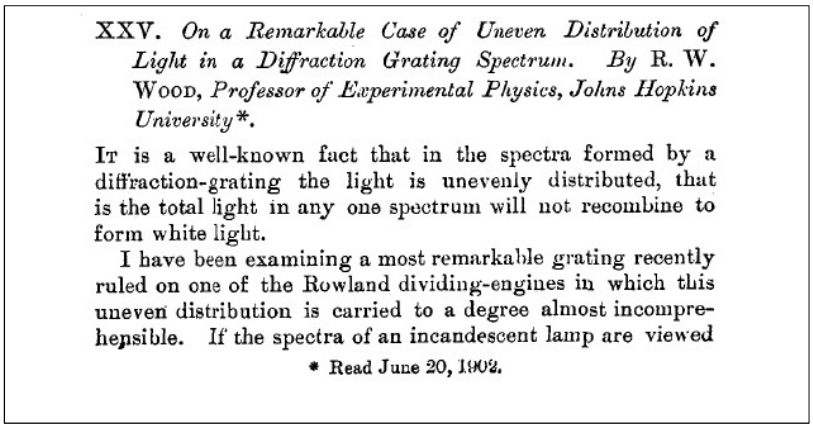

XXV. *On a Remarkable Case of Uneven Distribution of Light in a Diffraction Grating Spectrum.* *By* R. W. Wood, *Professor of Experimental Physics, Johns Hopkins University**.

It is a well-known fact that in the spectra formed by a diffraction-grating the light is unevenly distributed, that is the total light in any one spectrum will not recombine to form white light.

I have been examining a most remarkable grating recently ruled on one of the Rowland dividing-engines in which this uneven distribution is carried to a degree almost incomprehensible. If the spectra of an incandescent lamp are viewed

* Read June 20, 1902.

Figure 1.1 - First publication on the plasmonics [1].

The first theoretical treatment of these anomalies is undergone by *Lord Rayleigh* in 1907 [2] (figure 1.2). His "dynamical theory of the grating" was based on an expansion of the scattered electromagnetic field in terms of outgoing waves only. With this assumption, he found that the scattered field was singular at wavelengths for which one of the spectral orders emerged from the grating at the grazing angle. He then observed that these wavelengths, which have come to be called the *Rayleigh* wavelengths , λ_R correspond to the *Wood* anomalies [3]. Furthermore, these singularities appeared only when the electric field was polarized perpendicular to the rulings, and thus accounted for the S anomalies; for P polarization, his theory predicted a normal behavior near λ_R.

Wood's later papers [4, 5] however, suggest that P anomalies could sometimes be observed. *Palmer* [6, 7] very clearly demonstrated that P anomalies did exist in deeply ruled gratings. Thus, anomalies of both the S and P type were obtainable, but P anomalies were found only on gratings with deep grooves [3].

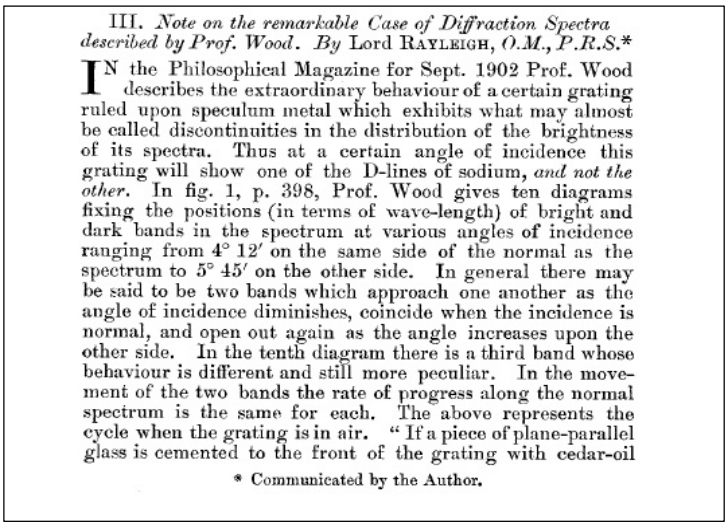

III. *Note on the remarkable Case of Diffraction Spectra described by Prof. Wood. By* Lord RAYLEIGH, *O.M., P.R.S.**

IN the Philosophical Magazine for Sept. 1902 Prof. Wood describes the extraordinary behaviour of a certain grating ruled upon speculum metal which exhibits what may almost be called discontinuities in the distribution of the brightness of its spectra. Thus at a certain angle of incidence this grating will show one of the D-lines of sodium, *and not the other*. In fig. 1, p. 398, Prof. Wood gives ten diagrams fixing the positions (in terms of wave-length) of bright and dark bands in the spectrum at various angles of incidence ranging from 4° 12′ on the same side of the normal as the spectrum to 5° 45′ on the other side. In general there may be said to be two bands which approach one another as the angle of incidence diminishes, coincide when the incidence is normal, and open out again as the angle increases upon the other side. In the tenth diagram there is a third band whose behaviour is different and still more peculiar. In the movement of the two bands the rate of progress along the normal spectrum is the same for each. The above represents the cycle when the grating is in air. " If a piece of plane-parallel glass is cemented to the front of the grating with cedar-oil

* Communicated by the Author.

Figure 1.2 - First publication on theoretical studies of plasmonics [2].

In the fifties, more experimentation was done on electron energy losses in gasses and on thin foils [8, 9]. The suggestion by *Pines* and *Bohm* [10-12] that the energy losses where due to the excitation of conducting electrons creating plasma oscillation or plasmon was a great step forward. Further research [9] revealed that the energy loss resulted from excitation of a surface plasma oscillation in which part of the restoring electric field extended beyond the specimen boundary. Therefore, the surface plasma oscillation could be affected by the presence of any film or contaminant on the specimen surface. This effect was later described in terms of excitation of electromagnetic 'evanescent' waves at the surface of the metal, and in the 1970's evanescent waves where described as a means to study ultra-thin metal films and coatings [13].

In the late sixties, optical excitation of surface plasmons by the method of attenuated total reflection was demonstrated by *Kretchman* [14, 15] and *Otto* [16]. Since then, surface plasmons have been intensively studied and their major properties have been assessed [17, 18].

1.2 SPR Optical Sensing

During the last two decades we have witnessed remarkable research and development activity aimed at the realization of optical sensors for the measurement of chemical and biological quantities. First, optical chemical sensors were based on the measurement of changes in absorption spectrum and were developed for the measurement of CO_2 and O_2 concentration [19]. In the 1980s, surface plasmon resonance (SPR) and related techniques exploited evanescent waves applied to the interrogation of thin films as well as biological and chemical interactions [20-23]. In these sensors the target quantity is determined by measuring the refractive index, absorbance and fluorescence properties of analyte molecules or a chemo-optical transducing medium [24, 25]. The potential of surface plasmon resonance for characterization of thin films

and monitoring processes at metal interfaces [26] was recognized in the late seventies. In 1982 the use of SPR for gas detection and biosensing was demonstrated by *Nylander* and *Liedberg* [23, 27, 28]. Since then SPR sensing has been receiving continuously growing attention from the scientific community.

Within the last few years, the possibility of implementing the surface plasmon resonance sensing principle into optical waveguide structures has attracted much attention. SPR sensors based on optical waveguides offer various advantageous features for sensing. Indeed, they are small in size, exhibit ruggedness, there is the prospect of fabrication of multiple and/or multichannel sensors on a single optical chip and, in conjunction with optical fibers, they may, be used for remote sensing applications.

Development of new SPR-sensing configurations as well as applications of SPR-sensing devices for the measurement of physical, chemical and biological quantities have been widely described. A great deal of work has been done in the exploitation of SPR for optical biosensing, as can be assessed from the fact more than 75% of the research papers deal with applications of SPR to detect biomolecular interactions. In this area, SPR, as a surface-oriented method, has shown a great potential for affinity biosensors, allowing real-time analysis of biospecific interactions without the use of labeled molecules. The SPR sensor technology has been commercialized by several companies and has become a leading technology in the field of direct real-time observation of the biomolecular interactions.

In the following a few recent applications of SPR sensors will be described, in particular their employment in the detection of environmental pollutants and in space missions.

1.2.1 Environmental Applications

Surface Plasmon Resonance biosensors have been demonstrated for the detection of many aqueous pollutants , as arsenic [29], ricin [30, 31], endocrine disruptors [32, 33], pesticides [34-37], methane [38], heavy metals [39], bacteria and toxins [40-42], copper ions [43] and others. Some of them have been tested in real lake water, surface water or groundwater samples.

Gaseous pollutants as NH_3 [44], CO [45], NO_2 [46], hydrogen [47, 48], SiO_2 [49], ammonia and amine gases [50], petroleum hydrocarbon vapors [51] are examples of additional compounds whose detection has been addressed by SPR arrangements.

Optical sensors based on the SPR phenomenon has also been applied in the framework of other medical and environmental applications, as food quality, safety analysis, detection of cancer, allergy and heart attack markers, dioxins, phenols and aromatic hydrocarbons, as reported in [52].

SPR sensors are particularly suited for pollutant and explosive detection because they only optically act on the surrounding ambient, therefore avoiding electric interaction. Moreover these sensors are able to provide extremely high sensitivities.

1.2.2 Space Applications

SPR based sensors are also well suited for astrobiologial missions. An example of application of these sensors on this environment is the *The Life Marker Chip (LMC)*, where SPR sensing is configured looking for the detection of organic or prebiotic molecules on the surface of planets or moons. The design aim of the LMC is to detect 20-25 biomarker molecules on 20-50 samples combining surface plasmon resonance and fluorescently labeled tracers. *Specific Molecular Identification of Life Experiment* (SMILE) has been proposed as a possible LMC (figure 1.3).

Light with wavelength 635 nm is coupled into the LMC by fiber coupling. The light is then guided by a Si_3N_4 (stoichiometric silicon nitride) waveguide (refractive index n=2.01) standing between SiO_2 (silicon oxide, n=1.47) top and bottom claddings. Locally, the top SiO_2 cladding layer is selectively removed. As shown in figure 1.3 in these regions the evanescent field is available for probing the fluorescent spots and the top cladding consists of water [53].

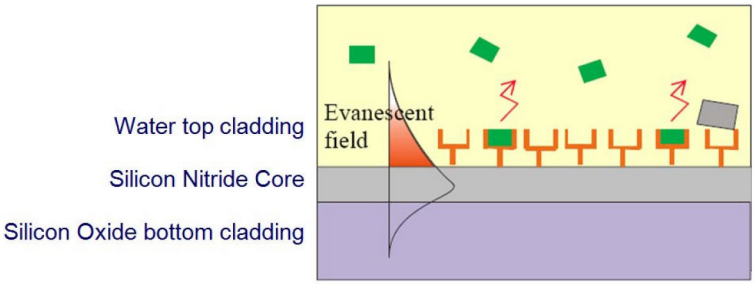

Figure 1.3 - Concept of the LMC: the evanescent field of the propagating light wave excites the fluorescent labels (green blocks) bound to the immobilized groups (red forks) on the chip surface [53].

1.3 The Outcome of Optic Based SPR Sensing

Due to all the favorable characteristics of optical fiber sensors, fiber sensing has been the focus of substantial research and development along the years and many solutions for field applications came out from this effort [54]. Following the degrees of freedom of the optical field, different classes of fiber sensors have been researched along the years, but it can be fairly stated that fiber optic sensors with spectral selectivity has been playing a major role in optical fiber sensor technology and all points out this trend will be strengthened in the future.

Within this general trend, the deposition of metals on the optical fiber to induce the phenomena of surface plasmon resonance has also been explored, being nowadays a rather successful optical sensing approach. This orientation started by *Jorgenson* and *Yee* in 1995 who fabricated the first optical fiber SPR sensor (figure 1.4) [55]. They proved that the optical fiber can be used as a substrate for metallic deposition and surface plasmon resonance sensing. The fiber used was chemically etched in order to remove almost all the cladding. The metal film deposition was made on that region of the fiber.

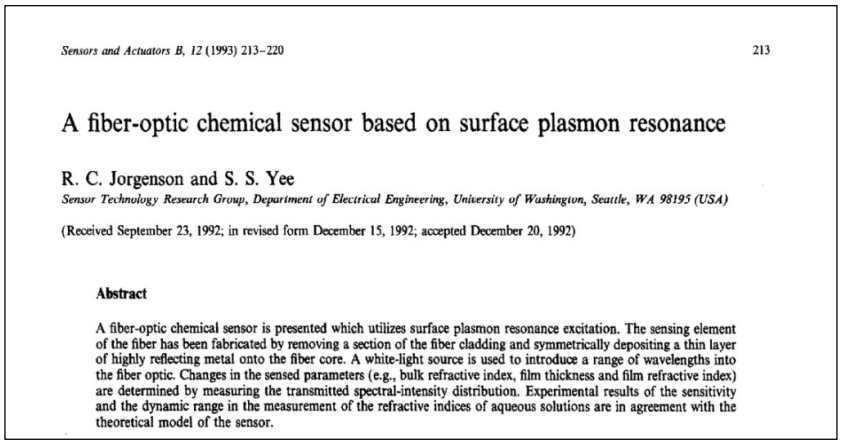

Sensors and Actuators B, 12 (1993) 213–220 213

A fiber-optic chemical sensor based on surface plasmon resonance

R. C. Jorgenson and S. S. Yee

Sensor Technology Research Group, Department of Electrical Engineering, University of Washington, Seattle, WA 98195 (USA)

(Received September 23, 1992; in revised form December 15, 1992; accepted December 20, 1992)

Abstract

A fiber-optic chemical sensor is presented which utilizes surface plasmon resonance excitation. The sensing element of the fiber has been fabricated by removing a section of the fiber cladding and symmetrically depositing a thin layer of highly reflecting metal onto the fiber core. A white-light source is used to introduce a range of wavelengths into the fiber optic. Changes in the sensed parameters (e.g., bulk refractive index, film thickness and film refractive index) are determined by measuring the transmitted spectral-intensity distribution. Experimental results of the sensitivity and the dynamic range in the measurement of the refractive indices of aqueous solutions are in agreement with the theoretical model of the sensor.

Figure 1.4 - First publication on SPR fiber optic sensors [55].

In 1995 *Tubb* et al. [56] demonstrated SPR sensing with a tapered optical fiber (such configuration was later studied by *Villatoro* et al. [57] bringing it to a high performance standard). In 1996, *Homola* et al. [58] used again the optical fiber as a substrate, but now considering a side polished optical fiber in order to get into the evanescent field of the core mode. These initial studies proved the feasibility of the optical fiber as a SPR sensing platform and established the potential in the sensing domain of the combination optical fiber + SPR, which has undergone continuous growth in the following years to an extent that nowadays become a reference when high performance environment optical sensing is on demand.

1.4 The New World of Plasmonics

Plasmonics is a subject that undergone tremendous progresses in the last decade following an accelerated development path, indicating the high impact it will have in fundamental and applied optics. Surely, optical sensing will strongly benefit from this movement but also many other areas in view the possibilities of optical imaging systems with nanometre-scale resolution, the availability of hybrid photonic-plasmonic devices, the substantial enhancement of semiconductor luminescence which opens the road to high efficient plasmon-assisted lightning, the feasibility of

plasmon antennas with large light capture characteristics, the foreseen viability of plasmonic nanocircuits which combine a large bandwidth with a high level of integration, and others. Therefore, to have a correct perspective of the reasons behind such huge promise and to draw a balanced picture of possible future progress paths in plasmonics based optical sensing, it is worthwhile to add here some paragraphs addressing general points of the subject [59].

1.4.1 SPR Sensing and Microstructured Optical Fibers

As briefly outlined in Section 1.3, plasmonics based optical sensing undergone a development leap when the sensor platforms expanded from the prism coupling system layout to structures supported by guided optics, particularly optical fibers and planar devices with input/output fibers. This movement permitted to address functionalities not possible with the classic approach, such as sensor miniaturization and remote operation. Pointing specifically to optical fiber SPR sensors, in the last decade various compact configurations enabling effective coupling between the fiber modes and the surface plasmonic waves have been investigated, such as those based on metalized side-tapered single mode and multimode optical fibers, metalized tapered fibers, metallized fiber Bragg gratings and others .

The consideration of standard optical fibers or derived structures (such as tapers, side-etched fibers, etc.) for SPR sensors faced two main difficulties (common also to planar waveguides), which have been limiting the performance level conceptually attainable with these platforms. The most fundamental one is the problem of phase matching of a waveguide core mode and the surface plasmonic wave (SPW), which implies the need the mode and the wave to have the same value for the corresponding effective refractive indices at the operation wavelength, generating what is known as a SPW of hybrid nature. In the case of a single mode waveguide, the effective refractive index of its core mode is close to that of the core material, which is typically higher than 1.45. On the other hand, the effective refractive index of a plasmon is close to that of the surrounding analyte, with the most often found situations associated to the presence of air (refractive index ~1.0) and water (refractive index ~1.33). Therefore, it is necessary to move to shorter wavelengths for the plasmon refractive index becomes high enough as to match that of a waveguide core mode (for the case of gold metal film, this requires $\lambda < 700$ nm). Phase match condition can be achieved at longer wavelengths incorporating in the sensing head an additional dielectric thin film with specific characteristics [60], approach with some disadvantages, one of them being added complexity. This phase matching problem can be attenuated by coupling to a plasmon through the high order modes of a multimode waveguide. These modes can have substantially lower effective refractive indices than the waveguide core index. Following this strategy, light has to be launched into a waveguide as to excite high order modes, with some of

them in conditions to be phase matched with a plasmon. However, as only a fraction of higher order modes fulfil this phase matching condition, only a fraction of total launched optical power will be coupled to a plasmon, therefore reducing sensor sensitivity. Moreover, as power distribution in high order modes is sensitive to the launching conditions this adds noise to the system due to fluctuations in the coupling setup.

A much more effective approach recently proposed involves decoupling the SPW from the fiber guided mode using a grating, therefore converting the hybrid SPW into a pure one [61]. As pointed out, the difference between the effective refractive index of the guided mode and the effective refractive index of pure SPW is large and requires a proper strategy to excite such surface plasmonic wave (wavelength tuning, consideration of waveguide higher order modes or the insertion of an additional layer). However, such gap can be bridged with a Bragg grating, which allows the wave-vector matching condition to be met. It was pointed out the potential of this approach to improve the sensitivity of SPR sensors. Indeed, in hybrid SPW the effective refractive index is only slightly different from the effective refractive index of the guided mode supported by the structure without the metal layer. This is because most of the energy is associated with the guided mode and only slightly weighted by the plasmon effective index. This condition means the hybrid mode is weakly sensitive to any change in the effective index of the plasmon, should it be altered by the presence or absence of a surrounding layer. For the case of a pure SPW, since almost all its energy is concentrated at the metal-dielectric interface, this scheme can be extremely sensitive to small changes in the refractive index of the sensed medium.

The other difficulty mentioned above is more practical and has to be with the packaging of a microfluidics setup, waveguide and a metallic layer into a sensing structure. Considering single mode fiber based sensors, to metalize a surface close to the core first one has to strip the fiber jacket and then polish the fiber cladding almost to the core to enable evanescent coupling with a plasmon. This is a time-consuming process that compromises fiber integrity and turns the sensor susceptible to mechanical failures. In addition, the integration of a metalized fiber piece into a microfluidics setup presents extra difficulties, thus increasing the overall fabrication complexity and cost.

The first difficulty pointed out is related with the reduced degrees of freedom available for sensors supported in standard fibers, which means the tuning of their characteristics must be done acting essentially on the sensor constituent materials, which are essentially those of the optical fiber (or planar waveguide) with a variability strongly constrained by the need to assure, first of all, high quality optical propagation. Therefore, not considering the Bragg grating coupling approach described above, the open ground is from the geometry side, assuming it can be overcome the

technological problems associated with the fabrication of fibers with operation essentially defined by their geometry.

The breakthrough associated with the development of microstructured optical fibers (MOF) is, to a large extent, associated with the flexibility provided by the possibility to change readily the cross section profile of the fiber, alternating silica and void regions and, with that, tailoring in a wide range the characteristics of the modal propagation. This amplitude allows an easy compromise of the guiding properties with those related with high performance plasmonic based optical sensing. Indeed, in a MOF supported SPR sensor, plasmons on a surface of a thin metal film can be excited by a Gaussian-like leaky mode of an effectively single mode waveguide. It has been demonstrated the effective refractive index of such mode can be designed to be considerably smaller than that of the core material, actually it can have a value from zero to that of the refractive index of the core material [62]. This enables efficient phase matching with plasmons at any wavelength of choice, while retaining highly sensitive response to changes in the refractive index of an analyte layer.

SPR sensing structures supported by MOF also considerably alleviate the second difficulty abovementioned. Microfluidics in these fibers is enabled by passing the analyte through the porous cladding, thus solving one of the packaging problems, as well as the fragility issue since no polishing is involved. Additionally, the internal propagation of the fluids increases the safety when dealing with the measurement of volatile or toxic samples. Deposition of metal layers inside the MOF can be performed either with high pressure CVD techniques or wet chemistry deposition techniques used in fabrication of metal covered hollow waveguides [63].

A recent development illustrates the potential of MOF for SPR sensing. A well-studied layout for a microstructured optical fiber is the three-hole fiber illustrated in figure 1.5(a) [64]. The silica fiber consists of three air holes, where cladding layers and gold layers are uniformly deposited in sequence. Since the size of the air holes can be tens of micrometers, fabrication of the multi-

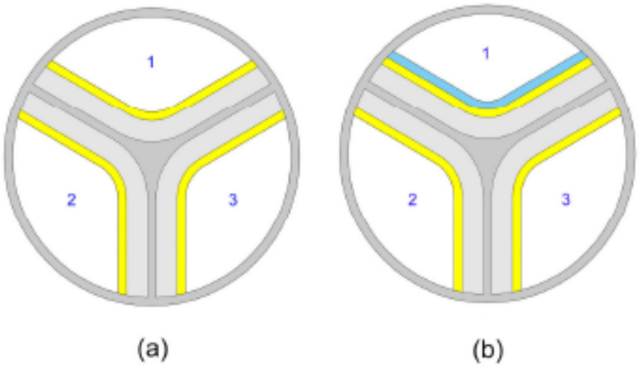

Figure 1.5 - Schematic of the three-hole microstructured optical fiber [64].

layered channel structures and the infiltration of sample into channels become easier. The cladding layers, with a refractive index slightly smaller than the fiber core, are introduced to tune the propagation loss of the sensor to a tolerable level. Polymers and down-doped silica are both candidates for the cladding layers. The gold layers, generally with a nano-scale thickness, can be coated via the technique of high-pressure microfluidic chemical deposition.

This structure was investigated to implement a dual-channel plasmonic sensor [65], with analyte A in one of the metalized holes (denoted as Channel 1) and analyte B in the other two holes (Channel 2&3). The study performed by the authors indicated the sensor in the standard configuration given in figure 1.5(a) fails to distinguish between the two analytes when there is a small refractive index difference between them (smaller than 0.01). So, it was proposed to introduce an asymmetry in the sensing structure by adding a high refractive index polymer layer on top of the gold surface of Channel 1, as illustrated in figure 1.5(b). In this case it turns possible to have two distinct SPR resonance dips, showing a spectral shift with refractive index variations with slopes of of 1535 nm/RIU (Channel 1) and 1550 nm/RIU (Channel 2&3). Assuming a resolution of 0.01 nm for the reading spectrometer, the corresponding refractive index minimum detectable variations are 6.51×10^{-6} and 6.45×10^{-6}, respectively.

The authors mention the capability of this structure in dual analyte sensing yields two applications. One is tracking two different analytes in one liquid sampling, where each analyte is captured by a functional material deposited in the corresponding channel. The other is sensing two different liquids samples simultaneously. Another interesting application of this device is to implement a sensor with referencing properties. For example, Channel 1 can be chosen as the sensing channel and channels 2 and 3 both work as reference channels, which are usually coated with receptors responding to the non-targeted molecules in the sample. Both the referencing signal and the sensing signal appear as absorption dips. The variation of the non-target molecules, which causes a shift of the referencing signal, also contributes to the shift of the sensing resonance. Hence, instead of monitoring a single resonance wavelength, the spectral separation of the two dips can be used to nullify the non-specific effects. In addition, the two resonances share almost the same instrumental noise and thermal instability, which also helps to eliminate external influences.

This example illustrates the possibilities in SPR sensing offered by platforms based in microstructured fibers. Moreover, to solve the two main difficulties identified for SPR sensors supported by standard optical fibers (and planar waveguides), it provides a level of flexibility for sensor design and tuning of performance level without parallel in other guided optics sensing approaches, further enhanced when the integration of grating structures is considered. It is therefore expectable to observe in the near future a growing level of R&D activity around the

combination of plasmonics and microstructured optical fibers towards advanced optical sensing functionalities.

1.4.2 Multiplexing of SPR Sensors

The reported R&D activity oriented to multiplexing of SPR sensors has been residual, although some efforts done on that direction in prism based sensors, as is the case of the work described by [66] where a dual-channel configuration was proposed. The truth is the prism coupling systems are not amenable to incorporate the multiplexing functionality, contrary to what happens when the optical fiber is considered. Indeed, the unique feature of the fiber being simultaneously sensing element and communication channel opens the intrinsic capability of this technology for sensor multiplexing, a characteristic that has been widely explored in the context of many areas addressed by fiber optic sensing, but not when considering SPR sensors, even when they are fiber based. This somehow surprising reality has reasons eventually rooted to that the background of the researchers that have been working out this type of sensors. Indeed, the illumination used is almost invariably at wavelengths in the 850 nm region, where the availability of high-performance fiber optic components is reduced, consequently not benefiting from the novel developments in optical fiber technology which are anchored to the telecommunications field, in particular from the high-tech optical fiber components available for the third telecommunications window (1550 nm), which are crucial for the development of effective fiber optic sensor networks. Some results were reported on fiber SPR sensors operating in this spectral region [67, 68], for all reasons a path to be reinforced in the future, opening the route for actively pursuing the topic of SPR sensor multiplexing.

1.4.3 Sensor Functionalization

A topic relevant for all optical sensing heads intrinsically sensitive to refractive index, but enhanced in the case of SPR based structures in view the performance level they exhibit which is compatible with ultra-low detection thresholds, derives from the circumstance in many situations the targeted measurand is not refractive index but another entity that can be detectable by variations it induces in the sensor surrounding index. As an example, the detection of Hydrogen with a SPR sensor can be achieved depositing a thin Palladium layer on the sensor structure, which has a refractive index that depends on the nearby Hydrogen concentration. In general, refractive index changes can be induced by a myriad of factors, which means the developing of a SPR sensor to detect a specific species implies the need to amplify those changes connected with its presence while minimizing the others associated to variations of any other parameter, a process known as

sensor functionalization. This is particularly acute in the domain of biochemical sensing because the intrinsic high sensitivity of SPR sensors is an appealing characteristic to detect very small concentrations of the targeted entity, admitting they induce refractive index changes larger enough compared with any other environmental related changes, which for the case have a noisy effect [69, 70].

In this domain substantial R&D effort has been done on how to detect specific molecules from groups of molecules. Here, one of the main problems is that recognition molecules may exhibit affinity to similar types of other unwanted molecules present in the environment. These unwanted ("noise") molecules will react with the biosensors and will alter the refractive index, affecting important sensor parameters such as sensitivity, detection accuracy and reproducibility. A second problem is related with nonspecific interactions between sensor surface with "noise" molecules and with background refractive index variations, which can arise from many factors, such as temperature, humidity and compositional fluctuations. These two issues demand the conception and development of robust functionalization approaches for SPR based optical sensors (actually, in most circumstances for all sensing platforms with refractive index intrinsic sensitivity), desirably with tuning ability to the type of entities targeted for measurement. This is a demanding challenge, particularly when addressing the biochemical area, and will continue to be a focus of intense research and development activity.

1.4.4 Nanostructured Plasmonic Sensors

In the last few years, plasmonic nanostructures have been exploited in several ways for plasmonic sensors [71, 72]. Therefore, surface-enhanced spectroscopies (SES), such as surface-enhanced Raman scattering (SERS) [73, 74], surface enhanced resonance Raman scattering (SERRS) [75], surface-enhanced infrared absorption (SEIRA) [76] or metal enhanced fluorescence (MEF) [77], are considered as some of the most important optical sensing techniques. They are all based on a significant amplification of the spectroscopic signal by electromagnetic field enhancement induced by localized surface plasmon resonance (LSPR). In particular, SERS was the most widely used SES as an extremely sensitive analytical technique for chemical or bio-analytical applications. Although single molecule detection has already been predicted and observed in SERS [74, 78], in most of the cases giant enhancements of the Raman signal were only reached for coupled nanostructures such as at interstitial sites in nanoclusters or nanostructured surfaces with closely spaced features [79, 80]. However, SERS behaviors at so-called hot spots are complex and usually show poor repeatability and reproducibility, which limit their use in biosensor applications. Particularly, the LSPR excitations at such interstitials or on nanoparticle sharp edges are highly dependent on the excitation polarization [81]; as a consequence, the SERS signal will show in the

same way a strong dependence on the excitation polarization [82]. For example, using nano-ellipses as SERS-active substrates, intense Raman signals could only be obtained when the excitation polarization is parallel to the major axis of the nano-ellipses [83]. Such polarization dependence also brings limitations to the actual sensing applications because rigorous management of polarization in the measurements set-up will be required. This could be an important drawback especially when the light polarization control cannot be easily completed such as in optical fiber [84] or when the SERS substrate cannot be placed precisely in the right orientation. Further developments for technology transfer of such optically based sensors will depend on their robustness and simplicity for non-physicists users (biologist, medical doctors, others).

Most of the SPR biosensors commercially available at present use surface plasmon polaritons (SPPs), which are excited on continuous Au or Ag films in the attenuated total internal reflection (ATR) geometry [85]. Owing to the resonant photon-SPP coupling conditions, namely the specific combination of the wave vector and wavelength, SPPs provide an extremely small detection limit exceeding 10^{-5} refractive-index units (RIU), which can be further improved using phase-sensitive interferometry schemes [86]. However, the SPP-based approach still needs an improvement in sensitivity for the detection of small analytes and does not always satisfy modern requirements of biotechnology advancing towards new nanoscale designs and promising the manipulation on the nanoscale level of size-based selectivity and selective chemical and biochemical nano-architectures. Localized surface plasmons (LSPs) of metallic nanostructures seem much more suitable to match these new trends, as well as to bring new functionalities, such as spectral tenability [87] and strong enhancement of the local electric field [88]. However, LSP-based sensors are known to provide at least an order of magnitude lower sensing response to refractive index change compared with SPPs, with sensitivities not exceeding 100-300 nm per RIU in spectral interrogation schemes as well as 10 times smaller probe depth [89], making them applicable for only a very limited number of biological species. Understanding these problems in sensing applications of existing plasmonics structures also induced focus on newly emerging plasmonic metamaterials, composite structures consisting of subwavelength-size components. The objective is to design a sensor-oriented metamaterial that is capable of supporting similar or more sensitive guiding modes than SPPs. The metamaterial based approach may additionally offer the advantages of nano-architectures, i.e., enable large effective area and the possibility of guiding and imaging capabilities beyond the diffraction limit [90], as well as the feasibility of nanomanipulation and nanotrapping [91].

1.5 Final Remarks

The coherent interaction of the photon and the electron which generates an hybrid structure named *Plasmon,* with its own properties which shows flavours of the characteristics of the free electron and of the free photon, is a phenomenon known since the beginning of the twenty century, but can be fairly stated it was only recently that the conceptual relevance of such hybrid entity was grasped, from where a huge technological impact has been emerging. This statement becomes obvious when it is realized with plasmons optical sub-wavelength imaging turns possible, overcoming the constraints of the optical diffraction limit which has always been assumed to be an absolute one. The field of science that deals with this hybrid entity is identified as ***Plasmonics*** and is nowadays one of the most fascinating fields of Photonics and the focus of a worldwide R&D activity that takes place at a breathtaking pace.

Plasmonic has also strongly impacted the domain of optical sensing, starting from the modest demonstration of this possibility in the 1970's. Up to the end of the century SPR based optical sensing progressed to a point it became the technique providing the best sensitivity in measurement of refractive index changes of the sensor surrounding and was demonstrated the advantages associated with the utilization of the optical fiber as a platform to host this sensing principle. But was the outcome of nanoscience and nanotechnology at the turn of the century that opened the door to rather large horizons for Plasmonic in general and plasmonics-based optical sensing in particular. This new reality brought to the forefront the nanoengineering of materials and, consequently, the new world of the metamaterials became accessible. The implications of this are rather difficult to foresee but no doubt the breakthroughs will be tremendous in science and technology, and surely optical sensing will not be an exception particularly when high performance interrogation approaches are considered to read out the status of the sensors as is the case of phase interrogation.

The research undergone in the context of this PhD programme was oriented to the analytical study of the performance of SPR based fiber optic sensing heads with different geometries and material compositions when coupled to optical phase interrogation. To do this first the theoretical background of Plasmonics was reviewed which is the focus of next chapter.

2

Theoretical Background of Plasmonics

Summary: *This chapter presents the physical concepts that define the Surface Plasmon Polaritons phenomenon and the conditions for their existence on dielectric-metal-dielectric slabs. The propagation of electromagnetic fields into a multilayer structure will also be discussed. This theory consequently allows understanding and model surface plasmon resonance based sensors.*

2.1 Electromagnetic Theory of Surface Plasmons

In this section, an electromagnetic theory of optical waveguides based on solving Maxwell's equations using the modal method will be presented. The Maxwell's equations for a space without free charges are [85]:

$$\nabla \times \vec{E} = -\mu\, \partial\vec{H}/\,\partial t \tag{2.1}$$

$$\nabla . \varepsilon_0 \varepsilon_r \vec{E} = 0 \tag{2.2}$$

$$\nabla \times \vec{H} = \varepsilon_0 \varepsilon_r \vec{E}/\,\partial t \tag{2.3}$$

$$\nabla . \mu\vec{H}=0 \tag{2.4}$$

where the relative permittivity is $\varepsilon = \varepsilon_0 \varepsilon_r$, where ε_0 is the free-space permittivity, the magnetic permeability is μ and E and H are the electric and magnetic fields, respectively.

For linear, isotropic and non-magnetic materials ($\mu = \mu_0$) from the above equations it comes out

$$\Delta\vec{E} - \mu_0 \varepsilon_0 \varepsilon_r\, \partial^2\vec{E}/\,\partial t^2 = \nabla(\vec{E}.\nabla \ln(\varepsilon_0 \varepsilon_r)) \tag{2.5}$$

$$\Delta\vec{H} - \mu_0 \varepsilon_0 \varepsilon_r\, \partial^2\vec{H}/\,\partial t^2 = (\nabla \times \vec{H}) \times \nabla \ln(\varepsilon_0 \varepsilon_r) \tag{2.6}$$

from where comes out wave equations. Here, the vector differential operators ∇ and Δ are defined as follows:

$$\nabla . \vec{A} = \frac{\partial A_x}{\partial x} + \frac{\partial A_y}{\partial y} + \frac{\partial A_z}{\partial z} \tag{2.7}$$

$$\nabla \times \vec{A} = \left(\frac{\partial A_y}{\partial z} - \frac{\partial A_z}{\partial y}\right)\mathbf{x}_0 + \left(\frac{\partial A_z}{\partial x} - \frac{\partial A_x}{\partial z}\right)\mathbf{y}_0 + \left(\frac{\partial A_x}{\partial y} - \frac{\partial A_y}{\partial x}\right)\mathbf{z}_0 \tag{2.8}$$

$$\nabla g = \frac{\partial g}{\partial x}\mathbf{x_0} + \frac{\partial g}{\partial y}\mathbf{y_0} + \frac{\partial g}{\partial z}\mathbf{z_0} \tag{2.9}$$

$$\begin{aligned}\Delta\vec{A} = (\partial^2 A_x/\,\partial x^2 + \partial^2 A_x/\,\partial y^2 + \partial^2 A_x/\,\partial z^2)\mathbf{x_0} + \\ \left(\partial^2 A_y/\,\partial x^2 + \partial^2 A_y/\,\partial y^2 + \partial^2 A_y/\,\partial z^2\right)\mathbf{y_0} + \\ (\partial^2 A_z/\,\partial x^2 + \partial^2 A_z/\,\partial y^2 + \partial^2 A_z/\,\partial z^2)\mathbf{z_0}\end{aligned} \tag{2.10}$$

the scalar coordinates are (x, y, z), the vector $\vec{A}(x,y,z) = \left[A_x(x,y,z), A_y(x,y,z), A_z(x,y,z)\right]$, $g(x,y,z)$ is a scalar function and $\mathbf{x_0}, \mathbf{y_0}, \mathbf{z_0}$ are unit vectors.

If we assume the electromagnetic wave to propagate along the z axis and time dependence of the fields to be $\exp(-i\omega t)$ where ω is the angular frequency and $i = \sqrt{-1}$, from the equations abovementioned can be derived the following

$$E = e(x,y)\exp[i(\beta z - \omega t)] \tag{2.11}$$

$$H = h(x,y)\exp[i(\beta z - \omega t)] \tag{2.12}$$

where β denotes the propagation constant of an electromagnetic mode.

A illustrated in figure 2.1, let's consider an optical waveguide composed of three homogeneous media with permitivities:

$$\varepsilon(x) = \varepsilon_3 = n_3^2, \qquad x > d, \tag{2.13}$$

$$\varepsilon(x) = \varepsilon_2 = n_2^2, \qquad -d \le x \le d, \tag{2.14}$$

$$\varepsilon(x) = \varepsilon_1 = n_1^2, \qquad x < -d, \tag{2.15}$$

where d is the waveguiding layer half-width and n_i $(i = 1,2,3)$ is the refractive index of the *i* layer. Notice ε_i and n_i are generally complex permitivities and refractive indices.

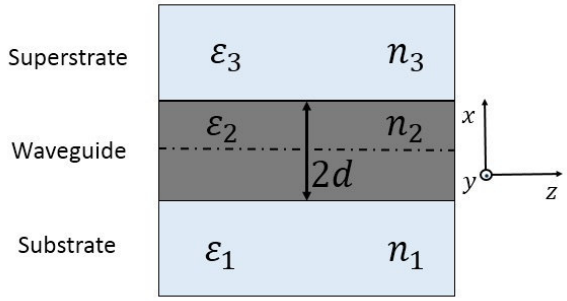

Figure 2.1 - Section of a planar waveguide with a step refractive index profile.

By orienting the layers in the y-z plane as shown in figure 2.1, the field vectors can be written as:

$$E = e(x)\exp[i(\beta z - \omega t)] \tag{2.16}$$

$$H = h(x)\exp[i(\beta z - \omega t)] \tag{2.17}$$

and the wave equations are:

$$(\Delta_{transverse} + \omega^2 \varepsilon \varepsilon_0 \mu_0 - \beta^2) e_i = 0 \tag{2.18}$$

$$(\Delta_{transverse} + \omega^2 \varepsilon \varepsilon_0 \mu_0 - \beta^2) h_i = 0 \tag{2.19}$$

where $(i = x, y, z)$.

The solutions of the equations 2.18 and 2.19 set above produce two different modes, one with $h_z = 0$ called Transverse Magnetic (TM) and one with $e_z = 0$, denominate Transverse Electric (TE). Substitution of the field profiles equations 2.16 and 2.17 into 2.18 and 2.19, respectively, yields for the transversal components of the field vectors [85]:

$$\frac{\partial^2 e_y(x)}{\partial x^2} + (\omega^2 \varepsilon \varepsilon_0 \mu_0 - \beta^2) e_y(x) = 0 \quad \text{for TE modes} \tag{2.20}$$

$$\frac{\partial^2 h_y(x)}{\partial x^2} + (\omega^2 \varepsilon \varepsilon_0 \mu_0 - \beta^2) h_y(x) = 0 \quad \text{for TM modes.} \tag{2.21}$$

From equations 2.1-2.4 and the definition of cross product:

$$\frac{\partial e_z}{\partial y} - \frac{\partial e_y}{\partial z} = -i\omega\mu h_x \tag{2.22}$$

$$\frac{\partial e_x}{\partial z} - \frac{\partial e_z}{\partial x} = -i\omega\mu h_y \tag{2.23}$$

$$\frac{\partial e_y}{\partial x} - \frac{\partial e_x}{\partial y} = -i\omega\mu h_z \tag{2.24}$$

$$\frac{\partial h_z}{\partial y} - \frac{\partial h_y}{\partial z} = i\omega\varepsilon e_x \tag{2.25}$$

$$\frac{\partial h_x}{\partial z} - \frac{\partial e_z}{\partial x} = i\omega\varepsilon e_y \tag{2.26}$$

$$\frac{\partial h_y}{\partial x} - \frac{\partial h_x}{\partial y} = i\omega\varepsilon e_z \tag{2.27}$$

assuming

$$\frac{\partial}{\partial y} = 0 \tag{2.28}$$

and

$$k_i^2 = \omega^2 \varepsilon_i \varepsilon_0 \mu_0 - \beta^2, \;\; i = 1, 2, 3 \tag{2.29}$$

the solutions of equations 2.20 and 2.21 for TE modes are:

$$e_y(x) = a_i^+ \exp(ik_i x) + a_i^- \exp(-ik_i x) \tag{2.30}$$

$$h_x(x) = \frac{\beta}{\mu_0 \omega} [a_i^+ \exp(ik_i x) + a_i^- \exp(-ik_i x)] \tag{2.31}$$

$$h_z(x) = \frac{-k_i}{\mu_0 \omega} [a_i^+ \exp(ik_i x) - a_i^- \exp(-ik_i x)] \tag{2.32}$$

and for TM modes are:

$$h_y(x) = b_i^+ \exp(ik_i x) + b_i^- \exp(-ik_i x) \tag{2.33}$$

$$e_x(x) = \frac{-\beta}{\varepsilon_i \varepsilon_0 \omega} [b_i^+ \exp(ik_i x) + b_i^- \exp(-ik_i x)] \tag{2.34}$$

$$e_z(x) = \frac{k_i}{\varepsilon_i \varepsilon_0 \omega} [b_i^+ \exp(ik_i x) - b_i^- \exp(-ik_i x)]. \tag{2.35}$$

a_i and b_i are the amplitude of Transverse Electric (TE) and Transverse Magnetic (TM) fields, respectively, and i=1, 2, 3, denotes the different sections of the planar waveguide (figure 2.1). The superscript signs + and – in a and b show, wave propagation in the $+x$ or $-x$ direction. In the first and third layer the fields decay exponentially with the distance to the second layer that represents the metal, so $a_1^+ = a_3^- = 0$ and $b_1^+ = b_3^- = 0$.

The boundary conditions of the Maxwell's equations are such that the components of the electric and magnetic fields parallel to the boundaries of the layers must be continuous at the borders of the second layer (x = d and x = −d). As a result the previous equation for TE modes may be expressed as:

$$e_y(x = d) = a_2^+ \exp(ik_2 d) + a_2^- \exp(-ik_2 d) = a_3^+ \exp(ik_3 d) \tag{2.36}$$

$$h_z(x = d) = \frac{-k_2}{\mu_0 \omega}[a_2^+ \exp(ik_2 d) + a_2^- \exp(-ik_2 d)] = \frac{-k_3}{\mu_0 \omega}[a_3^+ \exp(ik_3 d)] \tag{2.37}$$

$$e_y(x = -d) = a_2^+ \exp(-ik_2 d) + a_2^- \exp(-ik_2 d) = a_1^- \exp(ik_1 d) \tag{2.38}$$

$$h_z(x = -d) = \frac{-k_2}{\mu_0 \omega}[a_2^+ \exp(-ik_2 d) - a_2^- \exp(ik_2 d)] = \frac{-k_1}{\mu_0 \omega}[a_1^- \exp(ik_3 d)] \tag{2.39}$$

The surface wave definition demands the existence of scattered fields without incident waves [92]. Therefore the determinant of the associated matrix E (equation 2.40) must be equal to zero and thus formula 2.41 can be found:

$$E = \begin{bmatrix} 0 & k_2 \exp(-ik_2 d) & -k_2 \exp(ik_2 d) & k_3 \exp(ik_3 d) \\ 0 & \exp(-ik_2 d) & \exp(ik_2 d) & -\exp(ik_3 d) \\ -\exp(ik_1 d) & \exp(ik_2 d) & \exp(-ik_2 d) & 0 \\ -k_1 \exp(ik_1 d) & k_2 \exp(ik_2 d) & -k_2 \exp(-ik_2 d) & 0 \end{bmatrix} \tag{2.40}$$

$$[(k_2 - k_1)(k_3 - k_2)] \exp(i2k_2 d) + [(k_2 + k_1)(k_3 + k_2)] \exp(-i2k_2 d) = 0. \tag{2.41}$$

For TM modes instead can be written:

$$h_y(x = d) = b_2^+ \exp(ik_2 d) + b_2^- \exp(-ik_2 d) = b_3^+ \exp(ik_3 d) \tag{2.42}$$

$$e_z(x = d) = \frac{k_2}{\varepsilon_2 \varepsilon_0 \omega}[b_2^+ \exp(ik_2 d) - b_2^- \exp(-ik_2 d)] = \frac{k_3}{\varepsilon_3 \varepsilon_0 \omega}[b_3^+ \exp(ik_3 d)] \tag{2.43}$$

$$h_y(x = -d) = b_2^+ \exp(-ik_2 d) + b_2^- \exp(ik_2 d) = b_1^- \exp(ik_1 d) \tag{2.44}$$

$$e_z(x=-d)=\frac{-k_2}{\varepsilon_2\varepsilon_0\omega}[b_2^+\exp(-ik_2d)-b_2^-\exp(ik_2d)]=$$

$$\frac{-k_1}{\varepsilon_1\varepsilon_0\omega}[b_1^-\exp(ik_3d)] \tag{2.45}$$

and the null determinant of the matrix T (equation 2.46) leads to the equation 2.47.

$$T=\begin{bmatrix} 0 & \exp(-ik_2d) & \exp(ik_2d) & -\exp(ik_3d) \\ -\exp(ik_1d) & \exp(-ik_2d) & \exp(ik_2d) & 0 \\ 0 & -(\frac{k_2}{\varepsilon_2})\exp(-ik_2d) & (\frac{k_2}{\varepsilon_2})\exp(ik_2d) & -(\frac{k_3}{\varepsilon_3})\exp(ik_3d) \\ (\frac{k_1}{\varepsilon_1})\exp(ik_1d) & -(\frac{k_2}{\varepsilon_2})\exp(ik_2d) & (\frac{k_2}{\varepsilon_2})\exp(ik_2d) & 0 \end{bmatrix} \tag{2.46}$$

$$[(\frac{k_1}{\varepsilon_1}-\frac{k_2}{\varepsilon_2})(\frac{k_2}{\varepsilon_2}-\frac{k_3}{\varepsilon_3})]\exp(ik_2d)+$$

$$[(\frac{k_1}{\varepsilon_1}+\frac{k_2}{\varepsilon_2})(\frac{k_2}{\varepsilon_2}+\frac{k_3}{\varepsilon_3})]\exp(-ik_2d)=0 \tag{2.47}$$

It can be additionally observed that

$$\exp(i2k_2d)=\cos(2k_2d)+i\sin(2k_2d) \tag{2.48}$$

$$\exp(-i2k_2d)=\cos(2k_2d)-i\sin(2k_2d) \tag{2.49}$$

and the following parameters can be settled:

$$\gamma_1=-i\,k_1 \tag{2.50}$$

$$\gamma_3=-i\,k_3 \tag{2.51}$$

2.2 Surface Plasmons on Metal-Dielectric Interface

A waveguide consisting of a semi-infinite metal with a complex permittivity $\varepsilon_m=\varepsilon_m'+i\varepsilon_m''$, and a semi-infinite dielectric with permittivity $\varepsilon_d=\varepsilon_d'+i\varepsilon_d''$, where ε_i' and ε_i'' are the real and the imaginary parts of ε_i (i is m or d), see figure 2.2, can be treated as a limiting case of a three-layer waveguide (figure 2.1) with a metal substrate, a dielectric superstrate, and a waveguiding layer with a thickness equal to zero.

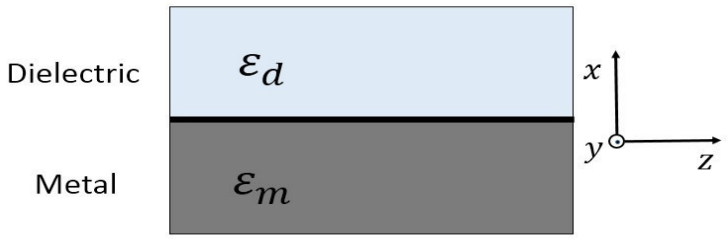

Figure 2.2 - A metal–dielectric waveguide.

The interaction of Surface Plasmon Polaritons (SPP) on a metal-dielectric interface can be modeled from equations 2.29, 2.41, 2.47, 2.48, 2.49, 2.50 and 2.51 when it is considered:

$$d = 0$$

$$k_2 = \varepsilon_2 = 0$$

$$\gamma_1 = \gamma_m$$

$$\varepsilon_1 = \varepsilon_m$$

$$\gamma_3 = \gamma_d$$

$$\varepsilon_3 = \varepsilon_d$$

For TE modes equation 2.41 becomes

$$\tan(2k_2 d_2) = \frac{\gamma_m k_2 + \gamma_d k_2}{k_2^2 - \gamma_m \gamma_d} = 0 \tag{2.52}$$

and considering equation 2.29 it leads to

$$\gamma_m = -\gamma_d \tag{1.53}$$

demonstrating that SPP cannot be bound to a metal-dielectric interface for TE modes [17, 85]. For TM modes equation 2.47 changes into

$$\tan(2k_2 d_2) = \frac{\left(\frac{\gamma_m}{\varepsilon_m}\right)\left(\frac{\varepsilon_2}{k_2}\right) + \left(\frac{\gamma_d}{\varepsilon_d}\right)\left(\frac{\varepsilon_2}{k_2}\right)}{1 - \left(\frac{\gamma_m \varepsilon_2}{\varepsilon_m k_2}\right)\left(\frac{\gamma_d \varepsilon_2}{\varepsilon_d k_2}\right)} = 0 \tag{2.54}$$

which leads to:

$$\frac{\gamma_m}{\varepsilon_m} = -\frac{\gamma_d}{\varepsilon_d} \tag{2.55}$$

and from equation 2.29 it can be found that consequently

$$\beta = \frac{\omega}{c}\sqrt{\frac{\varepsilon_d \varepsilon_m}{\varepsilon_d + \varepsilon_m}}, \tag{2.56}$$

which is the solution for a bounded-mode SPP [17, 85].

The real part of the refractive index of a media is associated to the effective refractive index while its imaginary part is related with light absorption inside the medium itself. For lossless metals and dielectrics ($\mathrm{Im}(\varepsilon_m) = \mathrm{Im}(\varepsilon_d) = 0$), equation 2.56 represents a guided mode, providing that $\mathrm{Re}\,(\varepsilon_m)$ and $\mathrm{Re}\,(\varepsilon_d)$ have a different sign and $\mathrm{Re}\,(\varepsilon_m) < -Re\,(\varepsilon_d)$. Dielectrics usually have $\mathrm{Re}\,(\varepsilon_d) > 0$ and real metals absorb the electromagnetic field, which means $\mathrm{Im}(\varepsilon_m) \neq 0$. This allows bounded SPP, in this case named evanescent modes, to exist even for $\mathrm{Re}\,(\varepsilon_m) > -Re\,(\varepsilon_d)$ if $\mathrm{Re}\,(\varepsilon_m) < 0$ and $|\mathrm{Im}\,(\varepsilon_m)| \ll |\mathrm{Re}\,(\varepsilon_m)|$. The real part of the propagation constant β is related to the SPP propagation speed while its imaginary part gives information about the SPP attenuation.

The propagation length L is the distance at which the SPP energy decreases of $1/e$, therefore it can be defined as [85]

$$\mathrm{L_{SPP}} = \frac{1}{[2\beta'']}. \tag{2.57}$$

The electromagnetic (E-M) fields have a maximum intensity at the metal-dielectric interface and decrease exponentially with the distance from the latter.

The skin depths at which the E-M fields decrease of $1/e$ are, according to [17]

$$\mathrm{l_{SPP,m}} = \frac{\lambda}{2\pi} Re\left(\frac{\sqrt{\varepsilon_m + \varepsilon_d}}{\varepsilon_m}\right) \tag{2.58}$$

into the metal and

$$\mathrm{l_{SPP,d}} = \frac{\lambda}{2\pi} Re\left(\frac{\sqrt{\varepsilon_d + \varepsilon_d}}{\varepsilon_m}\right) \tag{2.59}$$

into the dielectric.

2.3 Surface Plasmons on Dielectric-Metal-Dielectric

A Dielectric-Metal-Dielectric Waveguide is composed of a metal film sandwiched between two semi-infinite dielectric media (figure 2.3). This kind of structure supports two TM modes that is two surface plasmons at the opposite boundaries of the metal film, when the metal film is much thicker than the penetration depth of a Surface Plasmon at each metal-dielectric interface. When the metal thickness decreases, coupling between the two surface plasmons occurs, giving rise to mixed modes of electromagnetic field [85].

Taking into consideration a symmetric waveguide, that is a dielectric-metal-dielectric interface where the two dielectric media are equal and regarding equations 2.29, 2.48, 2.49, 2.50 and 2.51 when

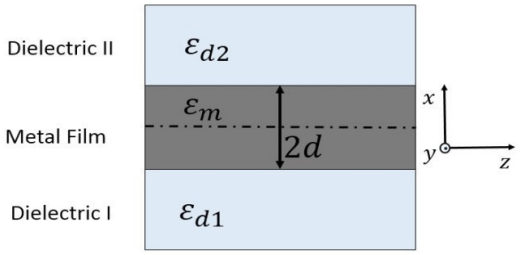

Figure 2.3 - Thin metal layer sandwiched between two dielectrics.

$$\varepsilon_1 = \varepsilon_3 = \varepsilon_d \tag{2.60}$$

$$\gamma_1 = \gamma_3 = \gamma_d \tag{2.61}$$

$$\varepsilon_2 = \varepsilon_m \tag{2.62}$$

$$k_2 = k_m \tag{2.63}$$

the solutions for TE modes from equation 2.41 is:

$$\tan(k_m d) = \frac{\gamma_d}{k_m} \text{ and} \tag{2.64}$$

$$\cot(k_m d) = \frac{-\gamma_d}{k_m} \tag{2.65}$$

while for TM modes equation 2.47 gives[17]:

$$\tan(k_m d) = \frac{\varepsilon_m \gamma_d}{\varepsilon_d k_m} \text{ and} \tag{2.66}$$

$$\tan(k_m d) = \frac{-\varepsilon_m k_d}{\varepsilon_d \gamma_d} \tag{2.67}$$

For a generic asymmetric waveguide the SPP modes are associated with the characteristic equation

$$tan(2k_m d) = \frac{\left(\frac{\gamma_1}{k_2}\right) + \left(\frac{\gamma_3}{k_2}\right)}{1 - \left(\frac{\gamma_1}{k_2}\right)\left(\frac{\gamma_3}{k_2}\right)} \tag{2.68}$$

for the TE modes and

$$\tan(2k_m d) = \frac{\left(\frac{\varepsilon_2 \gamma_1}{\varepsilon_1 k_2}\right) + \left(\frac{\varepsilon_2 \gamma_3}{\varepsilon_3 k_2}\right)}{1 - \left(\frac{\varepsilon_2 \gamma_1}{\varepsilon_1 k_2}\right)\left(\frac{\varepsilon_2 \gamma_3}{\varepsilon_3 k_2}\right)} \tag{2.69}$$

for TM modes [17, 85].

2.4 Excitation of Surface Plasmons

There are several configurations to induce surface plasmon resonances. In figure 2.4 some possible configurations are presented. In all of them the applied principle is the same: when the effective index of the light and the surface plasmon match, there is coupling between both fields, losses are induced, and heat dissipation occurs.

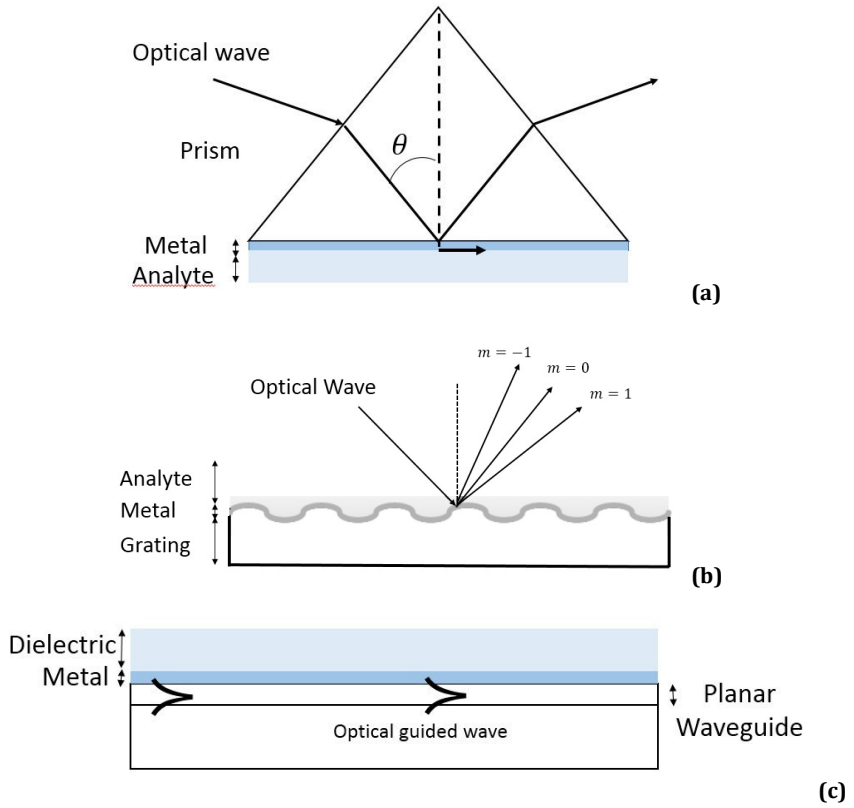

Figure 2.4 – Different SPR configurations (a) prism coupling (Kretschmann configuration).

(b) Grating coupling. (c) Waveguide coupling.

2.4.1 Kretschmann and Otto configurations

The prism coupler in the Kretschmann and Otto configurations employs the attenuated total reflection (ATR) method, where an incident beam (p-polarized light) propagates through a prism. The incident photon totally reflects at the prism base, and its evanescent field reaches the metal-dielectric interface, where the surface plasmon may be excited between the metal and the external medium. Excitation occurs when the component of the wavevector of the incident light parallel to the interface is equal to the surface plasmon wavevector, k_x, given by

$$k_x = \sqrt{\varepsilon_d}\frac{\omega}{c}\sin\theta = n_d k_0 \sin\theta \tag{2.70}$$

where $n_d = \sqrt{\varepsilon_d}$ is the dielectric refractive index, θ is the angle of incidence and $k_0 = \omega/c$ is the wavenumber of the incident light. Surface plasmons on the external medium/metal interface can be excited when the dispersion relation is fulfilled:

$$k_x = n_d k_0 \sin\theta = k_0\sqrt{\frac{\varepsilon_m \varepsilon_d}{\varepsilon_m + \varepsilon_d}} = k_{SP} \tag{2.71}$$

In the particular case of excitation of surface plasmons on the air/metal interface, the dispersion relation is given by

$$k_{SP} = k_0\sqrt{\frac{\varepsilon_m}{\varepsilon_m + 1}} \tag{2.72}$$

where ε_d and ε_m are the dielectric constants of the dielectric medium and metal, respectively. The corresponding wave vector diagram is shown in figure 2.5. This excitation reveals itself as a loss in the intensity of the light reflected out of the prism, and is achieved by varying θ until a minimum is observed in the intensity of the reflected light.

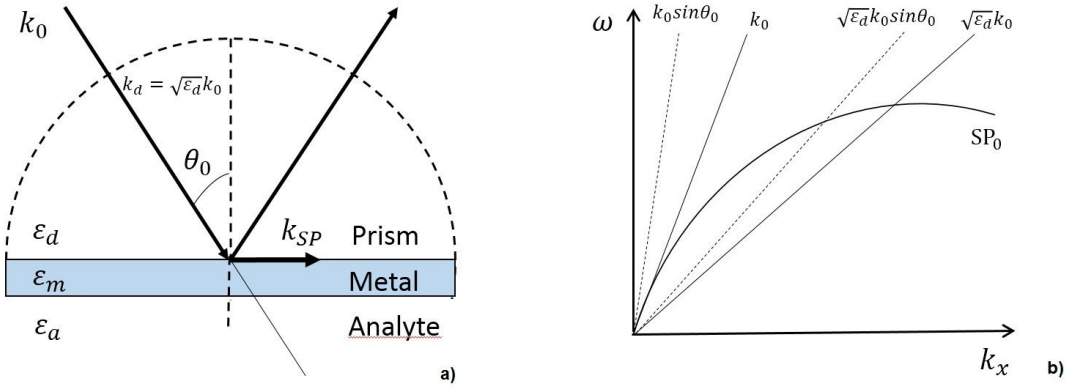

Figure 2.5 – (a) Reflection of light at the metal surface ($\varepsilon_m(\omega)$). The medium above the metal is a dielectric Material (ε_d) as a glass or silica; below the metal is the analyte, that can be air, vacuum or an aqueous medium (ε_a). (b) Dispersion diagram of the attenuated total reflection method (SP_0: Dispersion of surface plasmon at metal/air interface).

Mathematically, the phase matching condition is expressed as an equality between the plasmon vector and a projection of the wavevector of an incident wave along the interface. Since the plasmon excitation condition depends resonantly on the value of the refractive index of the external medium within 100-300 nm from the interface, this method is widely used for detection, with high sensitivity, of biological binding events over the metal surface.

This excitation is known as the attenuated total reflection (ATR) intensity. Two different ATR configurations have been used to excite surface plasmons: Otto configuration, and Kretschmann-Raether configuration.

The Otto configuration [93] is depicted in figure 2.6 (a), where the dielectric prism (ε_d) is separated from a half metal surface (ε_m) by an air or dielectric slit (ε_a) at a distance d, which is in the order of $\lambda_0/\sqrt{\varepsilon_d}$. When the light is reflected at the boundary of the prism, the evanescent field can couple to the surface plasmon on the interface of air and metal.

Besides the Otto-configuration, the Kretschmann-Raether configuration [14] is commonly used to excite surface plasmons on thin metal films. As shown in figure 2.6 (b), the metallic layer ε_m, with a thickness of several tens of nanometers, is in contact with the prism ε_d. The electromagnetic field decays exponentially inside the film and excites the surface plasmon on the interface of the metal and air.

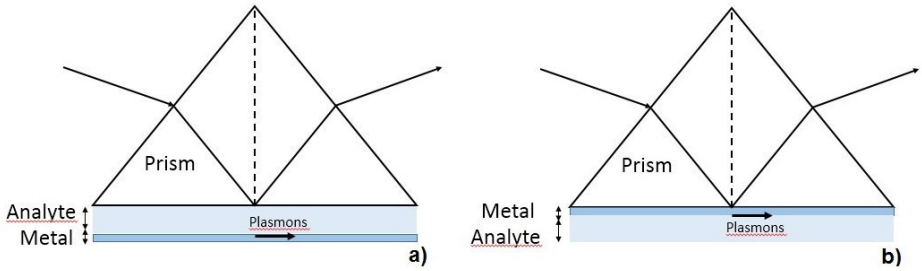

Figure 2.6 - (a) Otto configuration. The analyte (dielectric or air) lies between the prism and the metal surface. (b) Kretschmann-Raether configuration. The metal film is in contact with the prism.

It is worthwhile to mention that surface plasmons can be excited via a rough surface (corrugated surface, grating, etc.), and the strong electromagnetic field is built up at the surface [17]. The reverse process also can take place: surface plasmons propagating along the metal-dielectric interface can be transformed into light beams via the roughness of the surface, so that the surface plasmon field becomes radiative and a strong light emission results. These processes are significant in experiments and have been applied for enhanced light emission from rough or sinusoidal surfaces, photoemission enhanced by surface plasmons, strong Raman scattering, or generation of second harmonics in the strong surface plasmon field.

Otto and Kretchman configurations are the most widely used configurations. Usually, the bulk surface plasmon devices based on prisms have great flexibility and high signal-to-noise ratio, which allow high resolution measurements. These configurations have been applied for surface analysis and biological sensing as, for example, changes in the refractive index of a bulk analyte or test molecules. The evanescent field will affect the coupling conditions required for the excitation

of the surface plasmons at a specific wavelength. In order to compensate for this change in the coupling conditions, the angle θ has to be varied until maximum attenuation is obtained for the reflected light. When the Kretschmann-Raether configuration is applied for surface analysis, the change in θ or shift in the position of the resonance minimum is related to the observed change at the surface of the metal. Improvements to the architecture of the device, with the introduction of multichannel sensing capabilities and dual channel sensor with wavelength interrogation, permitted the demonstration of sixteen channel sensor with intensity measurement involving a CCD camera [94, 95].

2.4.2 Grating Coupling

Coupling by a diffraction grating [17] is achieved when light is coupled into the waveguide, and then is transmitted along the waveguide onto the grating. When the light ($k_0 = \omega/c$) hits a grating with a grating period Λ at an incidence angle θ, its component on the surface can have wave vectors $k_0 \sin\theta \pm mG$, where m is an integer and $G = 2\pi/\Lambda$. Surface plasmons will be excited when the following condition is accomplished:

$$k_x = k_0 \sin\theta \pm mG = k_0 \sqrt{\frac{\varepsilon_m \varepsilon_d}{\varepsilon_m + \varepsilon_d}} = k_{SP}. \tag{2.73}$$

Figure 2.7 shows a grating coupler scheme and its k-vector diagram. The incoming wave, with $k_0 \sin\theta$, is transformed into surface plasmons by addition of $\Delta k = G$. The resonance is observed as a minimum in the reflection of the light. Equation 2.73 shows that changes in the propagation constant in response to changes in the refractive index at the grating will cause a change in the output coupling angle θ. The observed shift in the output coupling angle θ is related to the changes occurring at the grating surface.

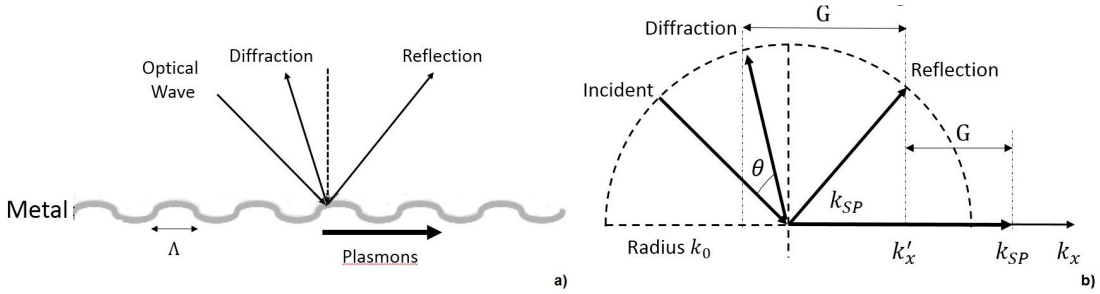

Figure 2.7 - (a) The grating coupler used to excite surface plasmons. (b) Wave vector diagram of the input coupler. k_0 is the wave vector of the incident light (k_{SP} is the wave vector of the surface plasmons and $G = 2\pi/\Lambda$, where Λ is the grating period).

2.4.3 Waveguide Coupling

In the case of waveguide coupling, the phenomenon is similar to what happens in the prism configurations (Otto and Kretschmann-Raether configurations). However, the former configuration has several advantages when compared with the ATR configurations, such as higher simplicity, small size and the sensor interaction strength, offering additionally the same high resolution measurements that the ATR approach can reach.

The light propagates along the waveguide with a transverse magnetic polarization. This transverse magnetic mode has its principal component of the magnetic field parallel to the substrate and the waveguide surface, and normal to the propagation direction, while the principal component of the electric field is normal to the substrate surface [96]. Coupling of light to the metal surface results in the generation of a plasmon, with an associated electromagnetic field that extends about 100-300nm above and below the metal surface, as shown in figure 2.8.

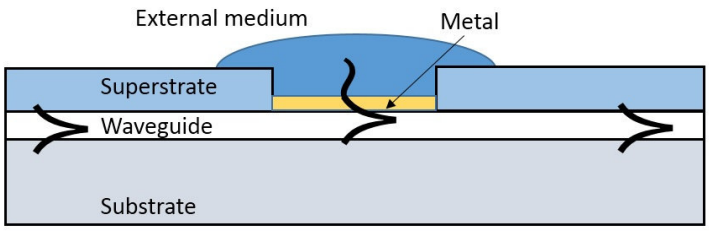

Figure 2.8 - Side view of an integrated waveguide device with SPR excitation.

Excitation is shown by a loss in the intensity of the light coupled out of the waveguide substrate when compared to that initially launched into the waveguide. This loss is a direct result of the radiative nature of the surface plasmon. The refractive index of the materials above and below of the metal (substrate and superstrate region) affect the amount of intensity coupling of the plasmon. Small variations in the refractive index of the external medium (superstrate region) result in large changes in the attenuation of the waveguide mode that can be seen in the transmitted signal.

The SPR sensors based on integrated optics is one of the most promising approaches to develop multiplexed integrated sensors in a single chip, able to simultaneously measure different samples. The use of optical fibers presents the highest level of miniaturization of surface plasmon resonance sensors based on the waveguide design, and allows operation free from mechanical misalignment problems that are often present in bulk configurations. The SPR sensors analysed in this work are built in optical fiber, so the next section is dedicated to a general analysis of surface plasmon resonance in optical fiber sensors.

2.5 Theoretical Study of Optical Fiber based Surface Plasmon Resonance Sensors

All the simulations in this work were inspired on the model similar to the one described by Esteban [97]. The numerical model was established from Fresnel's equations, where the analyte/metallic layer interface was modeled by a multilayer system.

In this model the core of the fiber is replaced by an equivalent planar layer with the same thickness as the original core, as shown in figure 2.9. The optical fiber is replaced by a system of five layers: the first one (layer 1) corresponds to the core of optical fiber with refractive index n_{co} ($n_{co}^2 = \varepsilon_{co}$); the second layer (layer 2) is the clad of optical fiber; the third one (layer 3) is a metallic layer characterized by a dielectric constant function given by ε_m; the layer 4 represents a dielectric layer used to tune the plasmonic resonance; and a last layer (layer 5) is the external medium (analyte) with a dielectric constant ε_a, as shown in figure 2.9. The evanescent field that seeps into the cladding is similar to the one produced by the core of a single mode fiber, under the same conditions. The simulation assumes the transfer matrix formalism [98], which is based on the calculation of light propagation through a multilayer medium consisting of (N-1) isotropic and homogeneous layers.

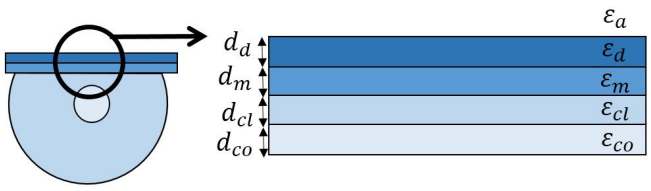

Figure 2.9 - Equivalent planar model of an optical fiber based plasmonic structure.

2.5.1 Reflection Coefficient

This electromagnetic analysis of light reflection on a multilayer system relies on solving the Maxwell's equations subjected to boundary conditions. A schematic illustration of the system is presented in figure 2.10. The amplitude of the E (electric field) and H (magnetic field) vectors in the first (E_0 and H_0) and last (E_N and H_N) layers are related by:

$$\begin{bmatrix} E_0 \\ H_0 \end{bmatrix} = [M] \times \begin{bmatrix} E_N \\ H_N \end{bmatrix}, \tag{2.74}$$

where the transfer matrix M is

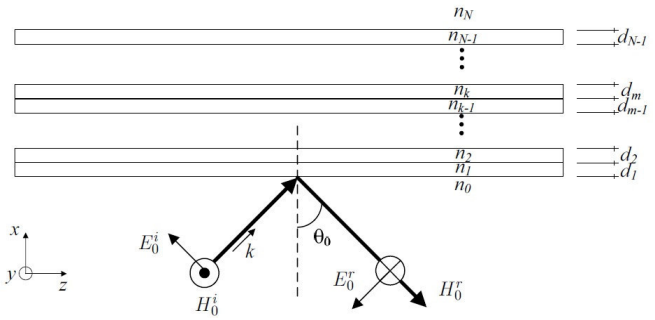

Figure 2.10 - Electric and magnetic field vectors of p-wave at the inner surface of the multilayered system.

$$[M] = \begin{bmatrix} M_{11} & M_{12} \\ M_{21} & M_{22} \end{bmatrix} = \prod_{k=1}^{N-1} \left(\begin{bmatrix} \cos\delta_k & \frac{-i\sin\delta_k}{\eta_k} \\ -i\eta_k \sin\delta_k & \cos\delta_k \end{bmatrix} \right), \tag{2.75}$$

where δ_k is the phase in the k^{th} layer, given by

$$\delta_k = \frac{2\pi}{\lambda} n_k \cos\theta_k \times (x_k - x_{k-1}) = \frac{2\pi d_k}{\lambda} (\varepsilon_k - n_0^2 \sin^2\theta_0)^{1/2}, \tag{2.76}$$

where n_k is the refractive index of the k^{th} layer, d_k is the thickness of the k_{th} layer along the x-axis, the incidence angle is θ_0, and λ is the wavelength of the light propagating into the system. The parameter η_k is the optical admittance, and is defined as a function of the polarization state as

$$\eta_k^s = \left(\frac{\varepsilon_k}{\mu_k}\right)^{1/2} \cos\theta_0 = (\varepsilon_k - n_0^2 \sin^2\theta_0)^{1/2} \quad \text{for s} - \text{wave (TE)} \tag{2.77}$$

and

$$\eta_k^p = \left(\frac{\varepsilon_k}{\mu_k}\right)^{1/2} \times \frac{1}{\cos\theta_0} = \frac{\varepsilon_k}{\eta_k^s} \quad \text{for p} - \text{wave (TM)} \tag{2.78}$$

Finally, the reflectance R of the whole multilayer structure is provided from the Fresnel reflection coefficients r_s and r_p:

$$R_s = |r_s|^2 = \left| \frac{(M_{11}^s + M_{12}^s \cdot \eta_N^s)\eta_0^s - (M_{21}^s + M_{22}^s \cdot \eta_N^s)}{(M_{11}^s + M_{12}^s \cdot \eta_N^s)\eta_0^s + (M_{21}^s + M_{22}^s \cdot \eta_N^s)} \right|^2 \tag{2.79}$$

$$R_p = |r_p|^2 = \left| \frac{(M_{11}^p + M_{12}^p \cdot \eta_N^p)\eta_0^p - (M_{21}^p + M_{22}^p \cdot \eta_N^p)}{(M_{11}^p + M_{12}^p \cdot \eta_N^p)\eta_0^p + (M_{21}^p + M_{22}^p \cdot \eta_N^p)} \right|^2. \tag{2.80}$$

The simulation of these equations has been widely used in the literature [99, 100]. In order to get a sensor in the expected range several simulations were made, always based on the Fresnel formalism assuming a planar equivalent geometry to the etched optical fiber or to the tapered optical fiber.

To find the refractive indices of the layers involved in the simulation, different models were taken into account, depending on the nature of the layer. The dielectric function, ε_m, corresponding to the metal film was obtained following the Drude Model [101]. The frequency-dependent optical properties of gold in the visible/near-UV range can be represented by the contribution of this model. According to the modified Drude model, the real and imaginary parts of the metal nanoparticle dielectric functions are given by expressions 2.81 and 2.82 [101],

$$\varepsilon'_m(\lambda) = 1 - \frac{\lambda^2\lambda_c^2}{\lambda_p^2(\lambda^2+\lambda_c^2)} \tag{2.81}$$

$$\varepsilon''_m(\lambda) = \frac{\lambda^2\lambda_c^2}{\lambda_p^2(\lambda^2+\lambda_c^2)}, \tag{2.82}$$

where λ_p and λ_c denote the size dependent plasma and collision wavelengths of the nanoparticle, respectively.

The core and silica dielectric functions were calculated with the Sellmeier [102] equation 2.83,

$$\varepsilon_d(\lambda) = n_d^2(\lambda) = 1 + \frac{B_1\lambda^2}{\lambda^2 - C_1} + \frac{B_2\lambda^2}{\lambda^2 - C_2} + \frac{B_3\lambda^2}{\lambda^2 - C_3}, \tag{2.83}$$

where λ is the radiation wavelength, and $B_{1,2,3}$ and $C_{1,2,3}$ are experimentally determined Sellmeier coefficients.

2.5.2 Transmitted Power

Considering that all the guided rays are launched in the fiber using a collimated source and a microscope objective, the angular power distribution of rays guided in the fiber is given as [103]

$$dP \propto \frac{n_1^2 \sin\theta \cos\theta}{(1 - n_1^2 \cos^2\theta)^2} d\theta, \tag{2.84}$$

where θ is the angle of the ray with the normal to the core-cladding interface and n_1 is the refractive index of the core of the fiber. To calculate the effective transmitted power, the reflectance (R_p) for a single reflection is raised to the power of the number of reflections the specific propagating angle undergoes with the sensor interface. Hence, for *p*-polarized light, the generalized expression for the normalized transmitted power in an optical fiber based SPR sensor will be given as

$$p_{trans} = \frac{\int_{\theta_{cr}}^{\pi/2} R_p^{N_{ref(\theta)}} [n_1^2 \sin\theta \cos\theta/(1 - n_1^2 \cos^2\theta)^2]\, d\theta}{\int_{\theta_{cr}}^{\pi/2} [n_1^2 \sin\theta \cos\theta/(1 - n_1^2 \cos^2\theta)^2]\, d\theta} \tag{2.85}$$

where

$$N_{ref}(\theta) = \frac{L}{D \tan \theta} \tag{2.86}$$

and

$$\theta_{cr} = \sin^{-1}\left(\frac{n_{cl}}{n_1}\right) \tag{2.87}$$

Here, $N_{ref}(\theta)$ is the total number of reflections performed by a ray making an angle θ with the normal to the core–metal layer interface in the sensing region. L and D are the length of the exposed sensing region and the fiber core diameter respectively, and θ_{cr} is the critical angle of the fiber and n_{cl} is the refractive index of the cladding of the fiber.

2.5.3 Sensitivity and Quality parameter

Resonance wavelength (λ_{res}) is determined corresponding to the refractive index of the sensing medium (n_s) in the SPR sensor based on spectral interrogation. If the refractive index of the sensing medium is altered by δn_s, the resonance wavelength shifts by $\delta\lambda_{res}$. The sensitivity (S_n) of a SPR sensor with spectral interrogation is defined as [100]

$$S_n = \frac{\delta\lambda_{res}}{\delta n_s} \tag{2.88}$$

A quantity that takes into account the sensitivity and the detection accuracy of the sensor is identified as the of the Γ_λ-parameter SPR sensor, which is inversely proportional to the width of the SPR response curve. If $\delta\lambda_{0.5}$ is the spectral width of the SPR response curve corresponding to 50% reflectivity, this parameter is defined as

$$\Gamma_\lambda = \frac{\delta\lambda_{res}}{\delta\lambda_{0.5}} \tag{2.89}$$

To denote the overall performance of the sensor, a quality parameter is introduced. If $\delta\lambda_{0.5}$ is the spectral width of the SPR response curve corresponding to 50% reflectivity (full-width at half- maximum of the SPR dip), the quality parameter (χ) is defined as [104]

$$\chi = \frac{S_n}{\delta\lambda_{0.5}}. \tag{2.90}$$

2.6 Optical Sensing based in Optical Fibers Coupled to SPR Phenomenum

The importance of surface plasmon resonance fiber optic sensors in the field of chemical, biological and environmental sensing has notably increased in the last years. Consequently, many

different configurations and analytes have been studied in the literature [59]. However, the demanding requirements of SPR systems impose the necessity of improving the performance beyond that of the bulk configurations in order to fully exploit the advantages of optical fibers.

The optical fiber can be an almost ideal platform for surface plasmon resonance, for chemical and biological sensors, where some measurements have to be made in hazard or difficult to access places. Optical fiber configurations already demonstrated advantages when compared with other surface plasmon resonance configurations due to their mechanical flexibility, and the possibility to transmit optical signals at remote distances.

In an optical fiber the polarization can be TE or TM, although only the TM polarization will excite the plasmon. The excitation in an optical fiber is not based on the incidence angle of the light, as in the Otto or Kretschmann-Raether configurations, but by modulation of the intensity or wavelength of the resonance, i.e., the output signal can be processed taking into account the total power transmitted through the device, as it is usual with D-type fiber based sensors, or by analysing the spectral properties of the transmitted signal. To excite efficiently a surface plasmon, the phase matching condition between a plasmon and a waveguide mode has to be satisfied, which mathematically amounts to the equality of their modal propagation constants ($k_{SP} = k_{waveguide}$, which corresponds to the equality of their effective refractive indices). In optical fiber SPR configurations, there is always the need to get near the core in order to allow the electromagnetic radiation to seep into the metallic layers and external medium. So, the cladding of the optical fiber must somehow be reduced, to let the evanescent field interact with the external layers [5].

Several configurations have been made to improve the performance of fiber optic SPR sensors [105]. Some of the most important layouts are related with tapered and tip optrode optical fiber geometries, coupled to the consideration of different metallic elements. These structures were studied looking for the maximization of their sensing characteristics, as reported after chapter 3 which is devoted to an outline of interrogation techniques oriented to SPR-based optical fiber sensors.

3

Interrogation of Plasmonics Sensing Structures

Summary: *This chapter presents a worked review of the different techniques to interrogate plasmonic based sensors, addressing in particular the performance level that can be achieved with each of the interrogation approaches. These include angular interrogation, spectral interrogation, intensity interrogation and phase interrogation.*

3.1 Introduction

The interaction of light wave with surface electrons in metals generating a plasmonic wave can change the characteristics of the light in terms of amplitude, spectral distribution, phase, and polarization. Any change in the wave vector of surface plasmon will change any of these characteristics. Change in the dielectric constant or the refractive index of the dielectric medium resulting in the change in wave vector of the surface plasmon can be determined by knowing the changes in one of these properties. This is the principle of surface plasmon resonance (SPR)-based sensors. On the basis of change in light characteristics, the measurement techniques can be classified as angular, wavelength, intensity, and phase with their associated interrogations approaches. Historically, angular interrogation was the first to be widely considered, but later the others are becoming increasingly appellative, in particular the spectral (wavelength approach) and phase reading when extremely high sensitivities are on demand.

This chapter reviews different techniques to perform interrogation of SPR-based sensors along the indicated modulation mechanisms but, in advance, it can already be stated two favourable characteristics for this type of sensing systems, namely: i) to be supported by optical waveguide platforms, either fiber optics or planar integrated optics layouts with input/output fibers; ii) interrogation in the spectral domain to benefit from wavelength encoded operation. As detailed later, this can be done directly by monitoring the deep of the SPR loss band, which requires a spectral analyzer or a tunable laser to scan a wavelength range that contains the extreme of the SPR signature. An indirect approach relies on reading the optical power that propagates through the sensor in two wavelengths, one in each side of the loss band. This can be achieved using two lasers, or by illuminating the sensor with broadband light and the spectral interrogation lines be defined by two FBGs [106]. Previous calibration permits to obtain from these two readings a parameter only dependent on the spectral position of the SPR loss band and highly sensitive to its displacement.

The resolution of a SPR sensing head depends not only on its intrinsic sensitivity to the measurand but also on the performance of the interrogation technique considered. To benefit from the wavelength encoded characteristics of these sensors the interrogation approach above briefly outlined or variants shall be adopted. As also indicated, when better resolutions are on demand this approach can be complemented by the consideration of an additional interrogation technique which shows better performance. Eventually, the most favorable one would be phase reading, associated with the fact light that propagates through the sensor at two different locations of the SPR spectral loss band will experience different phase delays. Therefore, phase interrogation can be achieved by illuminating the sensor with a laser line with emission in the region of the SPR loss band where is maximum the slope of phase variation with the measurand induced band spectral

shift. Considering SPR can only exist for TM polarization, the TE wave will accumulate a SPR immune phase delay when propagates through the sensor structure, therefore providing a reference to the sensing effective TM wave.

In the following sections, each of the main interrogation techniques that have been reported in the literature to recover the information from plasmonic based optical sensors will be described and, for that, was considered instructive to refer to the original research published by the pioneers of these techniques.

3.2 Angular Interrogation

3.2.1 General Considerations and Historical Background

In the attenuated total reflection (ATR) configuration, a transverse magnetic TM polarization light passes through a prism and reflects at the metal/dielectric interface above the critical angle, exciting a Surface Plasma Wave (SPW). At certain angles and wavelengths, the energy associated with the incident radiation will couple with the SPW. The loss of this energy is observed as a dip in the reflectivity spectrum. The interaction between the analyte and the recognition element produces a change in the refractive index, which manifests itself as a shift in the SPR dip. Therefore precise and accurate determination of the minimum in the spectrum is essential in detection of the analyte. For the case of angular interrogation, the information about the measurand variations is obtained from the shift in the prism incident angle required to maintain the resonance condition.

In 1983s, Biedberg and co-workers at Linkoping University (Sweden) reported the first SPR sensor based on angular interrogation [27]. This sensor can be used in gas detection and was based on prism configuration. In the early 1990s, an angular modulation based SPR sensor consisting of a light-emitting diode (LED) and a detector array with imaging optics was introduced [107]. As shown in figure 3.1, a divergent beam produced by the LED was collimated and focused by means of a cylindrical lens to produce a wedge-shaped beam of light, which was used to illuminate a thin gold film on the back of a glass prism containing several sensing areas (channels). The imaging optics consisted of one imaging and one cylindrical lens ordered in such a way that the angular spectrum of each sensor channel was projected on separate rows of the array detector [108]. This design has been adopted by Biacore and resulted in a family of commercial SPR sensors

with high performance (resolution down to 1 × 10^{-7} RIU) and multiple sensing channels (up to four).

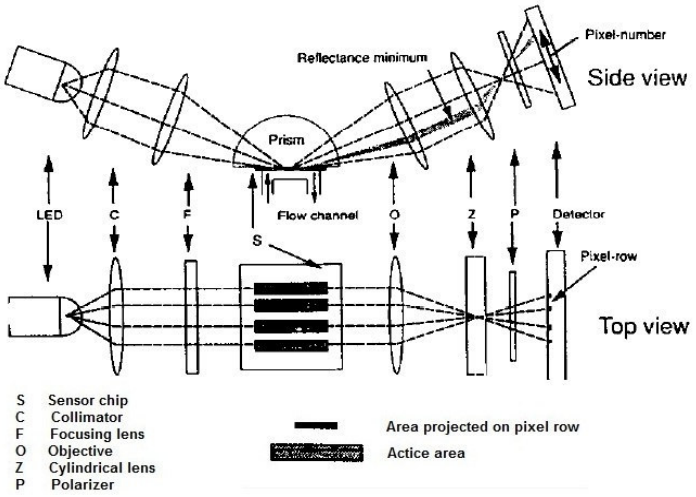

Figure 3.1 - The configuration of SPR sensor based on angular modulation [107].

In 2004, Thirstrup et al. integrated several optical elements into a single sensor chip [109]. In this approach, the cylindrical focusing optics utilized to create a beam of a desired angular span was replaced by a diffraction grating of a special design incorporated into the sensing element [110, 111]. A wide parallel light beam was diffracted by the focusing grating and focused into a small spot on the SPR measuring surface. The reflected light followed a similar path, producing a parallel beam with an angular spectrum superimposed across the beam. A two dimensional photodetector was used to measure the angular spectrum of the reflected light for several parallel channels. This design offered a compact SPR platform with a resolution of about 5 × 10^{-7} RIU [111]. In 2006, Hong et al. presented self-constructed angular interrogation based SPR sensor that can be used as an immunosensor enough to analyse the antigen–antibody interaction [112]. An angular interrogation-based SPR sensor was constructed with the Kretschmann–Raether geometry of the attenuated total reflection method, as shown in figure 3.2(a), the light source used was a laser diode with a fixed wavelength of 635 nm and a bandwidth of ≈5 nm. A polarizer was positioned in front of the incident light to obtain the transverse magnetic polarized light. This procedure preceded the making of a wedge-shaped beam of light by way of a planocylindrical glass lens. The light passing through the planocylindrical glass lens was focused onto the fused silica prism combined with a protein chip. The reflected wedge-shaped beam of light from the protein chip was projected onto a one-dimensional CCD detector. The range of the measurable angle in this configuration was approximately 6°. Figure 3.2(b) shows SPR spectra for different thicknesses of Au films on the glass substrates as a function of the incidence angle. The detection limit of the minimal refractive index variation was calculated to be 1.4 × 10^{-4} RIU.

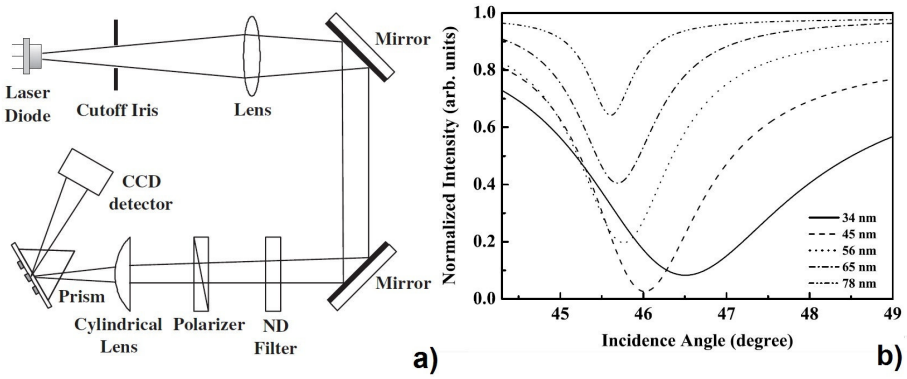

Figure 3.2 - (a) Schematic diagram of the wedge-shaped beam type angular interrogation-based SPR sensor. (b) SPR spectra obtained from the various thicknesses of Au films on the glass substrates as a function of the incidence angle [112].

3.2.2 Principle of the Technique

For a prism of fixed refractive index and fixed wavelength of the light source, the resonance condition is satisfied at a particular angle of incidence called resonance angle (θ_{res}). At resonance, the transfer of energy of incident light to surface plasmons takes place resulting in the reduction in the intensity of the reflected light. In a sensing device based on the prism and angular interrogation method, the intensity of the reflected light is measured as a function of angle of incidence θ for fixed values of frequency, metal layer thickness, and dielectric constant of the sensing medium. At resonance angle, a sharp dip is observed due to an efficient transfer of energy to surface plasmons as shown in figure 3.3.

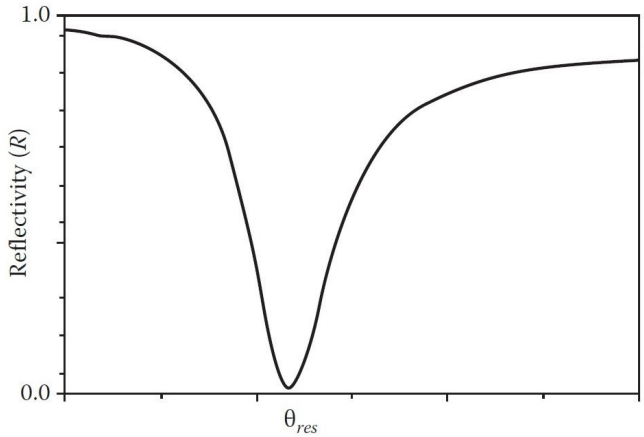

Figure 3.3 - A typical SPR curve in angular interrogation. At certain angles and wavelengths, the energy associated with the incident radiation will couple with the SPW. The loss of this energy is observed as a dip in the reflectivity.

The plot can also be obtained with the help of Fresnel's equations for the three-layer system. For a given frequency of the light source and the dielectric constant of the metal film, one can determine the dielectric constant (ε_d) of the dielectric medium by using resonance condition (Equation 2.71), if the value of the resonance angle (θ_{res}) determined experimentally is substituted. The resonance angle is very sensitive to the variation in the refractive index of the dielectric medium. If the refractive index of the dielectric medium is changed, the resonance angle will change accordingly. A graph between the resonance angle and the refractive index of the dielectric medium serves as the calibration curve of the sensor. Any increase in the refractive index of the dielectric medium increases the resonance angle.

3.2.3 Performance of the Technique

Sensitivity of an SPR sensor based on angular interrogation depends on how much the resonance angle shifts with a change in the refractive index of the sensing layer. If the shift is large, the sensitivity is large. Figure 3.4 shows a plot of reflectance as a function of angle of incidence of the light beam for sensing layer with refractive indices n_d and $n_d + \delta n_d$. Increase in the refractive index by δn_d shifts the resonance curve by $\delta\theta_{res}$ angle. The sensitivity of an SPR sensor with angular interrogation is defined as [113]

$$S_n = \frac{\delta\theta_{res}}{\delta n_d} \tag{3.1}$$

The detection accuracy of an SPR sensor depends on how accurately and precisely the sensor can detect the resonance angle and hence the refractive index of the sensing layer.

Apart from the resolution of the angle-measuring device, the accuracy of the detection of resonance angle depends on the width of the SPR curve. The narrower the SPR curve, the higher is the detection accuracy. Therefore, if $\delta\theta_{0.5}$ is the angular width of the SPR response curve corresponding to 50% reflectance, the detection accuracy of the sensor can be assumed to be inversely proportional to $\delta\theta_{0.5}$. A quantity that takes into account the sensitivity and the detection accuracy of the sensor is identified as the Γ_θ-parameter SPR sensor defined as [113]

$$\Gamma_\theta = \frac{\delta\theta_{res}}{\delta\theta_{0.5}}. \tag{3.2}$$

It has been shown that modern SPR sensing systems based on the angular interrogation are capable of an angular sensitivity of 140 degrees/RIU and a resolution of 5×10^{-7} RIU [111].

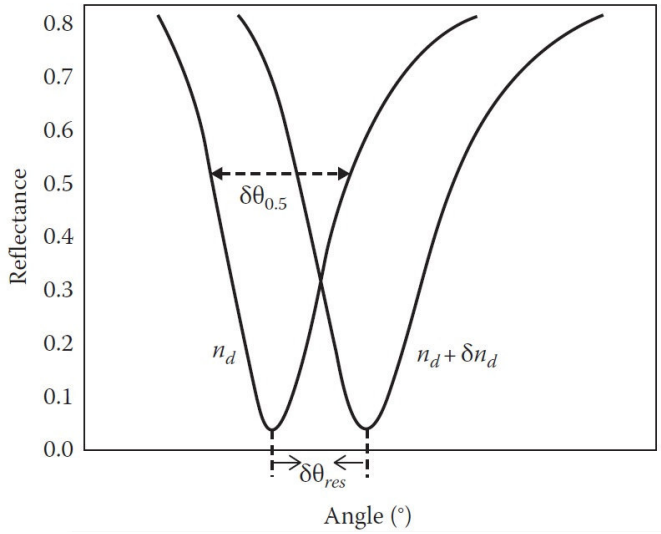

Figure 3.4 - SPR curves for different refractive indices of the sensing medium in the cases of angular interrogation.

3.3 Wavelength Interrogation

3.3.1 General Considerations and Historical Background

In SPR sensors with wavelength modulation, a surface plasmon is excited by a collimated light wave containing multiple wavelengths, typically a beam of polychromatic light. The excitation of surface plasmons is observed as a dip in the wavelength spectrum of reflected light. The wavelength yielding the strongest coupling is measured and used as a sensor output.

An SPR sensor with wavelength modulation and parallel channel architecture was reported in 2002 by Homola's group [114]. In this sensor, which is shown in figure 3.5, a polychromatic light from a halogen lamp was collimated into a large-diameter parallel beam, which was launched in a prism coupler. The light reflected from different sensing channels was collected by different output collimators coupled and transmitted to different inputs of a spectrograph. The SPR sensor of this design was demonstrated to be able to resolve refractive index changes down to 2×10^{-7} RIU [115].

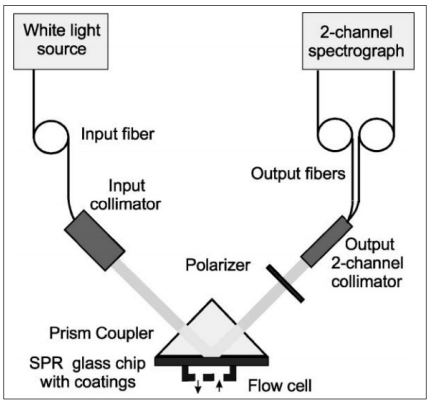

Figure 3.5 - Dual-channel surface plasmon resonance sensor based on wavelength interrogation [114].

An SPR sensor with wavelength division multiplexing (WDM) of sensing channels was proposed by Homola et al. [94]. In this approach, signals from multiple surface plasmons excited in different areas of a sensing surface are encoded into different regions of the spectrum of the light wave. Two configurations of WDM-SPR sensors have been developed [116, 117]. In the first configuration, a wide parallel beam of polychromatic light is made incident onto a sensing surface consisting of a thin gold film, a part of which is coated with a thin dielectric film. As the presence of the thin dielectric film shifts the coupling wavelength to a longer wavelength (compared to the bare gold), the reflected light exhibits two dips associated with the excitation of surface plasmons in the area with and without the overlayer [116]. The second configuration of WDM-SPR sensor employs a special prism coupler in which a polychromatic light is sequentially incident on different areas of the sensing surface at different angles of incidence. Due to the different angles of incidence, the surface plasmons in different regions are excited with different wavelengths of the incident light [117]. Therefore, the spectrum of transmitted light contains multiple dips associated with surface plasmons in different areas of the sensing surface. The WDM-SPR approach was combined with the parallel architecture, yielding an eight-channel SPR sensor with a resolution around 1×10^{-6} RIU [117].

SPR optical fiber sensors also attracted considerable attentions due to their advantages. In 1993, Jorgenson et al. [118] designed an SPR fiber-optic sensor based on wavelength interrogation (figure 3.6). They used a multi-mode fiber optic as the optical coupling element, and presented two configurations.

In one of them (*in-line transmission-based SPR sensor*) it is used the wavelength-interrogation technique and installed an SPR sensor by using a conventional polymer-clad silica fiber with partly removed cladding and an active SPR metal layer deposited symmetrically around the exposed section of the fiber core. A common silica step index fiber optic has a numerical aperture of 0.3. The fiber supports internal propagation of light at an angle of 78.5–90° with respect to the normal

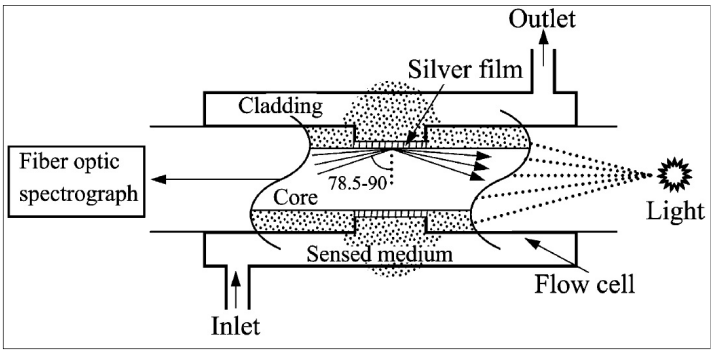

Figure 3.6 - Illustration of the SPR fiber optic sensing element reported by Jorgenson et al. [118].

of the core/cladding interface. Within this incident angle range, the SPR coupling wavelength for water is predicted to be 560–620 nm. The white light is used as source of a range of optical wavelengths guided into the optical fiber. The light output of the optical fiber is measured by a spectrograph. This approach allows construction of miniaturized fiber-optic SPR probes with limited areas of interaction and about 10 mm in length. The fiber-optic SPR sensor is capable of detecting variations in the refractive index within the operating range 1.2–1.4 RIU (refractive index units) with a resolution up to 5×10^{-5} RIU at higher refractive indices of analyte with a resonant wavelength resolution of 0.5 nm [118].

The second configuration (*Terminated reflection-based SPR sensor)* considers a sensor that utilizes a micro-fabricated mirror at the end of the probe to reflect the light back through the fiber based on the same principles as the in-line transmission based SPR sensor, so the light travels through the sensing area twice. The sensing length can be half the length of the sensing area of the in-line transmission based SPR sensor keeping the same sensitivity. The mirror is fabricated using electron-beam deposition.

Obando et al. [119] studied how reproducibility and robustness were affected by choice of fiber, isolation of the mirror from the sensing area, and orientation of the probes in the metal-layer sputter-deposition chamber in the manufacture of SPR dip-probes. Their work showed that optimizing the process yields sensors with a batch to batch reproducibility as low as 0.5 nm in locating the SPR spectral minima.

Iga et al. [120] developed a novel heterocore structure for a fiber optic SPR sensor. This structure was fabricated with a multi-mode graded index fiber as a signal transmission line whose core diameter was 50 μm. A 10-mm long single mode fiber segment was inserted as a sensing interface whose core diameter was 3.1 μm. A 50 nm silver layer was uniformly deposited around the cladding surface for SPR excitation. Since this structure did not need to eliminate the cladding layer of fiber, the fiber sensor probe would not be as vulnerable as those prepared with

conventional techniques. Using this SPR sensor, resolutions were obtained with values of 2.1×10^{-4} and 1.5×10^{-4} at refractive indices of 1.333 and 1.398, respectively.

Most recently, Zhao et al. [121] studied the potential for the modulation of SPR resonance wavelength with a multi-layer structure. The multi-layer modulation technique used in their sensor was confirmed to enhance the sensitivity of the SPR optical fiber sensor by adjusting the SPR resonant wavelength. In this study, the sputtering processed deposited 20nm of TiO_2, 11nm of SiO_2 and 30 nm of gold film on the material surface to change the refractive index. For operation in the refractive index regions of 1.32 and 1.36, the sensitivities in wavelength interrogation of the SPR optical fiber with the single gold thin film and multi-layers modulation were 1.08×10^{-5} RIU and 1.74×10^{-6} RIU, respectively.

3.3.2 Principle of the Technique

In the aforementioned method, the wavelength of the excitation light is kept constant, while the angle of incidence is varied. If the angle of incidence is kept constant and the excitation light source is polychromatic, then (2.77) will be satisfied at one particular wavelength of the light source where the maximum transfer of energy from the source to the surface plasmon wave will take place. This particular wavelength is called the resonance wavelength (λ_{res}) and the method is called wavelength interrogation. As shown in figure 3.7, at resonance wavelength, a sharp dip is observed due to an efficient transfer of energy to surface plasmons. Wavelength interrogation is mostly used in optical fiber–based SPR sensors where all the guided rays are launched and the light source used is polychromatic.

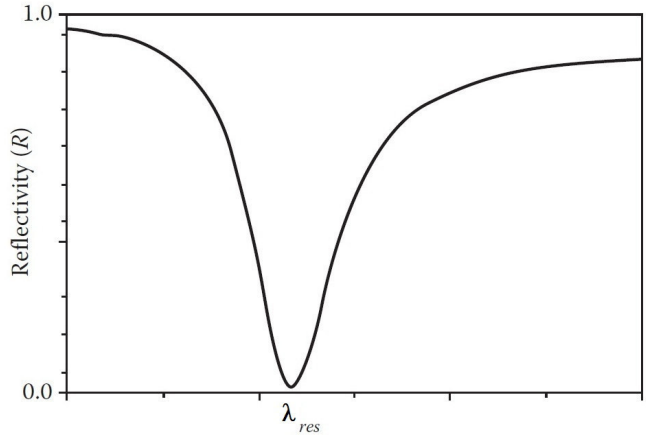

Figure 3.7 - A typical SPR curve in wavelength interrogation. At certain wavelength and angle, the energy associated with the incident radiation will couple with the SPW which is observed as a dip in the reflectivity.

3.3.3 Performance of the Technique

SPR sensing based on wavelength interrogation depends on shift of resonance wavelength when refractive index of sensing medium is changed. Figure 3.8 shows a plot of reflectance as a function of resonance wavelength for sensing layer with refractive indices n_d and $n_d + \delta n_d$. Increase in the refractive index by δn_d shifts the resonance curve by $\delta\lambda_{res}$. Following the same approach explained in the prior section about angular interrogation, the sensitivity of an SPR sensor with wavelength interrogation is defined as

$$S_n = \frac{\delta\lambda_{res}}{\delta n_d} \tag{3.3}$$

while Γ_λ-parameter referenced to wavelength is established as

$$\Gamma_\lambda \equiv \frac{\delta\lambda_{res}}{\delta\lambda_{0.5}} \tag{3.4}$$

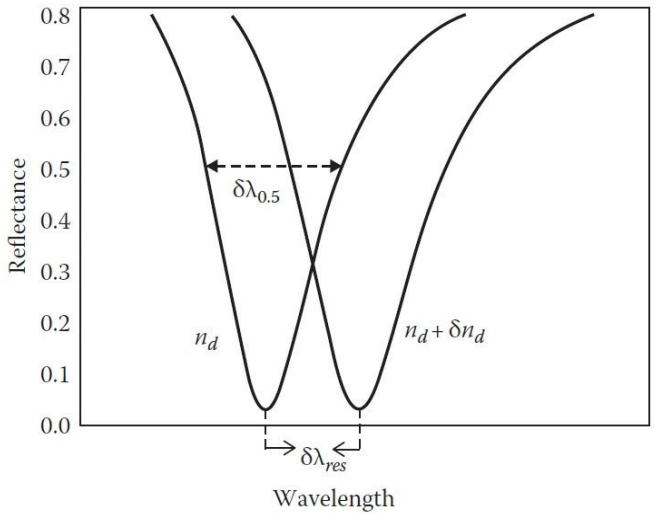

Figure 3.8 - SPR curves for different refractive indices of the sensing medium in the cases of wavelength interrogation.

SPR sensors based on wavelength modulation that have been employed include prism [114], optical fibers [121], and grating [122] based approaches. In section 3.3.1, were presented examples of the performance of the SPR sensors under wavelength interrogation. It could be seen that sensors based on a multi-layer modulation technique, as reported by Zhao et al. [121], offer better sensitivities. Indeed, sensitivities under wavelength interrogation improved from 1.08×10^{-5} RIU when considering an optical fiber with a single gold thin film to 1.74×10^{-6} RIU when a multi-layers was considered.

3.4 Intensity Interrogation

3.4.1 General Considerations and Historical Background

Intensity interrogation of SPR sensors occurs when the polychromatic incident light is incident at the SPR structure at a fixed angle, so when the refractive index of the surrounding medium changes the angular resonance condition also changes, therefore the intensity of reflected light at the same angle as the incident one also changes by an amount which depends on the angular shift of the resonance condition, which means the monitoring of such intensity can indicate the variation of the medium refractive index after proper calibration. SPR sensors based on intensity modulation focuses mainly on the two important aspects: improving performance (sensitivity, resolution) and increasing throughput.

To increase the sensitivity of intensity-modulated SPR sensors, Lechuga's group proposed an approach based on combination of the magneto-optic activity of magnetic materials and a surface plasmon resonance in a special multilayer structure [123]. They demonstrated an improvement in sensitivity by a factor of 3 compared to a conventional intensity-modulated SPR sensor and a refractive index resolution of 5×10^{-7} RIU [123].

A typical example of a high-throughput SPR sensor is the so called SPR imaging layout shown in figure 3.9 which is based on intensity interrogtion [124, 125]. In a typical SPR configuration of this type, a beam of light passes through a prism coupler and is made incident on a thin metal film at an angle of incidence close to the coupling angle. The intensity of reflected light depends on the strength of the coupling between the incident light and the surface plasmon and, therefore, can be correlated with the distribution of the refractive index at the surface of the metal film.

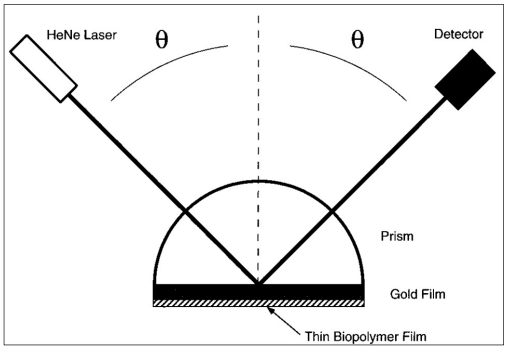

Figure 3.9 - A typical SPR scanning instrument with intensity interrogation [125].

Corn's group has researched these systems for over a decade. In their earlier works, they employed a HeNe laser as a source of illumination[125]. However, a highly coherent light source

generated images with parasitic interference patterns that were disturbing SPR measurements. In 1997 they improved their SPR instrument by introducing an incoherent light source and a near-infrared (NIR) narrow band-pass filter [126]. Using this approach, they detected hybridization of short (18-base) oligonucleotides at concentrations as low as 10 nM [127] (this was estimated to correspond to a refractive index resolution in the 10^{-5} RIU range). The use of a white light source and a band pass filter was also advocated by Yager's group[128]. They demonstrated that by tilting the interference filter, an operating wavelength of the SPR imaging sensor can be tuned [128]. Later they demonstrated that their SPR imaging instrument operating at a wavelength of 853 nm can provide a refractive index resolution of 3×10^{-5} RIU [129]. In 2005, Corn's group reported SPR sensing with a special multilayer structure supporting long-range surface plasmons; however, the use of long-range surface plasmons led only to minor sensitivity improvements of 20% (experiment) and 40% (theory) compared to the conventional SPR layout [130].

A dual-wavelength SPR system was reported by Zybin et al. [131]. In their SPR sensor, they used two sequentially switched-on laser diodes, and the intensities of the reflected light at the two different wavelengths were measured and the sensor output was defined as the difference of these two signals. A refractive index resolution of 2×10^{-6} RIU was achieved when the signal was averaged over a large beam diameter (6 mm^2).

Campbell's group reported an SPR imaging system with a controllable angle of incidence [132, 133]. This feature allows SPR patterns to be acquired sequentially at different angles of incidence and selection of the optimum angle of incidence for the SPR measurements. With a HeNe laser as a source of light, their sensor was able to measure simultaneously in 120 sensing channels with a refractive index resolution of 2×10^{-5} RIU. Recently, they claimed an improvement in sensor resolution down to 5×10^{-6} RIU [134].

Recently, Piliarik et al. investigated SPR sensing with an elliptically polarized light [135] and concluded that a change in the polarization of light induced by the coupling of light to a surface plasmon can be exploited to significantly improve the sensitivity and operating range of these SPR sensors. In addition, this approach, provides high-contrast SPR patterns (with a low background), which are well suited for automated analysis.

Homola's group developed an SPR sensing approach based on polarization contrast and excitation of surface plasmons on spatially patterned multilayers [136]. In this configuration, as illustrated in figure 3.10, a prism coupler with an SPR chip containing a spatially patterned multilayer structure was placed between two crossed polarizers. The output polarizer blocked all of the light reflected from the (inactive) areas outside the sensing areas, generating high-contrast patterns. Two types of SPR multilayers with opposite sensitivities to refractive index were employed, and the output signal was defined as a ratio of the intensities generated from the two neighboring

multilayers, therefore achieving immunity to optical power fluctuations. This sensor was shown to be able to detect refractive index changes down to 2×10^{-6} RIU and to detect short oligonucleotides (23-mers) at concentrations as low as 100 pM [137].

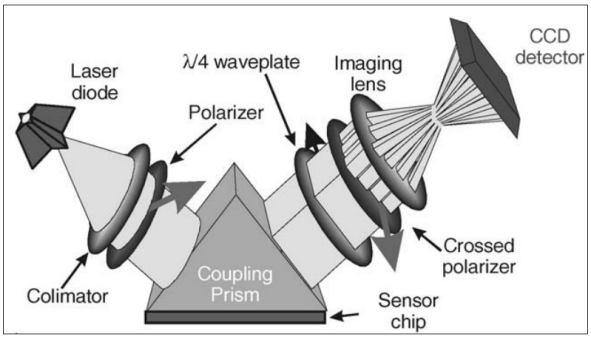

Figure 3.10 - Configuration of a SPR sensing system with polarization contrast and intensity interrogation [136].

3.4.2 Principle of the Technique

In this method, the wavelength of the light source and the angle of incidence of the light are kept constant. If the prism is used, then the intensity of the reflected light at a constant angle is measured as a function of the refractive index of the dielectric medium. An increase in refractive index will induce an increase in the resonance angle, and hence the intensity of the reflected light increases because of the shift in the SPR curve, as shown in figure 3.11. Knowing the intensity, the refractive index of the dielectric medium can be determined. Sometimes, two light emitting diodes (LEDs) of different wavelengths are used and intensities are measured at these wavelengths. The

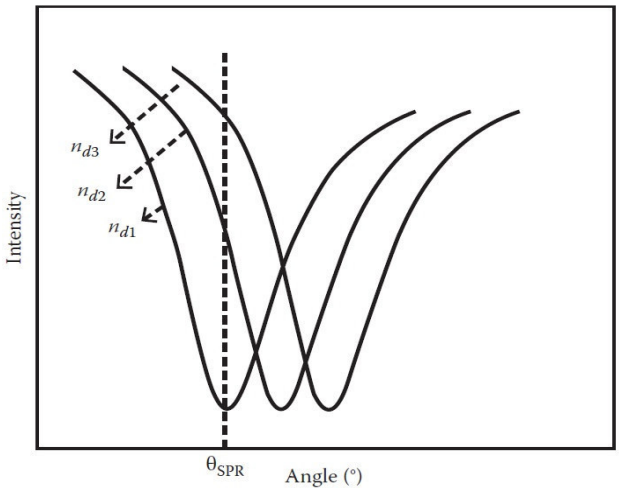

Figure 3.11 - Intensity interrogation of SPR sensors (the three curves are corresponding to three different refractive indices of surrounding the dielectric).

knowledge of change in differential intensities is used to determine the change in the dielectric constant of the medium.

3.4.3 Performance of the Technique

Different from the conventional optical setup performing angular interrogation, the laser and detection system are fixed but the incident angle can be changed through the employment of a paired off-axis parabolic mirrors and a set of rectangular mirrors. For the detection of intensity, first incident angle alters to obtain the SPR curve and then calculated the first-order differentiation of the original SPR curve. After that, the rectangular mirror moves to the corresponding position where the maximum slope happens. Subsequently, changes in the refractive index of the medium (n_a) originates angular displacement of the SPR curve, therefore a variation of the intensity level, I, incident on the photodetector. The sensitivity of the sensor is defined as

$$S = \frac{\delta I}{\delta n_a} \tag{3.5}$$

As shown in the prior section, the performance of the sensor reported by Homola's group has the highest sensitivity when compared with other sensing configurations based on intensity interrogation. This approach presented herein offers considerably enhanced sensitivity than the competing multichannel SPR sensing platforms and allows measuring changes in the refractive index as small as 2×10^{-6} RIU [137].

3.5 Phase Interrogation

3.5.1 General Considerations and Historical Background

Around the year 2000, the research group of Nikitin demonstrated two SPR sensor platforms based on interferometry [138, 139]. The first approach was based on the interference of the TM polarized signal beam with the TE-polarized reference beam [138], whereas the second method was based on a Mach-Zehnder interferometer combining TM polarized signal and reference beams, as shown in figure 3.12 [139]. This configuration was demonstrated in two modes: (a) phase contrast, which increases the sensor sensitivity and (b) "fringe mode", where there was a definite angle between the interfering beams and a pattern of interference fringes was superimposed on the image of the surface. Local variations in the phase of the signal beam resulted in bending and moving of the interference fringes. The reported refractive index

resolution was on the order of 10^{-7} RIU [139]. At the same time as Nikitin et al. published their work [139], a similar configuration of SPR sensor based on the Mach- Zehnder interferometer was reported by Notcovich et al. [140]. They used their system for measurement of the refractive index of gases and demonstrated a refractive index resolution on the order of 10^{-6} RIU [140].

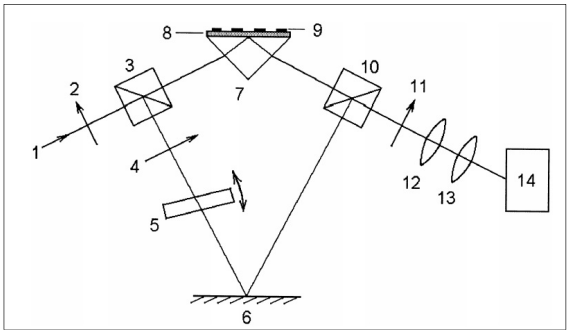

Figure 3.12 - Scheme of SPR sensor based on interferometry. (1) light beam; (2, 4) polarisers; (3, 10) beam-splitting cubes; (5) phase-retarding glass plate; (6) mirror; (7) SPR prism; (8) gold film; (9) patterned coating; (11) analyser; (12) imaging lenses; (14) CCD camera [139].

Wu et al. proposed a phase-modulation SPR sensor based on common-path, heterodyne interferometry [141]. Two acousto-optic modulators were used to split the incoming laser light from a HeNe laser into two linearly orthogonally polarized beams with a frequency difference of 60 kHz. These two light beams were merged into one beam by a polarization beam splitter. One portion of the beam was directed to a detector while the other was coupled into an SPR prism coupler. The TE and TM components of light reflected from a thin layer of gold on the base of the prism were recombined using a polarizer, and the output beam was received by a detector. SPR-induced phase shift was determined by an electronic phase meter (lock-in amplifier). The refractive index resolution of this design was estimated to be $\sim 2 \times 10^{-7}$ RIU [141].

Alieva and Konopsky developed an SPR sensor based on interference between a surface plasmon supported on a metal film and a bulk wave propagating at grazing angle just above the surface of metal [142]. This approach suppresses the sensitivity of the SPR method to variations in the refractive index of a liquid sample, which in SPR biosensors interfere with binding measurements.

Naraoka and Kajikawa reported a phase-modulation SPR sensor based on a rotating analyzer method [143]. In their approach, a linearly polarized light from a semiconductor laser was coupled to an SPR prism coupler and reflectivity was detected while the rotational angle of the analyzer was scanned. The phase difference between the TE and TM components of the reflected light were determined from the dependence of the reflectivity on the angle of analyzer. The refractive index resolution of their system was estimated to be below 2×10^{-7} RIU [143].

In recent years, SPR sensors with phase modulation have been extensively studied by the researchers at the Chinese University of Hong Kong and City University of Hong Kong. In 2002 Ho et al. reported an SPR sensor based on the Mach-Zehnder interferometer [144]. In that work, as shown in figure 3.13, an optical beam from an unpolarized HeNe laser passed through a prism coupler and the TM polarized component of the beam excited surface plasmons in two parallel sensing channels, one filled with a sample and the other with a reference solution. TE and TM polarization components of the output beam were split by a polarizing beam splitter. The optical path for TE polarization was modulated by means of a piezoelectric actuator. Finally, TM polarization was converted to TE polarization by a half-waveplate, and the two beams were recombined. The shift between the interference patterns for the measuring and reference sensing channels was measured. Resolution of this sensor was estimated to be about 3×10^{-6} RIU [144].

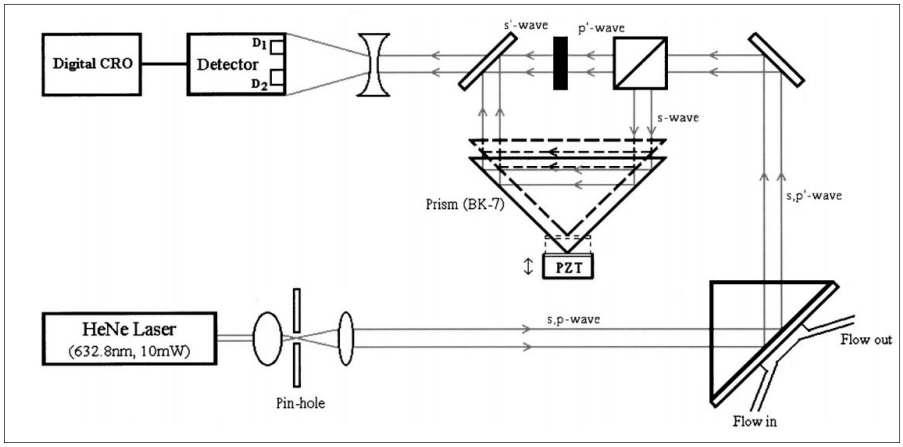

Figure 3.13 - Scheme of SPR sensor based on a Mach-Zehnder interferometer [144].

An alternative configuration of an SPR sensor with phase modulation was reported by Wu et al. in 2004 [145]. In this configuration, one Mach-Zehnder interferometer performed independent interference of TE and TM polarized components of a signal beam emerging from a prism coupler and a reference beam. Subsequently, the output TE and TM beams were separated in a Wollaston prism and directed to two separate detectors. A piezoelectric actuator modulated the optical path in a reference arm of the interferometer, producing a periodic intensity modulation in both TE and TM polarizations. The interference patterns for TE and TM polarizations were processed to reduce the noise and compensate for instabilities in the setup [146], with the sensor output determined as a mutual shift of the two patterns. Resolution of the sensor was estimated to be 5.5×10^{-8} RIU [145].

Another SPR sensor based on measuring the phase difference between TE and TM polarization components of light beam was reported by Ho et al. [147]. They used a single beam and a photoelastic phase modulator to introduce a carrier frequency so that the phase can be

determined by measuring the relative amplitude of the first harmonic signal. Resolution of the sensor was determined to be ~1.2×10^{-6} RIU [147]. In 2007, a phase modulation-based SPR sensor employing a Michelson interferometer was reported by Yuan et al. [148]. They used a Michelson interferometer with an SPR prism coupler inserted in one arm of the interferometer. This arrangement allows the TM polarized component of the light beam to incur a 2-fold phase shift compared with that in the Mach-Zehnder interferometer. Therefore, the sensitivity of the Michelson interferometer-based SPR sensor was twice as high as that of the SPR sensor with the Mach-Zehnder configuration. This improvement was demonstrated in a single experimental system incorporating both Michelson and Mach-Zehnder interferometers in which the refractive index resolutions were established to be 7.7×10^{-7} and 1.5×10^{-6} RIU, respectively [148].

In 2008, the highest refractive index resolution of 2.8×10^{-9} RIU was reported by Li and coworkers [149]. Comparing to the previously reported heterodyne-based SPR sensor [150], where phase was measured by the lock-in technique, active adjustment was employed by Li to equalize the amplitude of the reference and signal beams and the differential phase between them is subsequently retrieved by the amplitude modulation (AM) method which also helps to realize real-time measurement. The equalization of signal and reference beam amplitudes, as well as the common path setup in optical heterodyne technique, has helped to eliminate noise from laser intensity fluctuation and resulted in ultra-high resolution. In their experiment, apparent phase change was observable by adding 0.00001% sucrose to pure water, which corresponding to refractive index change of 1.4×10^{-8} RIU. As the signal magnitude is about 5 times of the noise level, the resolution of the device has been determined to be 2.8×10^{-9} RIU. Experiments conducted on glycerin water solution revealed a similar resolution of 7×10^{-9} RIU, while that on interaction between mouse-IgG/antimouse-IgG resulted in a sensitivity of 10 fg/mL (67 aM), which seems to be the highest ever achieved by SPR sensor.

3.5.2 Principle of the Technique

In this method, the phase difference between TM and TE polarized light in the reflection spectrum for a monochromatic light source is measured as a function of the refractive index of outer medium. It was determined that around the resonance angle, the variation in intensity of the reflected light is small when the refractive index changes, so the sensitivity is poor. The same does not happen if the parameter to be monitored turns out to be the phase difference between the p-

and s-components of the reflected light, as shown in figure 3.14, actually the other way around, i.e., it is the region of maximum phase sensitivity.

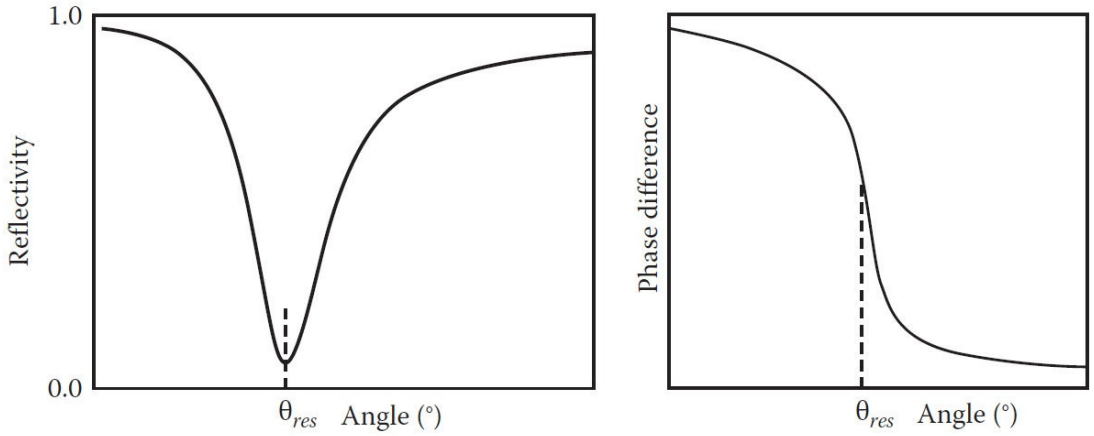

Figure 3.14 – Typical angular SPR curve (left) and the phase difference between the p- and s-components of the reflected light (right).

3.5.3 Performance of the Technique

Phase interrogation can be achieved by illuminating the sensor with a laser line with emission in the region of the SPR loss band where the slope of phase variation with the measurand induced band spectral shift has its maximum value. Considering that only the TM polarization component can couple to surface-plasmons and give rise to SPR, the TE wave will accumulate a SPR immune phase delay when propagating through the sensor structure, therefore providing a reference level to the sensing effective TM wave.

A possible classification for this interrogation approach is based on the way of generating these waves. When using a polarizer to obtain, from a single optical source, the TE and TM components which are made to interfere on the photodetector, the process is known as polarimetric interrogation. In the case where the TE and TM waves are provided by two distinct light sources with slightly different optical frequencies and are made to interfere resulting into a beat signal with frequency low enough to be resolved by the photodetection and amplification electronics, heterodyne interrogation is applied. Finally, if the reference wave propagates along a different spatial path and brought to interfere with the TM light on the photodetector, the approach is usually known as interference interrogation (though all the three processes rely on interference phenomena).

Phase interrogation has not been widely explored in the context of SPR sensors. Surely, it is more complex to implement, requiring more know-how on optical components, modulation

instruments and signal processing techniques, but eventually the main reason is the circumstance that most of the R&D community which has been working until recently in SPR sensing had a biochemical background, therefore with a tendency to use in their research spectroscopic equipment. This is going to change since plasmonics is now moving to fields other than sensing, such as imaging and data storage, bringing to the subject researchers with diverse backgrounds. A consequence of this dynamics is an improvement of the resolution values obtained for each of the three described phase reading approaches.

Following the approach outlined for the interrogation techniques described before, the sensitivity of SPR sensors relying on phase interrogation is defined as

$$S_{\phi} = \frac{\delta \phi_{p-s}}{\delta n_{\mathrm{d}}} \tag{3.6}$$

where ϕ_{p-s} is the phase difference between the p and s components of the reflected light.

As outlined in previous section, for the case of interferometric (heterodyne) interrogation, a value of 2.8×10^{-9} RIU was reported in 2008 [149], apparently the highest refractive index resolution obtained to this date; when considering interferometric (polarimetric) interrogation, under optimized conditions, it was obtained a resolution of 3.7×10^{-8} RIU [151]; for interferometric interrogation, a resolution down to 2.2×10^{-7} RIU was reported in 2011 [152].

3.6 Conclusion

To conclude this chapter, it may be useful to have a summary of the state-of-the-art concerning the interrogation of SPR sensors for refractive index measurement, as well as to add some comments addressing the implementation of these sensors with optical fiber support.

Most of this research was performed with classical sensing heads based on a prism coupling system in a Kretschmann configuration. The SPR induced phase change would be greatly amplified if the light undergoes multiple attenuated total reflections, as happens when the sensing platform is the optical fiber. This advantage is attenuated due to the propagation characteristics of the fiber. If it is multimode, each mode generates its own resonance dip at a specific wavelength, different from the other modes, resulting into a broadening of the full SPR resonance, factor that decreases the phase sensitivity (as well as the sensitivity expectable from the different interrogation approaches indicated in table 3.1). On the other hand, if in the sensing head a standard monomode fiber is considered, its small numerical aperture limits the incident angles from approximately 86.5 to 89.5 degrees (in the simplified picture of geometric optics), which is far from the critical angle, meaning a reduced phase shift occurs in each reflection.

Table 3.1 - Performance of SPR interrogation techniques.

SPR Interrogation	Angular	Wavelength	Intensity	Phase
Sensitivity	140 deg/RIU	-	-	-
Resolution (RIU)	5×10^{-7} RIU	1.74×10^{-6}RIU	2×10^{-6} RIU	2.8×10^{-9} RIU
Dynamic Range (RIU)	-	$>10^{-1}$	$>10^{-1}$	10^{-3}
Setup configuration	Gratings	Side-polished Optical Fiber	Prism Coupling	Prism Coupling
Wavelength (nm)	670	830	-	632.8
Reference	[111]	[121]	[131]	[149]

This feature indicates the need to consider a different type of sensing head in optical fiber based SPR sensing systems when the target is to achieve very high resolutions. Indeed, up to now no development effort has been done towards optical fibers well suited to SPR sensing, contrary to the large efforts done along the years to optimize the prism approach. Even in the recent appearance of microstructured optical fibers in SPR sensing, the focus was on the improvement of the access conditions of the measurand to the optical field and in the increase of the interaction area, which by itself increases the intrinsic sensitivity of the sensor, and not on the tailoring of the guidance mechanisms of the fiber to increase also its intrinsic sensitivity from this side. Eventually, a compromise needs to be found between these two mechanisms, a topic that certainly will be the target of future R&D activity. A possible path would be to consider for the sensing head a special fiber with material and geometric characteristics compatible with few modes light propagation associated to incident angles closer to the critical angle, providing a large interaction area of the optical field with the measurand in a region where it can have ready access, coupled to input/output standard single mode fibers, if necessary with a coupling transition region to reduce the connection loss. Desirably, the sensor shall operate in reflection not only because in such configuration the illumination fiber is additionally the return fiber, but also in view of the light double-pass in the sensing head, which further increases its intrinsic sensitivity.

Independently of the approach followed, it is fairly reasonable to state the study, development and application of optical fiber based platforms for high performance SPR sensors shall consider reading based on phase interrogation, eventually complemented with other approaches, particularly with wavelength encoding.

4

Optical Fiber SPR Sensing Structures with Single and Bimetal Layers

Summary: *This chapter develops the study of SPR based optical fiber sensing configurations integrating a single metal or a bimetallic layer. With the focus on phase interrogation, it is analyzed the performance associated with the utilization of different metals, namely silver, gold, copper, and aluminum when the tapered and the tip (optrode) optical fibers geometric layouts are addressed.*

4.1 Introduction

The basic approach to implement an optical fiber based SPR sensor relies on coating the fiber core with a metal layer showing characteristics adequate to induce plasmonic resonance in the conditions of light propagation in the optical fiber. Even so, and independently of the interrogation technique to be applied to read the measurand induced variation of the properties of such resonance signature, the type of metal to be used in a single layer, the possibility to include bimetallic layers with distinct combinations of metals, the addition of oxide layers of different materials, are all factors which, from the material side, strongly impact the performance of such sensing structures. But the geometric element is also important, therefore it is expectable different performances when standard fiber geometries, tapered configurations or optrode layouts are addressed. Naturally, the combination of the material and the geometric elements substantially increases the number of fiber optic based SPR sensing structures that may be feasible. Consequently, to perform a comparative assessment of their relative merits and drawbacks, it is important to build up a theoretical tool with characteristics that shall permit to expediently analyse each one of these possibilities.

A core element of the PhD programme was to construct and test such theoretical tool and apply it to the study of a variety of sensor architectures. The architecture of such model was outlined in Chapter 2 and here the focus will be on the analysis of the tapered and optrode layouts when single or bimetal layers are applied over the fiber. The performance of these sensing structures will be analyzed when the phase interrogation technique is applied.

4.2 General Considerations

In general, silver (Ag) and gold (Au) are the two main metals that are used for SPR sensor applications. As a matter of fact, Ag-based sensors are known for their narrow spectral width but they are chemically very unstable and are highly vulnerable to oxidation when used in liquid or gaseous environments. On the other hand, Au-based sensors are more sensitive but lesser accurate than Ag-based sensors. However, an Au layer is chemically very stable.

Keeping these features in mind, some research has been done about the idea of bimetallic structures but not in the sensing context [153]. In order to take the benefit of high sensitivity of Au and high detection accuracy of Ag, a SPR sensor based on resonant bimetallic layers was proposed a few years back [154]. It was shown that the bimetallic layers based sensor not only displayed a high shift of resonance angle as an Au based sensor, but also showed narrower resonance curve typical of an Ag-based sensor plus an additional advantage of protecting silver against oxidation.

Later on, significant modifications were made to this bimetallic layer based SPR sensor and a design of fiber optic SPR sensors with bimetallic layers was proposed [100]. The related design parameters were optimized in order to attain the best performance out of such bimetallic layers. Recently, the capability of other metals such as copper (Cu) and aluminum (Al) was analyzed for SPR sensor applications [155]. It was concluded that Cu and Al have the ability to be used to design a SPR sensor with a limitation that Cu is chemically vulnerable against oxidation and corrosion, therefore, protection of Cu film is required for a stable sensing procedure.

The performance of an optical fiber SPR sensor is usually evaluated in terms of its sensitivity. Several attempts have been made to improve the performance of a fiber optic SPR sensor [105, 156]. The consideration of tapered optical fibers has proved to be a useful concept to improve the sensor's performance [157]. For instance, a tapered optical fiber SPR microsensor based on white light excitation [158] and the use of dual-tapered and tetra-tapered fiber SPR probes for gas and liquid sensing have been proposed [159]. These structures present a substantial variation in evanescent field penetration along the tapered sensing region length. The evanescent field can be reached by the narrowing of the fiber cross section in the tapered region. Another approach, compatible with the mentioned mechanisms, is based on modifying the geometry of the sensing head (tip layout, often known as optrode design) to optimize the dynamic range and sensitivity [160-162]. These configurations are supported by beveling the distal end of the fiber probe, such as a chisel-tipped probe, where the top and bottom of the probe were polished to the same angle.

Such appealing characteristics of the bimetallic arrangement and SPR sensor structures induced the motivation of to study it further, which is the focus of this chapter.

4.3 Optical Fiber SPR Sensor with a Single Metal Layer

In this section, it is reported the study performed on an optical fibre based SPR sensing head incorporating a single metal layer, which can be gold (Au), silver (Ag), copper (Cu) and aluminum (Al). For each of them the performance of the sensor is assessed permitting to identify the best metal choice.

In this analysis, a sensing system consisting of a fibre core–metal film sensing medium is addressed as shown in figure 4.1. The fiber is a step-index multimode plastic clad silica fibre, with core diameter of 600 μm and 0.24 numerical aperture and a 1 cm long sensing region. It is assumed the oscillation angles to cover the full range determined by the fibre numerical aperture. The thickness of metal layer is taken as 50 nm and the refractive indices for the thin film materials

were obtained from experimental data available in the literature [163-166]. The results presented below were obtained directly from the equations derived in Chapter 2.

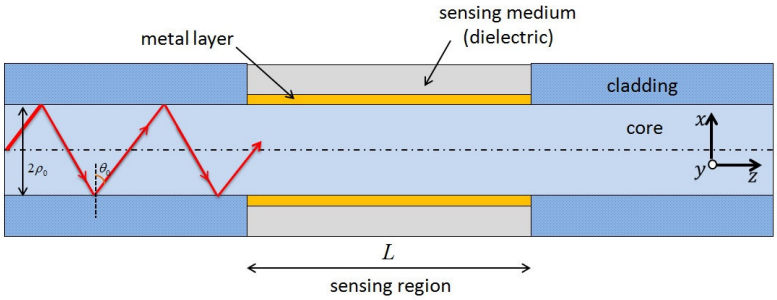

Figure 4.1 - Schematic diagram of an SPR sensor based on optical fibre.

Figure 4.2 shows the SPR transmittance curves for the SPR sensing head incorporating each of the four metals as the refractive index of the surrounding medium changes from 1.320 to 1.335 in steps of 0.005. From figure 4.2(a), it is clear that the resonance wavelength shifts from 560 nm to 599 nm for Au metal as the refractive index of the medium varies from 1.320 to 1.335. Similarly, from figure 4.2(b), for the case of Ag it is observed that the resonance wavelength shifts from 480 nm to 516 nm for the same variation range of the medium refractive index, while figures 4.2(c) and 4.2(d) reveal that the resonance wavelength shifts from 448 nm to 481 nm for Cu and 340 nm to 365 nm for Al respectively. Thus, the shift in the resonance wavelength is different for the various metals and it is maximum for Au and minimum for Al. Also, these figures reveal that Al exhibits the sharpest SPR dip while Au has the broadest SPR curve among all the four metals.

Figure 4.3 shows the variation of resonance wavelength with refractive index of the external medium for all the four metals. It is observed the resonance wavelength for each metal increases linearly with the increase of this index, following the same pattern. The slope of the resonance wavelength variation over the refractive index of the medium, i.e., the sensor sensitivity, is highest for the Au, while the lowest value occurs when the metal layer is of Al. Additionally, it can be observed the sensitivity for Ag is larger than that of Cu but is smaller than that of Au. This comparison only makes sense because of the nearly linear dependence of the shift resonance wavelength versus refractive index of the sensor surrounding, the whole range of refractive indices, i.e. 1.320 to 1.335, of the sensing medium. Table 4.1 summarizes the results obtained.

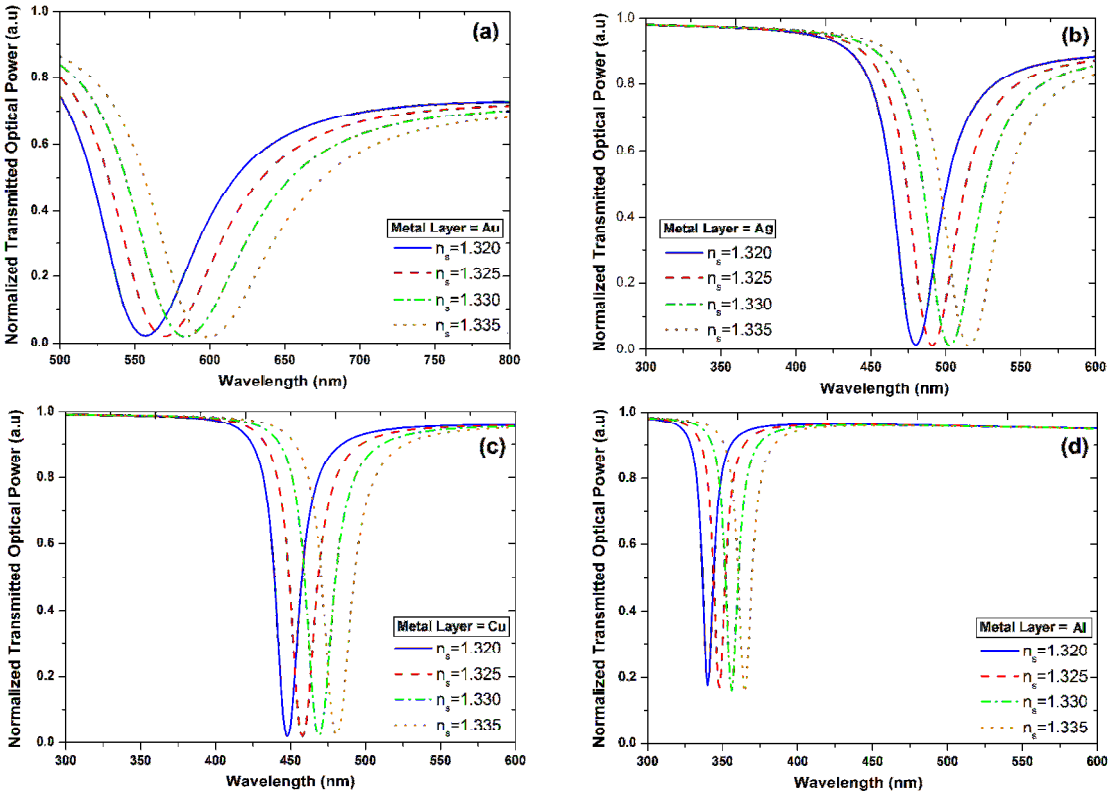

Figure 4.2 - Spectrum of the normalized transmitted optical power for the (a) Au, (b) Ag, (c) Cu, (d) Al metals sensing structure.

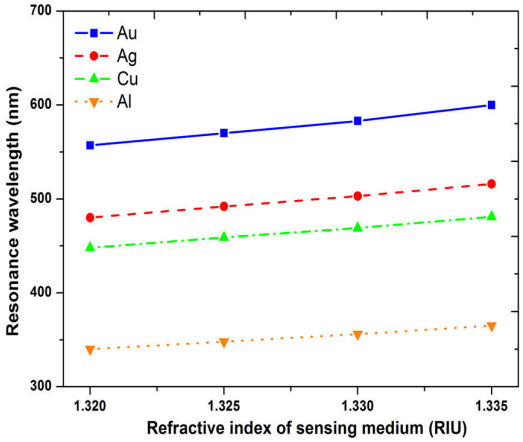

Figure 4.3 - Variation of resonance wavelength of the SPR sensor with refractive index of the external medium for each of the metals that overlay the optical fiber.

Table 4.1 - Comparison of the refractive index sensitivity of an optical fiber based SPR sensor incorporating a single metal layer when different metals are addressed.

Metal Layer	Sensitivity (μm/RIU)
Gold (Au)	2.87
Silver (Ag)	2.40
Copper (Cu)	2.20
Aluminum (Al)	1.67

It can be seen from this Table that the sensitivity obtained for the structure with a gold layer is the largest one (2.87 μm/RIU), while the smallest happens when aluminum is applied (1.67 μm/RIU), while intermediate values are obtained when layers of silver (2.40 μm/RIU) and copper (2.20 μm/RIU) are under concern.

In chapter 3, the Γ-parameter associated with the sensor response to a specific measurand variation was defined as the ratio of the variation of the value of the entity (angle, wavelength, intensity, and phase) where resonance occurs and the range of this entity corresponding to the width of the resonance at half-maximum. Here, the entity to be interrogated is the wavelength, so the Γ parameter and Quality Parameter (χ) are useful to be considered, which are expressed by equations (2.89) and (2.90).

For the sensing head structure deal with in this section, the values of the Γ (in wavelength, Γ_λ) and of χ were evaluated for the case of the most favourable arrangements, associated with layers of gold, silver and copper, with the results presented in Table 4.2. The sensor response was induced by a variation of the external refractive index from 1.320 to 1.335.

Table 4.2 - Comparison of the values for the Γ_λ and Quality Parameter (χ) for the SPR sensing heads incorporating thin films of gold, silver and copper.

Metal Layer	$\lambda_{n=1.320}$ (μm)	FWHM $\delta\lambda_{0.5}$ (μm)	Γ_λ	χ (RIU^{-1})
Gold (Au)	0.556	0.093	0.462	30.86
Silver (Ag)	0.480	0.042	0.857	57.14
Copper (Cu)	0.447	0.021	1.571	104.76

The observation of the data in the Table indicates the SPR sensor incorporating a layer of copper has the maximum Γ_λ parameter (1.571) and the maximum quality parameter (104.76 RIU^{-1}), while for a gold layer these values are, respectively, 0.462 and 30.86 RIU^{-1}, with the situation of the sensing head with a silver metal layer to show a performance between these two.

When the information derived from Tables 4.1 and 4.2 is combined, it turns out that for the case of the gold layer the sensor sensitivity reaches a maximum but its Γ_λ and χ parameters get the minimum values for the set of metals addressed. On the other way around, the sensitivity of the SPR sensor with a copper layer is the smallest one but the values for its Γ_λ and χ parameters got a maximum. Hence, in designing an optical fiber based SPR sensor, the proper metal should be chosen depending upon the performance parameter of interest, i.e. either sensitivity or the Γ_λ parameter along with the quality parameter.

Usually, the sensitivity performance is the critical factor, so it is privileged the layout which maximizes it when the Γ_λ parameter is not too low, in the case the one with the gold layer. An additional advantage of this option is its chemical stability, feature which does not happen when dealing with layers of aluminum and copper.

4.4 Optical Fiber SPR Sensor with Bimetal Layers

In order to take the benefit of high sensitivity of Au and high detection accuracy of Ag, a SPR sensor based on resonant bimetallic layers was proposed a few years back [154]. It was shown that the bimetallic layers based sensor not only displayed a high shift of resonance angle as an Au-based sensor, but also showed a narrower resonance curve as an Ag-based sensor, with the additional advantage of protecting silver against oxidation. Later on, significant modifications were made to these SPR bimetallic layers structures and a new design of fiber optic SPR sensors was proposed [100]. The related design parameters were optimized in order to attain the best sensing performance.

In this chapter a theoretical investigation is reported concerning the sensing characteristics of optical fiber sensors based on the plasmonic phenomenon and incorporating different bimetallic combinations made out of four metals: Ag, Au, Al, and Cu. The analysis follows the model outlined in chapter 2 with the due changes associated with the particular structure under study, which is shown in figure 4.4.

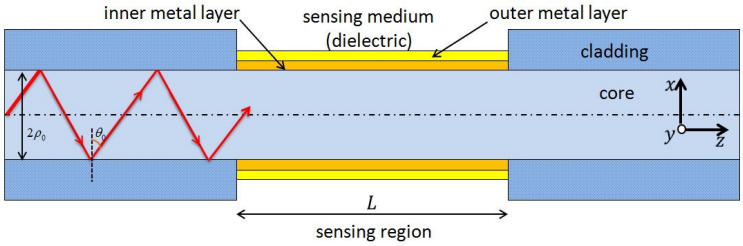

Figure 4.4 - Schematic diagram of an SPR sensor based on an optical fibre with bimetallic layer.

In this configuration the cladding around the core of a multimode step-index optical fiber is removed and is coated with a metal layer of thickness d_1. This inner layer is further covered with a thin layer of thickness d_2 of another metal and this outer layer is finally covered with the sensing layer. In the analysis, the total bimetallic thickness is taken as 50 nm and the layer thickness of the two metals is assumed as 25 nm each. Other relevant parameters had the values indicated in the context of the study addressed in previous section.

Figure 4.5 depicts the spectral transmittance curves for six different bimetallic combinations, namely (a) Au-Al, Ag-Al and Cu-Al and (b) Ag- Au, Cu-Au and Al-Au. In all these combinations, the first metal represents the inner layer whereas the second metal represents the outer layer. Ag and Cu are quite prone to oxidation and they are chemically not stable when used in liquid or gaseous milieu. Due to this reason only, Ag and Cu have not been considered as outer layers. Al and Au have been considered as an outer layer as they both are chemically stable. It is apparent from this figure that the bimetallic combinations are able to tune the position as well as the width of the SPR curve depending upon which two metals are coupled. For the same set of parameters and coefficients, the resonance wavelength range, which was around between 340 and 555 nm for the single metal case, is now constricted around between 385 and 615 nm. Also, the width of the SPR curve varies for different bimetallic combinations depending upon which two metals are clubbed together. Hence, it is quite worthwhile to estimate and figure out the best combination of two metals which can provide the best performance.

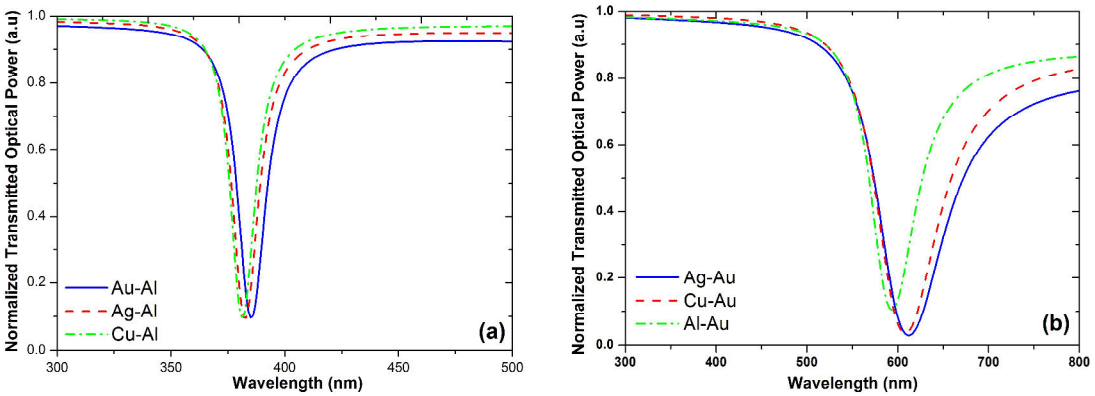

Figure 4.5 – Spectral resonance of the SPR optical fiber based sensing structure incorporating a bimetallic layer derived from the , combination of metals with (a) Al and (b) Au as outer metal layer (the refractive index of the surrounding medium is n_s=1.343).

Figure 4.6(a) shows the variation of sensitivity with inner layer, i.e., ratio of inner layer thickness to total bimetallic thickness, for six bimetallic combinations. The curves drawn are derived from the response of the SPR resonance to a variation of the external refractive index by a value δn_s=0.010.

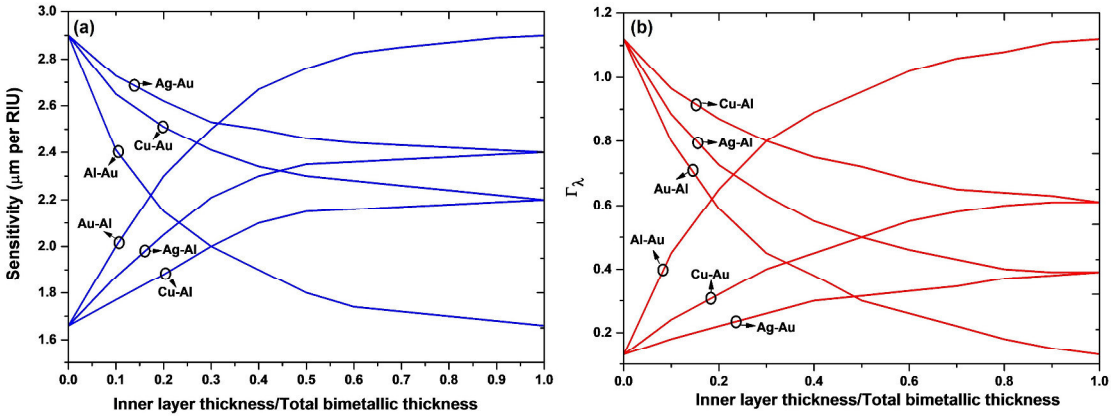

Figure 4.6 - Variation of (a) sensitivity, (b) Γ_λ with the ratio "inner layer thickness/total bimetallic thickness" for different bimetallic combinations. These parameters were obtained from the response of the SPR resonance to a variation of the external medium refractive index from 1.343 to 1.353 (δn_s=0.010).

The figure also contains the sensitivity of single metallic layers at points 0 and 1 on the x axis and it clearly vindicates the earlier observation that the single Au layer is the most sensitive layout, whereas the single Al layer is the least sensitive one. Au-Al and Ag-Au combinations also provide good sensitivity. However, it is the Au-Al case which provides the larger sensitivity when compared with all other combinations if the fraction of (inner) gold layer thickness is taken greater than 0.3. It implies that a thick Au layer with a very thin covering of Al layer (around 2–4 nm) is able to provide quite a large sensitivity. Figure 4.6(b) shows the corresponding variation in the Γ_λ parameter. As far as the single layer cases are concerned, it clearly suggests that the single Al layer provides the highest Γ_λ whereas the single Au layer provides the smallest one. Among the bimetallic combinations, Al-Au and Cu-Al are clearly better than all others. The Ag-Au combination provides the minimum values of the Γ_λ among all the cases.

Gathering all these results, it can be concluded that no single metal (among Ag, Au, Al, and Cu) is able to provide simultaneously reasonable values for all the performance parameters. However, when these metals are used in bimetallic combinations of a well-defined thickness ratio, one can find an overall sensing performance with high sensitivity and a good Γ_λ parameter along with a large operating range. Moreover, the results indicate that bimetallic SPR sensors can surpass the performance of single-layer systems, benefiting also from the enhanced chemical stability that yields facilitating the process of surface functionalization for selective biochemical sensing applications.

4.5 Optical Fiber SPR Sensor with Bimetal Layers in a Tapered Transmissive Geometry

The tapered optical fiber is the basis of many optical fiber devices and has become increasingly important over the years. This structure have attracted a lot of interest because of their use in a variety of applications, including interferometric devices [167, 168], directional couplers [169], sensors [170, 171], optical probes [172], dye lasers [173], optical coupling [174], microspheres coupling for whispering gallery modes [175, 176], and supercontinuum generation due to its enhanced nonlinearity [177].

These structures present a substantial variation in evanescent field penetration along the tapered sensing region length. The evanescent field can be reached by the narrowing of the fibre cross section in the tapered region, as shown in figure 4.7. When the effective refractive index of the surface plasmon mode approaches the value of the effective refractive index of a mode of the uncoated tapered fibre, resonant coupling between the modes with the same azimuthal order of both substructures can be observed at a specific combination of geometrical and material parameters, and a resonant dip is observed in the transmission spectrum. The penetration of the evanescent field, therefore the strength of light coupling with surface plasmons depends on the numerical aperture of the fibre, which is related to the light acceptance angle limit. Since the angle is fixed, these devices can operate in spectral shift mode or in power loss mode. In the spectral shift mode the transmission spectrum of the plasmon resonance shifts as the outer refractive index of the dielectric medium surrounding the structure changes. In the power loss mode, the total optical power transmitted at the plasmon resonance changes with the outer refractive index [178, 179].

In this section the behaviour of SPR sensing devices supported in tapered optical fibers and incorporating bimetal layers is studied. First, it is presented the approach applied to analyse these structures, then is it determined the optical power transmitted through them in the spectral region where plasmonic resonance occurs and, finally, is evaluated the performance of these sensing layouts under phase interrogation when addressing the detection of variations of the surrounding medium refractive index.

4.5.1 Modelling of the Tapered Sensing Structure

The structure of the sensing head under analysis is schematically illustrated in figure 4.7. It consists of a tapered layout with a bimetallic layer coating the waist region, directly onto the fiber core (it is assumed that the cladding has been removed in the waist and tapered segments). The length of the sensing and tapered regions is assumed to be L, with ρ_i and ρ_0 being the radii of the core in the uniform ($z < 0$ and $z > L$) and sensing ($L < z < 2L$) regions, respectively. The taper angle $\Omega = \tan^{-1}[(\rho_i - \rho_0)/L]$ is assumed to be constant in the tapered regions ($0 < z < L$ and $2L < z < 3L$), and we define the taper ratio as ρ_i/ρ_0. A geometric ray methodology combined with the transfer-matrix formalism for stratified optical media is applied here, following the approach of Gupta and co-workers [180-182].

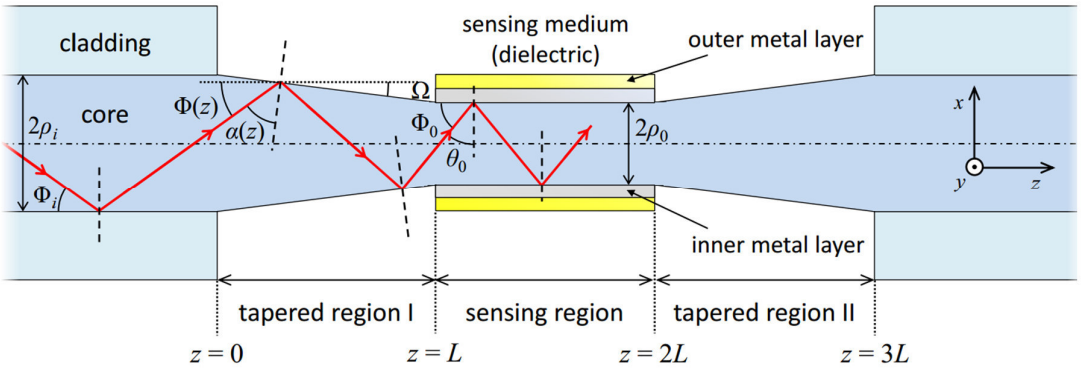

Figure 4.7 - Tapered optical fiber surface plasmon resonance sensor.

To describe the tapering effect on the propagation of a guided mode, we consider the corresponding optical ray that makes an angle Φ_i with the fiber axis. For constant doping and considering adiabatic tapering, this angle is transformed inside the tapered region according to:

$$\rho(z) \sin \Phi(z) = \rho_i \sin \Phi_i \qquad (4.1)$$

where $\rho(z)$ is the core radius at a distance z from the input end of the taper ($z = 0$). Defining α as the incidence angle of the optical ray with respect to the normal to the core/surrounding-medium interface in the tapered region I ($0 < z < L$), the previous equation may be expressed as:

$$\alpha(z) = \cos^{-1}\left(\frac{\rho_i \sin \Phi_i}{\rho(z)}\right) - \Omega \qquad (4.2)$$

where $\rho(z) = \rho_i - (z/L)(\rho_i - \rho_0)$ in the tapered region I. Equation (4.2) indicates that the angle $\alpha(z)$ depends on $\rho(z)$ for a given value of Φ_i, the angle of the propagating mode. Notice that as the radius $\rho(z)$ decreases, so does the angle $\alpha(z)$. Therefore, for a particular optical ray

launched at the input end of the taper to undergo total internal reflection throughout the entire length of the taper, the condition $\alpha(z) > \alpha_c = \sin^{-1}(n_s/n_{co})$ must be satisfied for $0 < z < L$ (n_0 and n_s are the refractive indices of the fiber core and of the surrounding medium, respectively). Using this condition together with (4.2) we arrive at an upper limit for the taper ratio ρ_i/ρ_0, given by:

$$\frac{\rho_i}{\rho_0} \leq \frac{n_0 \cos(\alpha_c + \Omega)}{NA} \tag{4.3}$$

where NA is the numerical aperture of the optical fiber. Since, in general, $\alpha_c >> \Omega$, the upper limit for the taper ratio given by (4.3) depends essentially on the type of optical fiber being used (through NA and n_{co}) and also on the sensing medium (through α_c, which depends on n_s).

In the sensing region the meridional optical ray undergoes a number of reflections given by:

$$N_{ref}(\theta_0) = \frac{L}{2\rho_0 \tan(\theta_0)} \tag{4.4}$$

where θ_0 is the angle of incidence of the optical ray with respect to the fiber/metal interface in the sensing region.

In order to evaluate the optical response of the sensing structure, we used the multilayer transfer-matrix theory applied to a four-layer system comprised of: (i) fiber-core, (ii) inner-metal, (iii) outer-metal, and (iv) probe-medium (Equation (2.81)). Since we are dealing with a multimode optical fiber, we consider that the propagation angles Φ_i of the guided modes launched at the input end of the taper ($z = 0$) are continuously distributed in the range $[0, \Phi_{i,max}]$, where $\Phi_{i,max} = \sin^{-1}(NA/n_{co})$ is the propagation angle of the guided mode with the highest order. At the output end of the taper ($z = L$), these angles are transformed by (4.1) to propagation angles Φ_0 in the range $[0, \Phi_{0,max}]$ and to angles $[\theta_{0,min}, \pi/2]$ with respect to the direction normal to the metallic coatings. The transmitted optical power at the output end of the fiber ($z = 3L$) is then given by:

$$P(\lambda) = \frac{\int_{\theta_{0,min}}^{\pi/2} [R_p(\lambda, \theta_0)]^{N_{ref}(\theta_0)} I(\theta_0) d\theta_0}{\int_{\theta_{0,min}}^{\pi/2} I(\theta_0) d\theta_0} \tag{4.5}$$

where $R_p(\lambda, \theta_0)$ is the reflectivity of the multilayer structure and

$$I(\theta_0) = \frac{n_{cl}^2 \sin\theta_0 \cos\theta_0}{1 - n_{cl}^2 \cos^2\theta_0} \tag{4.6}$$

is the intensity distribution between the continuum of guided modes.

In order to access the performance of phase interrogation of SPR based sensors supported by fiber taper structures, the (complex) Fresnel reflection coefficients r_s and r_p are expressed the polar form as:

$$r_s = |r_s|e^{i\phi_s}, r_p = |r_p|e^{i\phi_p} \tag{4.7}$$

Then, the phase difference variation $\delta\,\phi_{p,s}$ resulting from a single reflection at a given incident angle between the p and the s polarization components is:

$$\delta\phi_{p,s}(\theta_0) = \phi_p - \phi_s \tag{4.8}$$

and the total phase difference variation considering all the reflections inside the sensing region is given by:

$$\Delta\phi_{p,s}(\theta_0) = N_{\text{ref}}(\theta_0)\delta\phi_{p,s}(\theta_0) \tag{4.9}$$

Following the expressed in Chapter 3, the sensitivity of the sensing structure to the refractive index n_s of the surrounding medium is defined as

$$S_{n,\xi} = \frac{\delta\xi}{\delta n_s} \tag{4.10}$$

where $\delta\ \xi$ is the change in a given property of light (e.g. intensity, resonance wavelength or phase) due to a variation of $\delta\,n_s$ in the refractive index of the surrounding medium. Here, the focus is phase interrogation, where the property of light of interest is the phase difference $\Delta\,\phi_{p,s}$ between the p and s polarization components. In this case, the phase sensitivity to refractive index variations is then defined as $S_{n,\phi} = \delta\,(\Delta\,\phi_{p,s})/\,\delta\,n_s$.

4.5.2 Optical Transmission of the Sensing Structure

In our analysis, we have considered a step-index multimode silica optical fiber with core diameter of $2\rho_i$ = 600 μm and numerical aperture NA = 0.24. The sensing head comprises a tapered layout with a bimetallic coating on the region having uniform waist, as illustrated in figure 4.7. The bimetallic coating consists of an inner Ag layer and an outer Au layer with thicknesses 45 nm and 25 nm, respectively, and their refractive indices were obtained following the Drude Model. The sensing region had a length of L = 1 cm and the total length of the sensing head equal to 3L = 3 cm. The taper ratio ρ_i/ρ_0 varies from 1 (i.e. no taper) up to the maximum value of ~3 determined using (4.3), and the taper angle Ω changes accordingly through $\Omega\ =\ \tan^{-1}[(\rho_i - \rho_0)/L]$. The refractive index of the sensing layer is n_s= 1.333, which is the refractive index of water.

Figure 4.8 shows the transmitted optical power as function of the light's wavelength. It can be seen that for fixed bimetallic thicknesses the penetration of the evanescent wave inside the sensing region becomes deeper, with the consequent increase of the SPR peak loss. The tapering makes the angle of incidence of the rays more close to the critical angle, therefore it occurs a deeper penetration of the evanescent wave. Due to this reason, the coupling between the evanescent wave and the surface plasmon wave becomes much stronger and hence it can sense a very slight change in the refractive index of the surrounding medium, i.e., there is an increase of the device sensitivity.

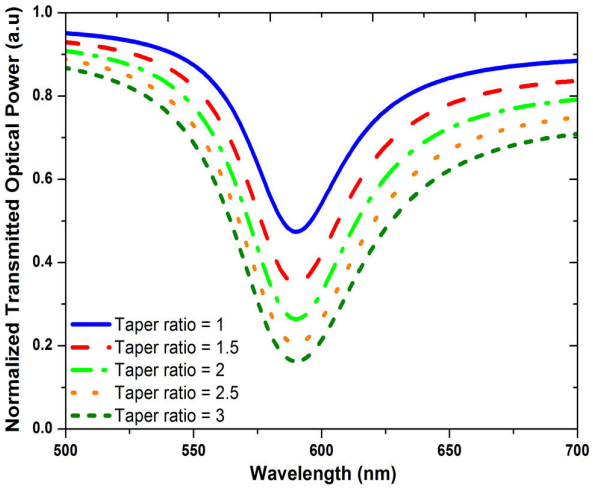

Figure 4.8 - Spectrum of the normalized transmitted optical power for a Ag-Au bimetallic sensing structure (d_1 = 45 nm – thickness of Ag layer and d_2 = 25 nm – thickness of Au layer) and different taper ratio when the surrounding medium having a refractive index of 1.333.

4.5.3 Performance of the Sensing Structure with Phase Interrogation

In this analysis the taper ratio = 2, L = 1 cm, NA = 0.25, Φ_i= 10° and the interrogation wavelength λ = 632.8 nm. First it was compared the sensing performance in phase interrogation of single-metal Au- and Ag-based structures with different thicknesses. Figure 4.9 shows the dependence of the phase difference $\Delta\phi_{p,s}$ between the TM (or p) and TE (or s) polarizations with the refractive index n_s of the surrounding medium, as well as the phase sensitivity $S_{n,\phi}$ (which corresponds to the derivative of the phase difference curves). The analysis was done for single metal layer of Au, figure 4.9(a), and Ag, figure 4.9(b), with the three different thicknesses of 50, 60 and 70 nm, values accessible to experimental validation. The best results were achieved for the thickness of 50 nm, resulting in phase sensitivities reaching 70000 degrees/RIU and 40000 degrees/RIU for Ag- and Au- single layers, respectively. The main drawback of this layout is that the refractive index values

for maximum phase sensitivity (around 1.35 for Ag and 1.31 for Au) do not correspond to the refractive indices associated with aqueous solutions.

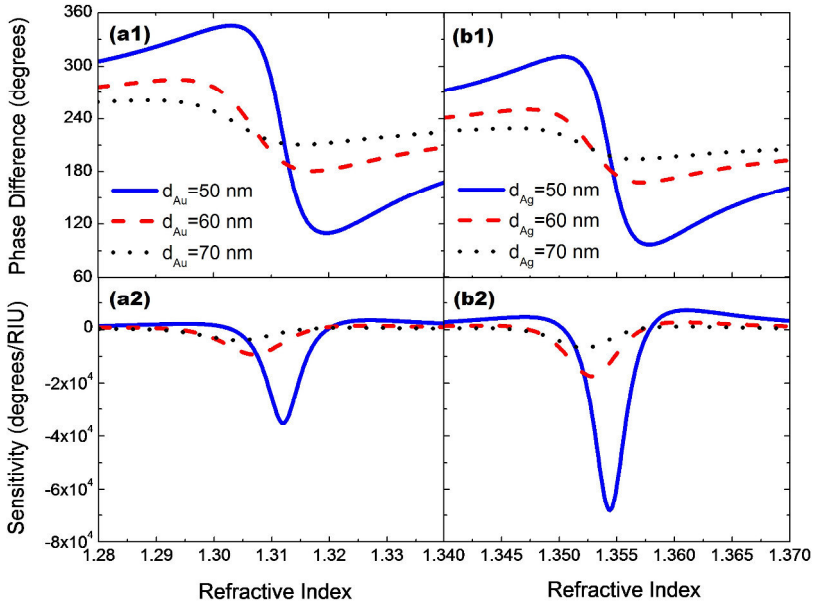

Figure 4.9 - Phase difference (between *p* and *s* polarizations) and phase sensitivity as function of the refractive index of the surrounding medium, for a single metal layer sensing structure comprised of 50, 60 and 70 nm thick (a) gold layer and (b) silver layer. The interrogation wavelength is 632.8 nm.

To overcome this issue and looking for the tuning of the operation point of the sensor, i.e., to configure it in order the sensor maximum sensitivity to occurs for a value of the external medium refractive index close to that of water, a Ag-Au bimetallic combination was studied in figure 4.10 shows the numerically calculated results for this bimetallic configuration for various combinations of (d_1, d_2), keeping constant the overall thickness at 50 nm.

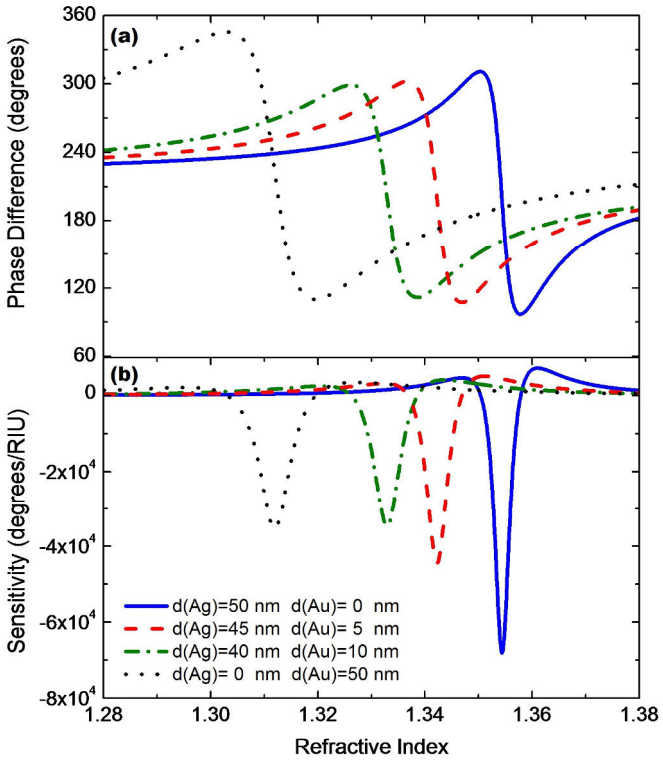

Figure 4.10 - Phase difference (between p and s polarizations) and phase sensitivity as function of the refractive index of the surrounding medium for different bimetallic sensing head combinations.

It can be observed that for the Ag-Au sensing head with d_1 = 40 nm (Ag) and d_2= 10 nm (Au) the maximum phase sensitivity occurs for refractive index values around 1.333, which is the refractive index of water at the interrogation wavelength considered. An additional positive feature of this structure is its enhanced chemical stability when compared with Ag-based SPR sensors.

Keeping this thickness combination, the phase difference $\Delta\phi_{p,s}$ and the phase sensitivity $S_{n,\phi}$ as function of the refractive index of the surrounding medium was investigated for different taper ratios (figure 4.11). It can be seen that $\Delta\phi_{p,s}$ varies between an upper and lower limiting values whose separation increases with increasing the taper ratio. This arises from the deeper penetration of the evanescent waves into the metals (in the sensing region), causing the phase of the p-polarization to become larger as compared to the s-polarization. Regarding the phase sensitivity $S_{n,\phi}$, one observes a variation by a factor of ~2 when different taper ratios are considered, reaching values up to 60000 degrees/RIU in the region around n_s = 1.333, the optimum working region at this interrogation wavelength. It can also be seen that tapering does not cause any shift in the optimum working region.

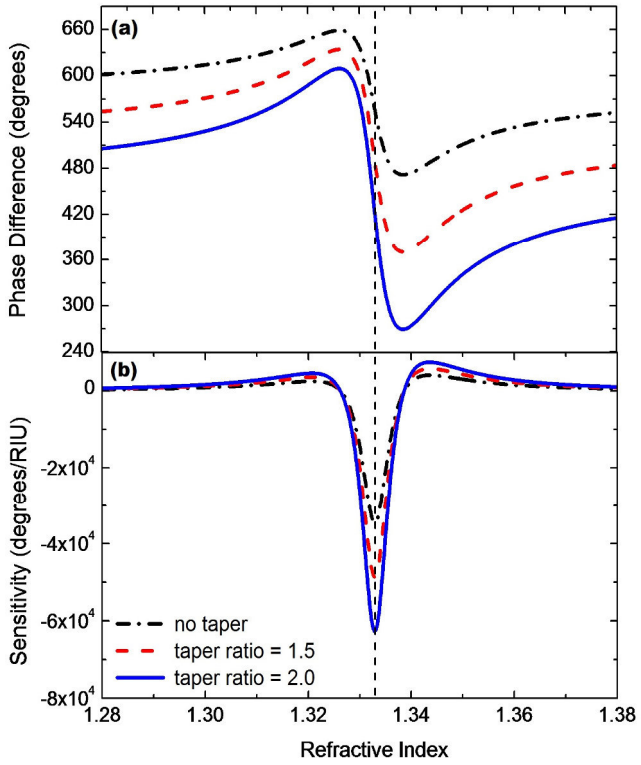

Figure 4.11 - (a) Phase difference (between *p* and *s* polarizations) as function of the refractive index of the surrounding medium and (b) associated phase sensitivity, for Ag-Au bimetallic structures (d_1 = 40 nm and d_2 = 10 nm) having different taper ratios. The interrogation wavelength considered is 632.8 nm, and the dashed vertical line at n_s = 1.330 indicates the point having maximum phase sensitivity.

The observation of figure 4.11 indicates the maximum phase sensitivity for an interrogation wavelength of 632.8 nm occurs when the refractive index of the surrounding medium is close to n_s = 1.333. It is important to identify the region of the SPR resonance spectrum associated with this value of n_s where maximum phase sensitivity to variations of n_s takes place. With this objective, the transmitted TM (p-polarized) optical power spectrum is plotted in figure 4.12 for the Ag-Au bimetallic sensing structure with taper ratio = 2, immersed in a surrounding medium with n_s = 1.333. It can be seen the interrogation wavelength associated with the maximum phase sensitivity (represented by the vertical line) corresponds to the SPR wavelength, a consequence of the Kramers-Kronig relations from where derives that in resonance the phase slope variation reaches a maximum.

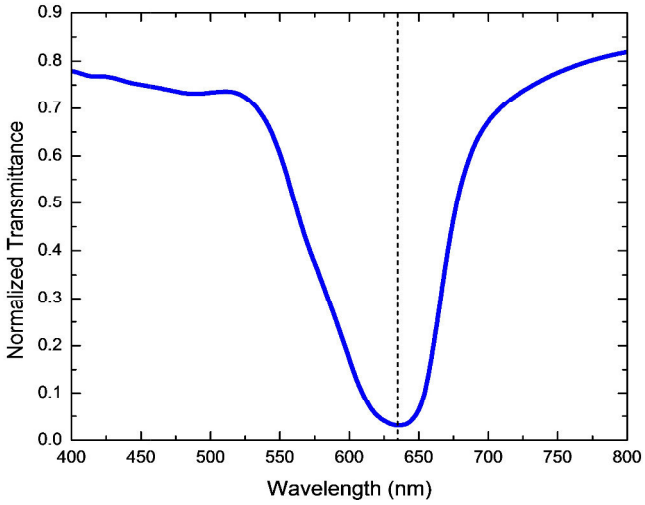

Figure 4.12 - Spectrum of the normalized transmitted optical power for the Ag-Au bimetallic sensing structure (d_1 = 40 nm and d_2 = 10 nm) with taper ratio = 2.0 and surrounding medium having a refractive index of 1.333. The dashed vertical line at 632.8 nm indicates the interrogation wavelength corresponding to maximum phase sensitivity.

Actually, the fact that the maximum phase sensitivity occurs in the SPR resonance, therefore with low level of optical power, may degrade the signal-noise ratio to a point that such high sensitivity does not have impact in the final phase reading resolution. Therefore, in principle shall be considered to operate in a wavelength where there is enough transmitted optical power, meaning the choice of an wavelength located in either side of the SPR transmittance curve. Its exact value may be determined from the compromise of sensitivity and available optical power to reach maximum refractive index resolution. This topic will be investigated next chapter in the context of another optical fiber based SPR sensing layout.

4.6 Optical Fiber SPR Sensor with Bimetal Layers in a Tip (Optrode)

As reported before, along the years a large number of fiber based sensing head layouts have been proposed to measure a broad range of parameters, relying on diverse interaction mechanisms of the measurand with the optical field One of the most attractive of those layouts is the reflective fiber tip configuration, where the sensor functionality occurs at the end of the optical fiber, therefore readily allowing point sensing at remote locations[183]. These fiber sensing devices are commonly identified as fiber optrodes, a generalization of the initial meaning of the word optrode, the combination of the words “optics” and “electrode”, indicating it strictly refers to the modulation of the optical field by the electric characteristics of an electrode which interacts with the targeted measurand [184]. To a large degree, fiber optrodes include a membrane at the tip of the fiber with its fluorescent and spectroscopic properties changing with the variation of the

measurand (typically a chemical or biochemical entity), inducing an intensity/spectral modulation of the light that returns along the fiber which is also the illumination channel [185]. However, other operation modes are possible, with particular importance the one associated with refractometry, where the sensing head is sensitive to the refractive index of the surrounding medium, which by itself can show a specific dependence with a certain chemical or biochemical parameter [186]. In such cases the SPR approach is a natural one, therefore in this section it is reported the study performed when the optrode layout in a tapered geometry and coupled to the plasmonic resonance phenomenon in a bimetal configuration is addressed.

To some extent, the organization of the section replicates the one delivered in the previous section, i.e., it starts by presenting the model used to study the properties of the sensing structure which, in broad terms, follows what was presented before with the modifications requested in view of the optrode layout, but then moves straightway to the analysis of the device sensing performance under phase interrogation.

4.6.1 Modelling the Optrode Sensing Structure

Figure 4.13 shows an optical fiber tip optrode with linear profile, in which the conical surface is coated with a double metal layer. The cone end is coated with a reflective thin film. The tip length is assumed to be L, ρ_0 and ρ_L denote the radii of fiber core and tip end, respectively.

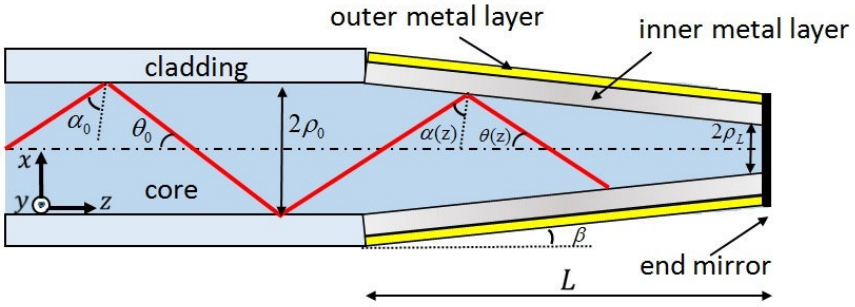

Figure 4.13 - Schematic illustration of the SPR fiber optrode under analysis. The top and bottom of the probe are polished to the same angle. The cladding of the optical fiber tip has been removed in the sensing region and replaced by a bimetallic film.

If θ_0 represents the propagation angle that the optical ray makes with the axis of the fiber, it is transformed to an angle θ(z) inside the taper following the transformation relation:

$$\rho_0 sin\theta_0 = \rho(z) sin\theta(z) \tag{4.11}$$

where ρ(z) is the taper radius at a distance z from the input end of the taper (z = 0). In the taper region, such optical ray reaches the interface with the metal-dielectric film at an angle of incidence, α(z), at coordinate z, which is related with the value α_0 in the non-tapered region as:

$$\alpha(z) = \cos^{-1}\left(\frac{\rho_0 \cos\alpha_0}{\rho(z)}\right) - \beta \tag{4.12}$$

where $\rho(z) = \rho_0 - (z/L)(\rho_0 - \rho_L)$ is the tip radius with the coordinate z and $\beta = \tan^{-1}\left(\frac{\rho_0 - \rho_L}{L}\right)$ is the taper angle. Notice that as the radius $\rho(z)$ decreases, so does the angle $\alpha(z)$. Therefore, for a particular optical ray launched at the input end of the taper to undergo total internal reflection throughout the entire length of the taper, the condition $\alpha(z) > \alpha_c = \sin^{-1}(n_s/n_{co})$ must be satisfied for $0 < z < L$ (n_s and n_{co} are the refractive indices of the surrounding medium and fiber core, respectively). Since $\alpha(z)$ becomes smaller along the propagation and considering (4.12), the above condition is fulfilled when

$$\cos^{-1}\left(\frac{\rho_0 \cos\alpha_0}{\rho_L}\right) - \beta > \alpha_c \tag{4.13}$$

This is the basic equation which permits to analyze the two relevant situations, namely for a fixed angle α_0 what is the maximum length of the optrode (taper) to keep the condition of total reflection along its length and the other way around, i.e., for a fixed taper length what is the minimum value for α_0.

Considering the first of these two situations, regarding (4.13) and assuming a fixed angle of incidence, the maximum taper length is:

$$L > \frac{\rho_0 - \rho_L}{tan\left[cos^{-1}(\frac{\rho_0 \cos\alpha_0}{\rho_L}) - \alpha_c\right]}, \tag{1.14}$$

On the other hand, when L is fixed, the minimum angle of incidence must satisfy:

$$\alpha_0 > cos^{-1}\left[\frac{\rho_L}{\rho_0} cos[\beta + \alpha_c]\right]. \tag{4.15}$$

The angle range of the rays at the coordinate z alters to $[\alpha_1(z), \alpha_2]$ due to the variation of fiber core diameter, where

$$\alpha_1(z) = cos^{-1}\left(\frac{\rho_0 cos\theta_{cr}}{\rho(z)}\right) - \beta, \tag{4.16}$$

$$\alpha_2 = \frac{\pi}{2} - \beta, \tag{4.17}$$

where $\theta_{cr} = \sin^{-1}(n_{cl}/n_{co})$ is the critical angle (n_{cl} and n_{co} are the refractive indices of the fiber cladding and core, respectively) [187].

The normalized transmitted optical power through the sensing region of the fiber tip follows equations (4.5) and (4.6) with the necessary adaptations

$$P_{trans} = \frac{\int_0^L dz \int_{\alpha_1(z)}^{\alpha_2} [R_p]^{N_{ref}} I(\theta) d\theta}{\int_0^L dz \int_{\alpha_1(z)}^{\alpha_2} I(\theta) d\theta}. \tag{4.18a}$$

where

$$I(\theta) = \frac{n_{cl}^2 \sin\theta\cos\theta}{(1 - n_{cl}^2 \cos^2\theta)} \tag{4.18b}$$

is the intensity distribution between the continuum of guided modes (assuming meridional excitation), R_p is the reflectivity of the multilayer structure and N_{ref} is the number of reflections the optical ray with propagation angle θ undergoes in the sensing region [40].

In order to evaluate the number of reflections, it is considered a length dL of the taper region around the coordinate z where the radius of the taper is ρ(z), as illustrated in figure 4.14.

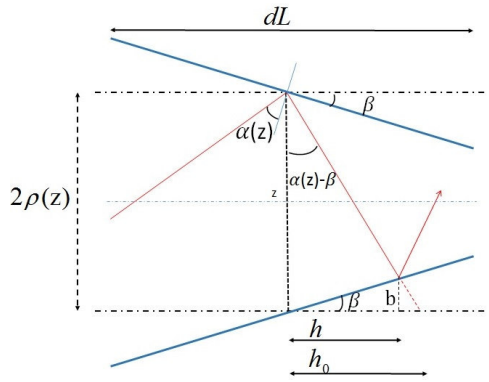

Figure 4.14. Schematic of a length *dL* of the taper region around the coordinate z where the radius of the taper is ρ(z).

With regard to this figure, $\tan(\beta) = b/h$ and $\tan[\alpha(z) - \beta] = (h_0 - h)/b$, therefore

$$h = \frac{h_0}{1 + \tan(\beta)\tan[\alpha(z) - \beta]}. \tag{4.19}$$

also,

$$h_0 = 2\,\rho\,(z)\tan[\alpha(z) - \beta] \tag{4.20}$$

With these relations, the equation for the longitudinal length advanced when the ray propagates from one side of the taper to the other is given by

$$h = \frac{2\rho(z)\tan[\alpha(z) - \beta]}{1 + \tan\beta\,\tan[\alpha(z) - \beta]} \tag{4.21}$$

The ray is reflected in the lower taper surface and propagates upwards towards the upper taper surface. To simplify, we can consider the same length h is advanced by the ray associated with this

upwards propagation (actually, the real value is smaller than h). Therefore, in the distance $2h$ we have a reflection, which means in the distance dL the number of reflections is

$$\delta N = \frac{1 + \tan(\beta)\tan[\alpha(z) - \beta]}{4\,\rho\,(\mathrm{z})\tan[\alpha(z) - \beta]}dz \tag{4.22}$$

Considering the full taper length, the number of reflections can be calculated as

$$N_{one\ path} = \int_0^L \frac{1 + \tan(\beta)\tan[\alpha(z) - \beta]}{4\,\rho\,(\mathrm{z})\tan[\alpha(z) - \beta]}dz \tag{4.23}$$

Since the configuration works in reflection, the total number of reflections is given by:

$$N_{ref} = 2N_{one\ path} = \int_0^L \frac{1 + \tan(\beta)\tan[\alpha(z) - \beta]}{2\rho(\mathrm{z})\tan[\alpha(z) - \beta]}dz \tag{4.24}$$

with $\alpha(z)$ given by (4.20). In order to access the performance of phase interrogation of SPR sensors supported by fiber structures, it is convenient to express the amplitude reflection coefficients r_s and r_p in the polar form as

$$r_s = |r_s|e^{i\phi_s}, r_p = |r_p|e^{i\phi_p}. \tag{4.25}$$

AS before, if $\left(\delta\phi_{p,s}\right)_j = \left[(\phi_p - \phi_s)_j\right]$ is the phase shift of the light between the p and s polarizations for reflection j, the total phase shift accumulated by the light that propagates in the optrode is given by

$$(\phi_p - \phi_s)_{total} = 2\sum_{j=1}^{N_{one\ path}} (\phi_p - \phi_s)_j. \tag{4.26}$$

The situation is somehow simplified if it is determined an average phase shift per reflection. At the input of the taper the angle of incidence can be considered to be α_0, which corresponds to a phase shift of $\left(\delta\phi_{p,s}\right)_{\alpha_0} = (\phi_p - \phi_s)_{\alpha_0}$; at the end of the taper the phase shift is $\left(\delta\phi_{p,s}\right)_{\alpha(L)} = (\phi_p - \phi_s)_{\alpha(L)}$, with $\alpha(L)$ obtained from (4.12) when $\rho(z) = \rho_L$. Therefore, an approximation for this average phase shift is given by:

$$(\delta\phi_{p,s})_{average} = \frac{(\delta\phi_{p,s})_{\alpha_0} + (\delta\phi_{p,s})_{\alpha(L)}}{2} \tag{4.27}$$

and the total phase shift accounting for all reflections inside the sensing region is:

$$\Delta\phi_{p,s} \equiv (\phi_p - \phi_s)_{total} = N_{ref}(\delta\phi_{p,s})_{average} \tag{4.28}$$

The evaluation of phase sensitivity is done with the same approach that was explained for the tapered structure regarding (4.10).

4.6.2 Performance of the Sensing Structure with Phase Interrogation

The analysis performed considered a multimode silica fiber with core diameter $2\rho_1$ = 600 μm, numerical aperture of 0.24 and sensing region L = 1 cm. The bimetallic combination consists of an inner Ag layer and an outer Au layer with thicknesses d_1 and d_2, respectively, and their refractive indices were fitted from experimental data available in the literature [163-166]. Concerning the metallic layers, the studies performed and reported before indicated that an Ag-Au sensing head with d_1 = 40 nm (Ag) and d_2 = 10 nm (Au) shows maximum phase sensitivity for refractive index values around the water value of 1.333. Accordingly to equation (4.24), the number of reflections is $N_{ref} = 14$. As mentioned in the prior section, the phase shift introduced in each reflection was assumed constant, the average of phase shift at the beginning of the taper $(\delta\phi_{p,s})_{\alpha_0} = (\phi_p - \phi_s)_{\alpha_0}$, with $\alpha_0 = 79^\circ$, and at the end of the taper $(\delta\phi_{p,s})_{\alpha(L)} = (\phi_p - \phi_s)_{\alpha(L)}$, with $\alpha_L = 68°$.

Figure 4.15 shows the effects of tip end radii in the phase difference $\Delta\phi_{p,s}$ and phase sensitivity $S_{n,\phi}$ as function of the refractive index of the surrounding medium for an interrogation wavelength of 632.8 nm. The observation of this data indicates the phase sensitivity increases when the tip end radius decrease, reaching a value of 1.25×10^5 degrees/RIU (at n_s = 1.333) when the radii of tip end is 150 μm.

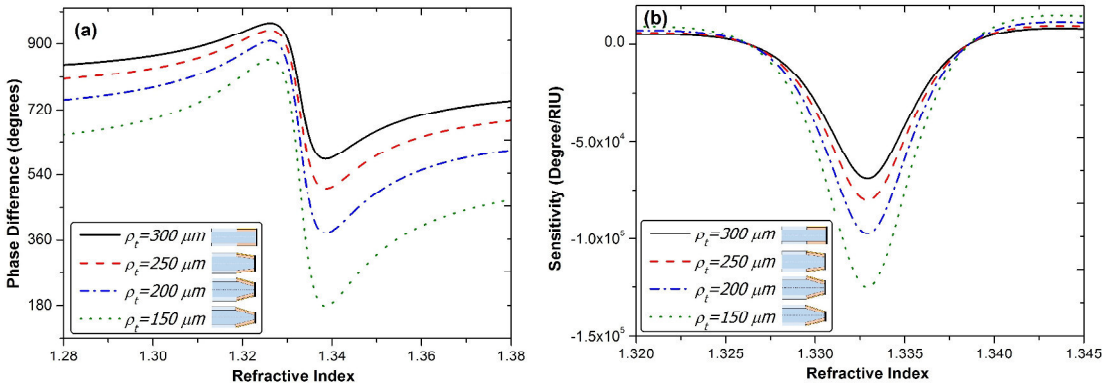

Figure 4.15 - Variation of (a) phase difference (between *s* and *p* polarizations) and (b) phase sensitivity as function of the refractive index of the surrounding medium for different radii of the tip end. The sensing structure comprised of a 40 nm silver + 10 nm gold layer and tip length of 1 cm. The interrogation wavelength is 632.8 nm.

It was also investigated the effects of optrode length in the phase difference between *s* and *p* polarizations when the tip end radius is 150 μ*m*. The results are shown in figure 4.16. The analysis of this data permits to conclude the phase sensitivity decreases when the tip length becomes smaller. Indeed, it reaches a value of 1.25×10^5 degrees/RIU for a tip length of 10 mm, which is reduced to 4.25×10^4 when such length is reduced to 4 mm.

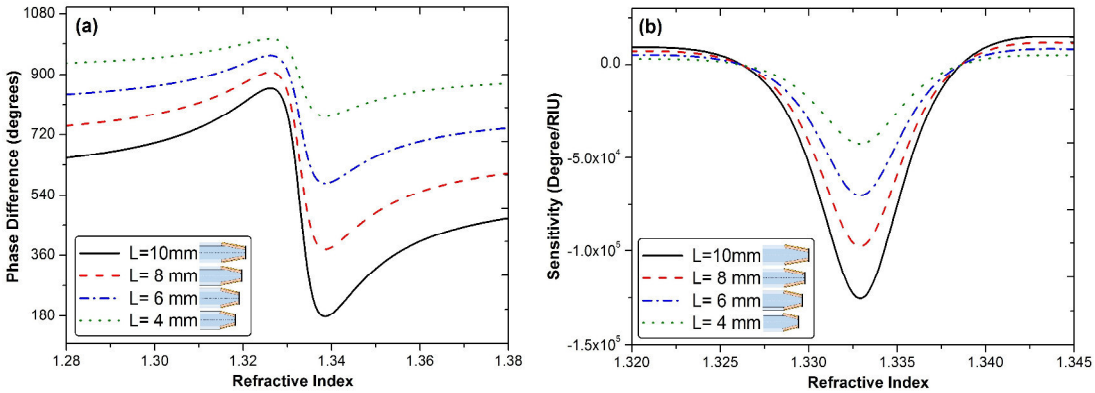

Figure 4.16 - Variation of (a) Phase difference (between *s* and *p* polarizations) and (b) phase sensitivity as function of the refractive index of the surrounding medium for different tip length. The sensing structure comprised of a 40 nm silver + 10 nm gold layer and the tip end radius is 150 μm. The considered interrogation wavelength is 632.8 nm.

The analysis presented here permits to guide the design of fiber optrodes highly sensitive to the surrounding medium refractive index by plasmonic interaction at a certain wavelength window and considering phase reading. The bimetallic combination is an effective approach, but other possibilities may be considered, particularly when looking for operation at other wavelength regions (mostly important around 1550 nm for sensing network applications), which can be achieved incorporating an outer oxide layer. This operation wavelength shift of fiber optic SPR based sensing structures is a topic addressed next chapters.

4.7 Conclusion

This Chapter addressed the study of optical fiber based SPR sensing structures incorporating a single metal or a bimetallic layer when phase interrogation is the readout technique. The metals included in this study were silver, gold, copper, and aluminum, and for the bimetallic configuration were considered the tapered and the tip (optrode) optical fiber geometric layouts.

The Chapter started by stating the motivations to analyze bimetallic layers instead of the usual single metal layer when optical fiber sensing structures based on the SPR phenomenon are under concern. Then, on the basis of the model exposed in Chapter 2, it was numerically evaluated the performance of single metal layer phase interrogated SPR sensors in standard optical fiber when targeting the measurement of refractive index changes of the surrounding medium. This provided the context to introduce the analysis of bimetallic configurations, the focus of the next section of the Chapter. Such analysis was later expanded to include two different sensor geometric layouts, one the transmissive tapered structure and the other the tip (optrode) reflective arrangement, which implied to adapt the previously developed theoretical approach to permit the numerical

evaluation of the performance of all these sensor patterns and, consequently, be able to determine their absolute and relative performances.

The results delivered in this chapter were obtained from a theoretical/computational analysis, not including experimental validation. On the strategy under way at the Center of Applied Photonics of INESC TEC to research and develop novel SPR sensing structures in optical fiber platforms/waveguides, all these components are tackled in a coherent plan involving several researchers, in particular PhD students, with complimentary focus, the one reported here connected to the study and modelling of these devices looking to guide the experimental work and to permit sensor performance optimization.

The phenomenon of plasmonic resonance associated with the metals addressed in this chapter typically occurs in the visible region of the electromagnetic spectrum, independently of being considered a single metal layer or a bimetal one. Theses wavelengths are not adequate for propagation of light in the standard optical fibers used in optical communication systems due to the presence of high losses. Indeed, theses fibers are designated for optimum light propagation in the spectral region around 1550 nm. Therefore, it would highly convenient to have SPR resonance at these wavelengths, which means the need to consider other layers in addition to the metal one. This is the topic to be addressed next chapter.

5

Optical Fiber SPR Sensing Structures with Hybrid Layers

Summary: *This chapter presents a theoretical investigation of optical fiber surface plasmon resonance sensors incorporating an internal metallic layer of silver covered with an oxide layer. The objective is to shift the resonance condition to longer wavelengths, therefore more suited to benefit from a broad range optical fiber technologies developed along the years within the context of optical fiber communications systems. Different oxide materials like titanium dioxide, silicon dioxide and aluminum oxide are considered aiming to achieve increased/enhanced sensitivity to refractive index variations of the external medium, particularly when addressing phase interrogation.*

5.1 Introduction

As exposed in detail in previous chapters, the resonant interaction of light with free electrons in metals originates loss bands in the light spectrum with a central wavelength that depends on the properties of the metal as well as of the surrounding medium, particularly its refractive index. This dependence is the principle of optical sensing based in plasmonics where, similarly to sensing structures based on fiber Bragg gratings and distributed feedback fiber lasers, the measurand information is encoded on the wavelength position of a spectral signature, with all the benefits which result from this characteristic [188].

As also indicated before, in the development process of SPR sensing soon it was recognized the obvious advantages of using the optical fiber as the SPR platform, starting by the fact of propagation in these waveguides in most of the cases is supported by the effect of total internal reflection, also central in plasmonic phenomena. Therefore, it has been observed a trend towards the consideration of the optical fiber as the privileged platform for SPR sensing [189]. Consequently, most of the recent developments in this field involve the combination of the optical fiber with nanostructures whose manufacturing became possible with the advances of the Nanosciencies and Nanotechnologies. It is the case of SPR layouts involving the combination of metal and oxide layers on the optical fiber surface, enabling the tailoring of the sensor performance, most notably its sensitivity and wavelength operation region [190].

On this context it is important to emphasize the efforts oriented to apply fiber optic SPR sensing structures at the third telecommunications window (around 1550 nm). Historically, it is known that SPR sensors have been focused to detect refractive indices of aqueous media, which means they are projected to be sensitive in the range of the refractive index of water (≈1.33). In the vast majority of the studies reported the optical fiber based SPR sensors operate around 640 nm, some in the 830 nm region, which are wavelengths where the availability of high-performance fibre optic components is reduced. To take advantage of the highly developed fiber optic technology, SPR fiber sensing must migrate to the third telecommunication window, surprisingly a move that has been quite slow. With bulk optics, SPR films have been designed to exhibit resonances in the 1500 nm region [191], and in this wavelength window a fiber optic taper-based SPR sensing head was reported for refractive index detection in the region of 1.44 [192]. Some years ago, it was demonstrated a 1500 nm fiber optic SPR sensor for aqueous media refractive index measurement based on a combination of a tilted fiber Bragg grating and a SPR film structure deposited at a lapped cladding region of the fibre [193]. The results reported indicate the feasibility of this approach, but it would be interesting to have a systematic approach to design and model the performance of fiber optic SPR sensors operating at these wavelengths.

This Chapter reports results obtained from a theoretical analysis of optical fiber based SPR sensors incorporating a double layer structure, an internal metallic silver (Ag) layer covered by an oxide layer. The analysis covers three different fiber geometries, the standard one where there is no change in the fiber geometry and a transmission layout is assumed, a tapered transmissive topology and a tapered reflective structure (tip or optrode identified configuration). The performance of these sensing structures is dependent on the interrogation technique considered with most of the results reported in this chapter associated with the phase interrogation approach.

5.2 General Considerations

The theoretical fundamentals of plasmonics outlined in Chapter 2 indicate almost any metallic layer with a dielectric medium attached can support a surface plasmon wave. The propagation constant of the surface plasmon wave propagating at the interface between a semi-infinite dielectric and metal can be written as,

$$k_{SP} = k_0 \sqrt{\frac{\varepsilon_m n_d^2}{\varepsilon_m + n_d^2}}, \tag{5.1}$$

where k_0 is the free space wave number, ε_m the dielectric constant of the metal ($\varepsilon_m = \varepsilon_m' + i\varepsilon_m''$) and n_d the refractive index of the dielectric. From equation 5.1 the surface plasmon wave may be supported by the structure providing the following relation is fulfilled:

$$\varepsilon_m' < -n_d^2. \tag{5.2}$$

At optical wavelengths, this condition is verified by several metals, gold and silver being the preferred materials for applications [105]. As discussed on Chapter four, Gold demonstrates a higher shift of resonance parameter to changes in the refractive index of sensing layer and is chemically stable. Silver, on the other hand, displays a narrower width of the SPR curve, favouring a higher SNR or detection resolution. The sharpness of the resonance curve depends upon the imaginary part of the dielectric constant of the metal. Therefore, silver which has a larger value of the imaginary part of the dielectric constant, shows a narrower width of the SPR curve, leading to a higher SNR or detection resolution. In what concerns the shift of the resonance curve it depends on the real part of the dielectric constant of the metal. This is larger in the case of gold than for silver and hence gold demonstrates a higher shift of resonance parameter to changes in the refractive index of sensing layer. Unfortunately, despite the great performance on sensing silver is too susceptible to oxidation.

A variety of other metals can sustain surface plasmon resonance, the basic condition the need to have conduction band electrons able to resonate with light at the appropriate wavelength. However, some of them are too reactive, as is the case of sodium (Na). Others are too broad in their SPR response, as copper or aluminum (Cu, Al). Although, the capabilities of copper (Cu) and aluminum (Al) for SPR sensor applications have also been analysed and it was established both metals have the ability to be used for SPR sensor sensing. Like silver, copper has the problem to be chemically vulnerable against oxidation and corrosion, therefore its protection is required for a stable sensing application.

The oxidation problems can be overcome introducing a cover dielectric layer between the metal layer and the external medium under measurement. Some of the dielectrics that can be used as the second dielectric layer are MgF_2, Ta_2O_5, SiO_2 or TiO_2 [194, 195], but there are some constraints associated with the utilization of this interface dielectric, the most relevant one the reducing of the sensor sensitivity since it is located just at the maximum of the surface plasmon wave field. Consequently, in the first days of SPR sensing, where the device platforms were built assembling bulk optics components, the inclusion of an interface dielectric layer was not popular, also because visible light sources were readily available permitting to induce plasmonic behaviour in these structures, with the additional bonus the alignment procedure could be performed with direct eye vision.

The situation started to change when the optical fiber moved to be an effective platform for SPR sensing. Now, the alignment issue was intrinsically solved but the working wavelength became a problem due to the propagation losses in the fiber, from one side, and also considering it would be rather convenient to work in the spectral region where the optical communication systems operate, so the plethora of high performance fiber optic devices became accessible with acceptable cost. Both factors pointed out to the high convenience to have optical fiber SPR based sensing structures tailored to work in the 1550 nm wavelength region. This could be achieved with the metals above indicated if a dielectric layer is included between the metal and the external medium, consequently the research oriented to have fiber optic structures of this type showing high refractive index sensing performance around 1550 nm became a rather hot topic.

This Chapter reports the study developed on this subject when the dielectric interface layer is an oxide. In particular, were analysed in detail fiber optic SPR sensing structures when the interface layer is titanium dioxide (TiO_2), silicon dioxide (SiO_2) and aluminum oxide (Al_2O_3).

5.3 Optical Fiber SPR Sensors with Metallic and Oxide Layers

The structure of the sensing head under analysis is schematically illustrated in figure 5.1. The sensing region is an uncladded fiber coated with a metallic layer followed by a layer of oxide material. The length of the sensing region is assumed to be L, ρ_0 the radius of the core and θ_0 the angle of incidence of the optical ray with respect to the normal to the core-cladding interface.

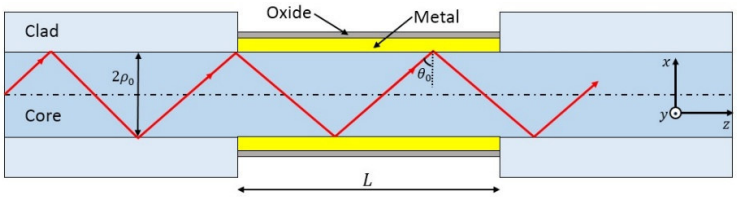

Figure 5.1 - Schematic illustration of the SPR sensing head under analysis. The cladding of the optical fiber has been removed in the sensing region and replaced by a metallic film covered with an oxide overlayer.

The choice of the metal for the internal layer was determined by the best performance achieved concerning the phase sensitivity of the double layer structure. Silver was found to be the most adequate metal, with the shape of the SPR resonance versus thickness of the silver layer (without the presence of the external oxide layer) shown in figure 5.2. The data shown was obtained assuming a silica fiber with 100 μm core diameter, numerical aperture of 0.24 and an uncladded length L = 1 cm. The refractive indices for the several materials mentioned in this Chapter were obtained from experimental data available in the literature [163-166].

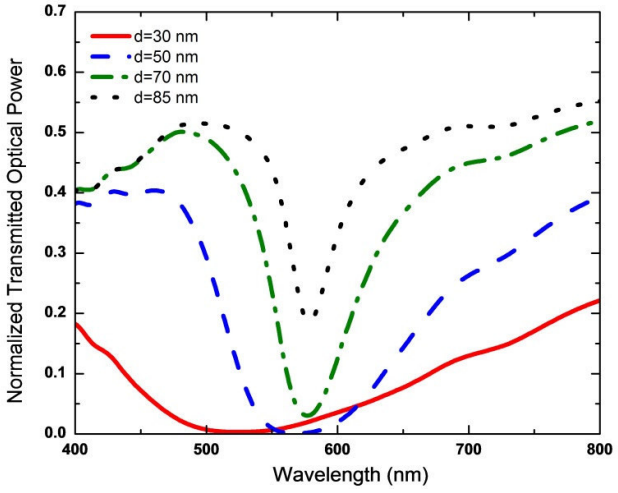

Figure 5.2 - Resonance of a fiber optic SPR structure with a single silver layer for several thicknesses (refractive index of the external medium: 1.33).

A relevant information is to establish the thickness of this silver layer that provides the best sensing performance when the oxide outer layer is added. When the silver layer is considered

alone the data of figure 5.2 indicates a thickness of 70 nm is the one which originates the SPR resonance with the most adequate characteristics for sensing. However, when the silver layer is combined with an outer layer of oxide, the thickness of 50 nm for the silver layer is the one that provides the best sensor performance, so this value was set for the analysis delivered in this Chapter.

Three different oxide materials were considered for the outer oxide layer, titanium dioxide (TiO_2), silicon dioxide (SiO_2) and aluminum oxide (Al_2O_3). It is known that the introduction of this layer modifies substantially the characteristics of the SPR resonance, most notably the spectral region where it appears [190]. This can be checked by the observation of figure 5.3 which shows the location and shape evolution of the resonance for different thicknesses of the oxide layer. The SPR sensing head is assumed to be surrounded by a non-dispersive external medium with refractive index of n_s = 1.33.

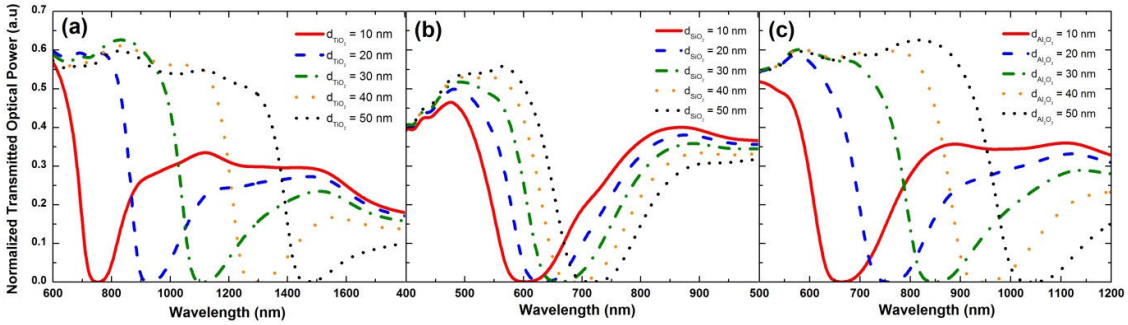

Figure 5.3 - Spectral behaviour of the double layer fiber optic SPR structure for different thicknesses of the oxide layer (TiO_2, SiO_2 and Al_2O_3 oxide materials are associated with (a), (b) and (c), respectively; refractive index of the external medium: 1.33).

The inclusion of a TiO_2 layer permits the largest displacement of the spectral response of the SPR resonance, turning possible to locate it within the 830, 1300 and 1550 nm telecommunication bands by adjusting the layer thickness within an interval technically feasible. This has also implications in the width of the resonance, which consistently becomes larger when it moves to longer wavelengths, as is shown in figure 5.4 which displays the spectral width of the resonance versus the thickness of the oxide layer.

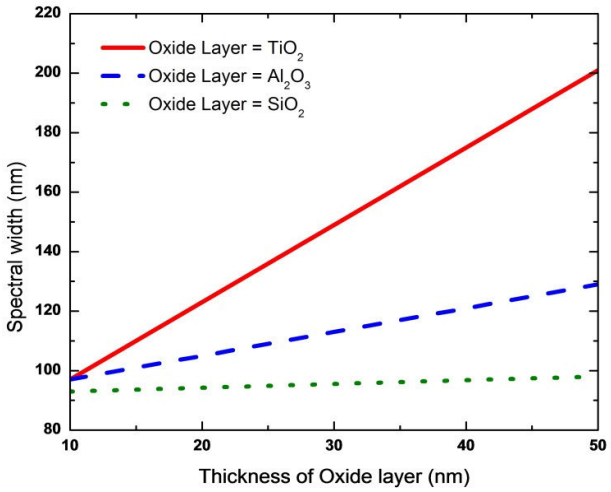

Figure 5.4 - Evolution of the spectral width of the SPR resonance (full width at the power level 6 dB above the minimum) as function of the thickness of the oxide layer. The refractive index of the external medium is assumed to be 1.33.

When addressing phase interrogation of the optic fiber based SPR sensing structure, a single oscillation angle of the light in the fiber, associated to a specific propagation mode, shall be considered (oscillation angle defined by the fiber axis and the light ray). The higher the numerical aperture of the fiber the larger this angle can be, meaning a smaller incident angle in the interface core-cladding of the fiber. In the fiber length where SPR occurs this condition favors the introduction of a larger phase difference $\Delta\phi_{p,s}$ between the TM and TE polarizations of the light in the reflection process, increasing the sensitivity to variations of the refractive index of the surrounding medium, n_s. Therefore, it is advantageous to consider an incident angle in the core-metallic layer interface just near the critical angle in the cladded fiber, which is $\theta_c \approx 80.5°$ for a fiber with numerical aperture of 0.24. As such, the phase interrogation analysis was performed assuming $\theta = 80.5°$.

Figure 5.5 shows the normalized transmittance and the phase difference $\Delta\phi_{p,s}$ versus n_s for layouts with TiO_2 and Al_2O_3 layers of 15 nm and 30 nm, respectively, which enable to operate the sensor in the first telecommunications window (the data is shown for λ = 830 nm; from the data shown in figure 5.3 (b), this wavelength is not accessible by considering a SiO_2 layer).

The analysis of this data shows that the maximum of the refractive index phase sensitivity occurs for n_s = 1.330 and for the case of the Titanium Dioxide layer, reaching a value of 3.2×10^6 degrees/RIU, while for the situation of aluminum oxide layer the value is 3.0×10^6 degrees/RIU for n_s = 1.328. In both cases, the condition of maximum phase sensitivity is on the SPR resonance, where the transmitted optical power is rather low. This means almost no light to detect, therefore decreasing substantially the signal-to-noise ratio. As such, a compromise

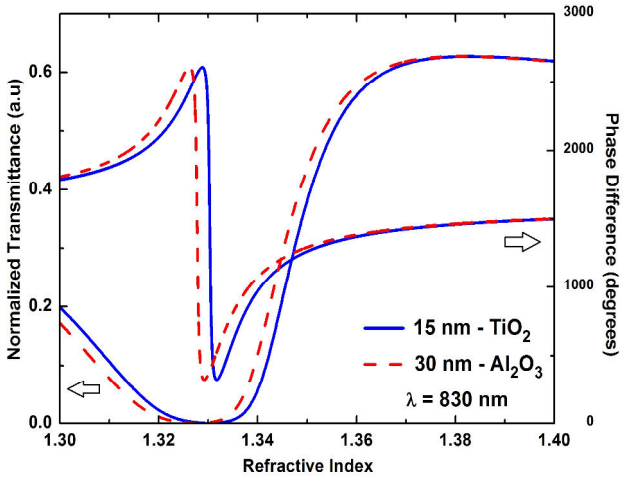

Figure 5.5 - Normalized transmittance and phase difference (between p and s polarizations) as function of the refractive index of the surrounding medium for an inner silver layer of 50 nm combined with a TiO_2 layer of 15 nm (solid curves) and a Al_2O_3 layer of 30 nm (dashed curves). The interrogation wavelength is 830 nm.

is needed so that the phase sensitivity is degraded to a certain extent while the signal-noise-ratio in the detection process increases, therefore reaching a situation of maximum resolution in the measurement of n_s.

For the sensing head to operate in the second (1300 nm) and third (1550 nm) telecommunications spectral windows, the observation of figure 5.3 indicates the need to consider an external layer of TiO_2 with thicknesses of 40 and 55 nm, respectively. The normalized transmittance and $\Delta\phi_{p,s}$ versus n_s are shown in figure 5.6.

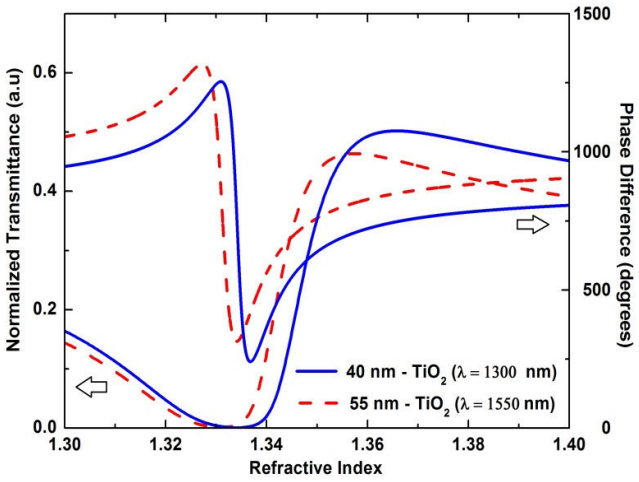

Figure 5.6 - Normalized transmittance and phase difference (between p and s polarizations) as function of the refractive index of the surrounding medium for an inner silver layer of 50 nm combined with a TiO_2 layer of 40 nm (solid curves) and a TiO_2 layer of 55 nm (dashed curves), associated to interrogation wavelengths of 1300 nm and 1550 nm, respectively.

From these results it turns out the maximum phase sensitivity has the value of 5.6×10^5 degrees/RIU (at n_s = 1.334) and 3.3×10^5 degrees/RIU (at n_s = 1.332) when the interrogation wavelengths are 1300 and 1550 nm, respectively.

As already outlined, when considering SPR sensors supported by optical fiber platforms it is advantageous to operate within these telecommunications windows, particularly the one in the 1550 nm region, due to a wide availability of high performance optical fiber technology at a relatively low cost, allowing the design and implementation of sensing structures with rather favorable characteristics.

As mentioned before, maximum phase sensitivity occurs in a region close to the dip of the SPR resonance, therefore with low level of optical power, which will degrade the signal-noise ratio to a point that such high sensitivity does not have impact in the final phase reading resolution. Therefore, shall be considered to operate in a wavelength where there is enough transmitted optical power, which means in principle it can be located in either side of the SPR transmittance curve. To investigate this aspect, it was analyzed the achievable phase sensitivity for different levels of transmittance in both sides of the SPR resonance, for the case being selected the situation associated with figure 5.6 and relative to an operating wavelength of 1300 nm. The results obtained are shown in figure 5.7.

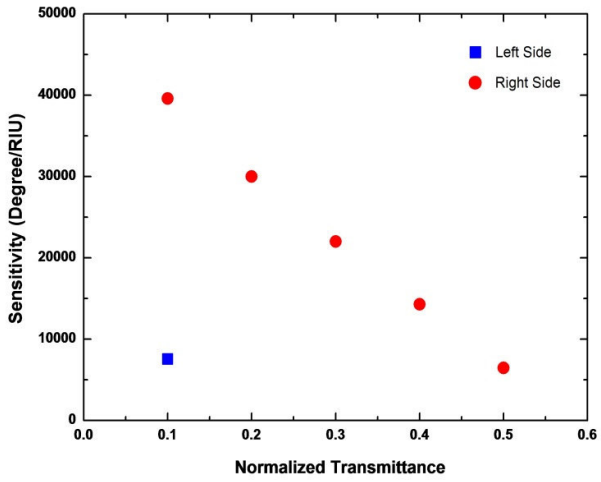

Figure 5.7 - Phase sensitivity versus normalized transmittance for a fiber optic SPR structure with an inner silver layer of 50 nm combined with a TiO_2 layer of 40 nm (interrogation wavelength of 1300 nm).

With the wavelength fixed, to access different transmittance levels means different refractive index of the surrounding medium. As expected from the observation of figure 5.3(a), due to the asymmetry of the SPR resonance, its left side provide limited freedom to the choice of the

operating pair (transmittance, sensitivity), indicating the preference to work out in the right side of the resonance.

Optical sensors based in the SPR phenomenon are inherently highly sensitive to variations of the external medium refractive index, permitting to detect very small changes of this measurand, for example variations induced by biochemical processes. Therefore, it is in the context of biochemical sensing that these devices are rather appellative, pointing out the relevance of optimizing their performance in the situation where the external medium is water. Consequently, for each type of the oxide layer it was determined the appropriate thickness in order to attain maximum sensitivity at the refractive index of water evaluated at the sensor operating wavelength.

Figure 5.8 shows the maximum phase sensitivity obtained when the operation wavelengths are 630 nm (a) and 830 nm (b). The most immediate outcome of the analysis of this data is that for the case of operation at 630 nm it is possible to find the required thickness for the oxide materials considered, TiO_2, SiO_2 and Al_2O_3. However, when moving to 830 nm, the layer of SiO_2 leaves to be an option, as the results shown in figure 5.3(b) already indicated.

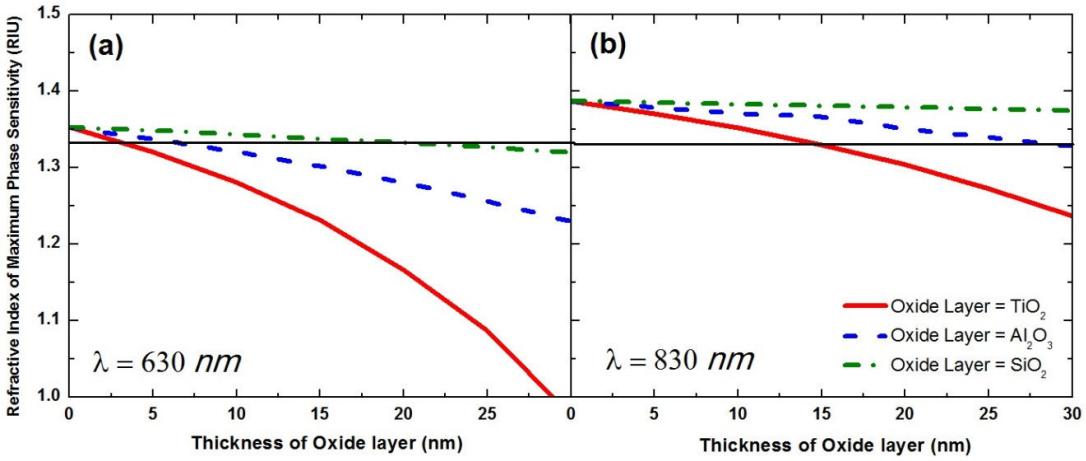

Figure 5. 8 - Thickness of the oxide layer required to operate with maximum sensitivity to changes of the refractive index of water, determined by the intersection of the horizontal line (that defines in the y-axis the water refractive index at the wavelength of operation) with the curves associated with different materials for the oxide layer. The interrogation wavelength is 630 nm (a) and 830 nm (b).

Figure 5.9 gives similar results but now considering as operating wavelengths 1300 nm (a) and 1550 nm (b). Again, the titanium dioxide option for the external layer permits to address operation at both wavelengths, eventually being feasible to consider a layer of aluminum oxide for 1300 nm interrogation, associated with a tackiness of ~86 nm, which is still technically feasible.

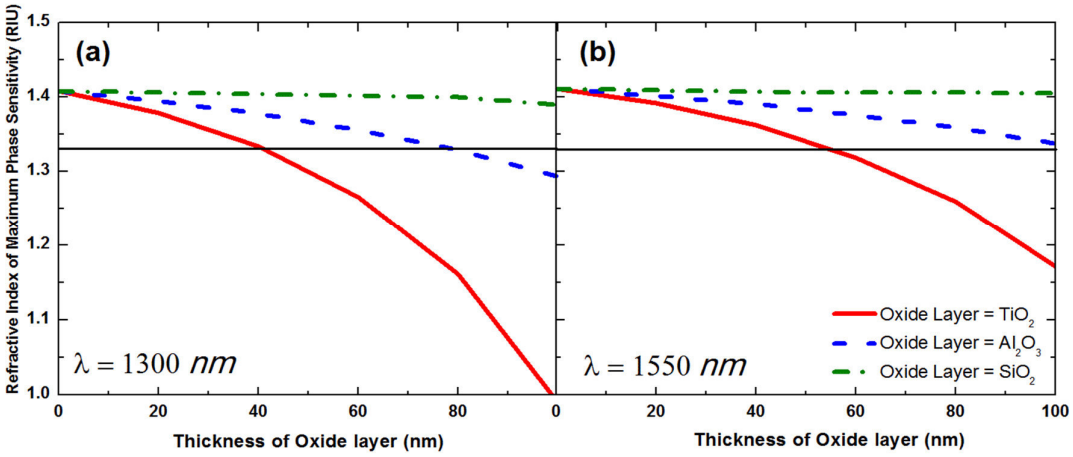

Figure 5.9 - Same as Fig. 5.8 but now with interrogation wavelengths of (a) 1300 nm and (b) 550 nm.

To summarize this section, the analysis presented here permitted to identify the main characteristics of SPR fiber optic sensing structures with a double layer of metal/oxide, particularly when phase interrogation is under concern, a readout approach which has been scarcely analyzed before. Two of these characteristics are particularly relevant, one the possibility to tune the sensor sensitivity to variations of the refractive index of the surrounding medium, the other the amenability to tune the measurement operation to a specific wavelength region, most notably the one around 1550 nm to benefit from the large portfolio of high performance fiber optic components available at these wavelengths. It was found the inclusion of an internal silver layer of 50 nm thickness permits the better performance for any of the three different oxide materials considered for the external layer (TiO_2, SiO_2, and Al_2O_3). Also, the results obtained shows the better flexibility is provided by the inclusion of a layer of titanium dioxide, approach that is compatible with tuning the sensor operation to a large wavelength window that includes operationally important wavelengths (630, 830, 1300 and 1550 nm).

5.4 Optical Fiber SPR Sensor with Metallic and Oxide Layers in a Tapered Transmissive Topology

In this section the same approach described above to analyze combinations of metallic and oxide layers which was done for normal optical fibers is implemented when tapered optical fibers are addressed. The structure of the sensing head under analysis is illustrated in figure 5.10. It consists of a fiber layout with a metal layer covered by an oxide layer. The length of the sensing region is assumed to be L, ρ_0 the radius of the core and θ_0 the angle of incidence of the optical ray with respect to the normal to the core-cladding interface. The modelling of this structure follows the approach presented in Chapter 4.

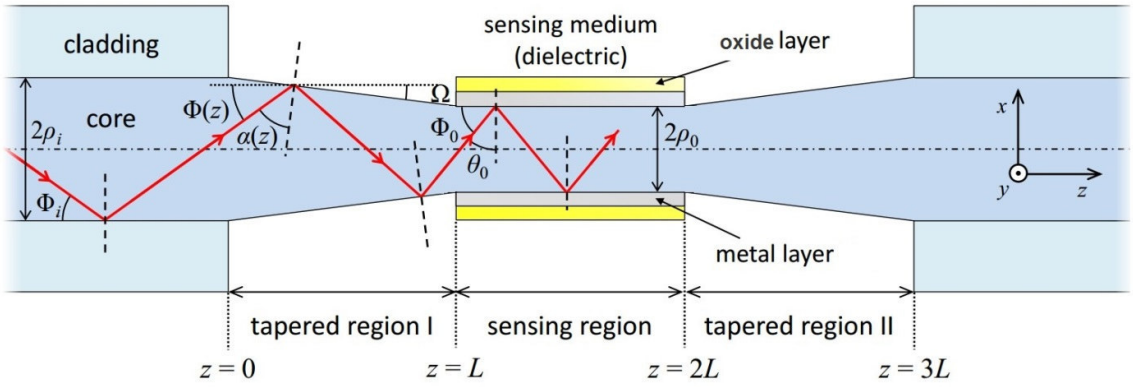

Figure 5.10 - Schematic illustration of the SPR fiber taper geometry under analysis.

It was considered a step-index multimode silica optical fiber with core diameter of $2\rho_i$ = 600 μm and numerical aperture NA = 0.24. The sensing head comprises a tapered layout with a metal + oxide coating on the region having uniform waist, as illustrated in figure 5.10. The sensing region has an extension of L = 1 cm, and the total length of the sensing head equals 3L = 3 cm. The taper ratio ρ_i/ρ_0 = 2 and the oscillation angle considered in this analysis is Φ_i= 10°. The SPR sensing head is assumed to be surrounded by a non-dispersive external medium with refractive index of n_s = 1.33.

As explained in the last section, when considering the sensor sensitivity the most adequate metal for the inner layer of silver. The thickness of this layer is also an important parameter, therefore it shall be chosen the value that optimizes de sensor performance. Figure 5.11 gives the SPR resonance for several values of the silver layer thickness (without the presence of the external oxide layer). When this layer is combined with an outer layer of oxide, the thickness of 80 nm for the silver layer provides the best sensor performance, so this value was set for the analysis from where comes out the results delivered in the following.

Figure 5.12 shows the effect of a coating layer with 20 nm of different oxides (TiO_2, Al_2O_3 and SiO_2) over a 80 nm layer of Ag, for two different interrogation wavelengths, (a) 632.8 nm and (b) 1550 nm. In this figure the phase difference between *s* and *p* polarizations and the corresponding phase sensitivities were considered. Notice that for a particular overlay material, the refractive index of the surrounding medium is different in the situation of resonance in each wavelength, as it should be because the other three degrees of freedom (oscillation angle, layers thicknesses and wavelength) are fixed.

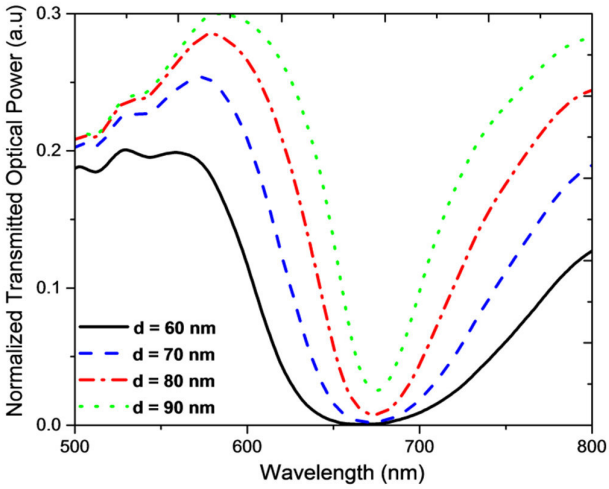

Figure 5.11 - Resonance of a fiber optic SPR structure with a single silver layer for several thicknesses (refractive index of the external medium: 1.33).

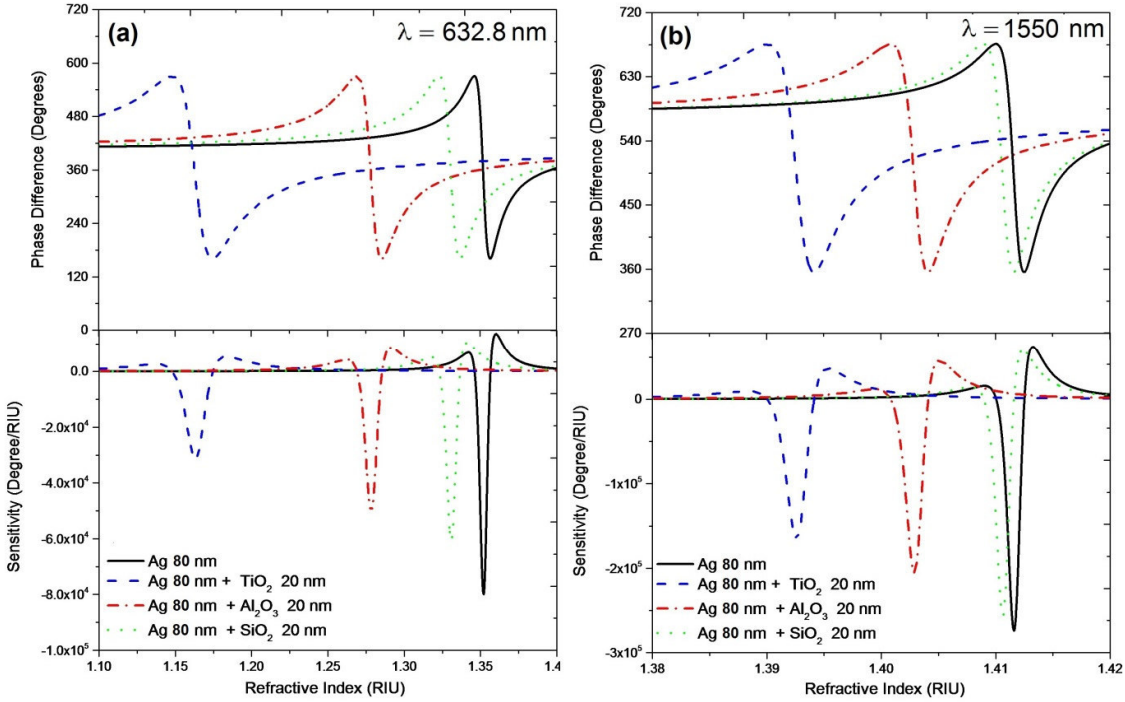

Figure 5.12 – Phase difference between the *s* and *p* light polarizations and associated phase sensitivity versus the refractive index of the surrounding medium for a single silver layer with 80 nm thickness and when this layer is covered by 20 nm of an oxide layer of TiO_2, Al_2O_3, and SiO_2. The interrogation wavelength is (a) 632.8 nm and (b) 1550 nm.

As expected, the introduction of an oxide layer decreases the phase sensitivity of the sensing structure to the refractive index of the surrounding medium. In the situation of a 632.8 nm interrogation wavelength, such reduction reaches values of ~60% and ~ 25% for the cases of TiO_2 and SiO_2 overlays, respectively. When this wavelength is 1550 nm, the performance improves with

the above figures getting the values of ~40% and ~ 10%. The case of the Al_2O_3 overlay stands in an intermediate position.

Following the approach applied for the situation of a normal optical fiber and outlined in the context of figure 5.8, to obtain maximum phase sensitivity close to the refractive index of water (n_s = 1.333 at 632.8 nm, and n_s = 1.318 at 1550 nm) were determined the required thickness values of the oxide layer. They were 3.8 nm, 7.4 nm and 22.0 nm for operation at 632.8 nm, and 55.5 nm, 106.0 nm and 507.0 nm considering the wavelength of 1550 nm, for overlays of TiO_2, Al_2O_3, and SiO_2 respectively

The inclusion of an oxide layer has also the benefit already identified when addressing an optical fiber with standard geometry, i.e. the shifting of the SPR resonance. This phenomenon is illustrated in figure 5.13. It can be seen that an oxide overlay of 20 nm thickness changes the spectral resonance more pronounced for the case of TiO_2.

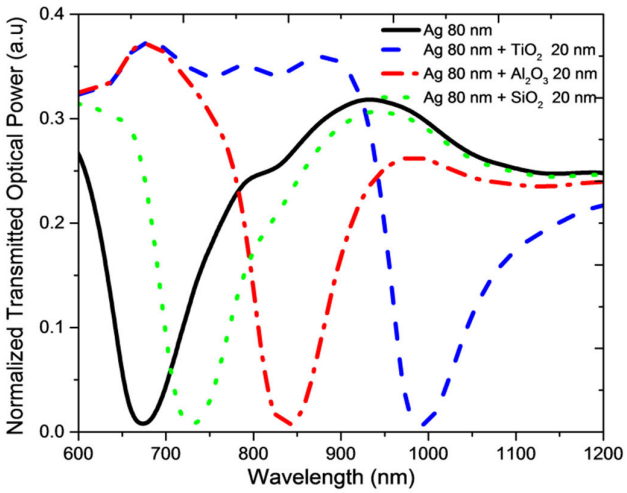

Figure 5.13 - Spectral behavior of the double layer fiber optic SPR structure with a single silver layer and 20 nm of oxide layers (TiO_2, Al_2O_3, and SiO_2) when the refractive index of the external medium is 1.33.

5.5 Optical Fiber SPR Sensor with Metallic and Oxide Layers in a Tip (Optrode) Geometry

The tip (optrode) geometry was studied in Chapter 4 within the context of fiber SPR structures incorporating bimetal layers. Following the same approach this configuration can be readily analyzed when the combination (inner metal layer, oxide layer) is addressed. It is shown in figure 5.14, where the conical surface is coated with an Ag thin film followed by a layer of oxide material; the cone end is coated with a reflective thin film. The tip length is assumed to be L, and ρ_0 and ρ_L have the usual meanings, i.e., denote the radii of fiber core and tip end, respectively.

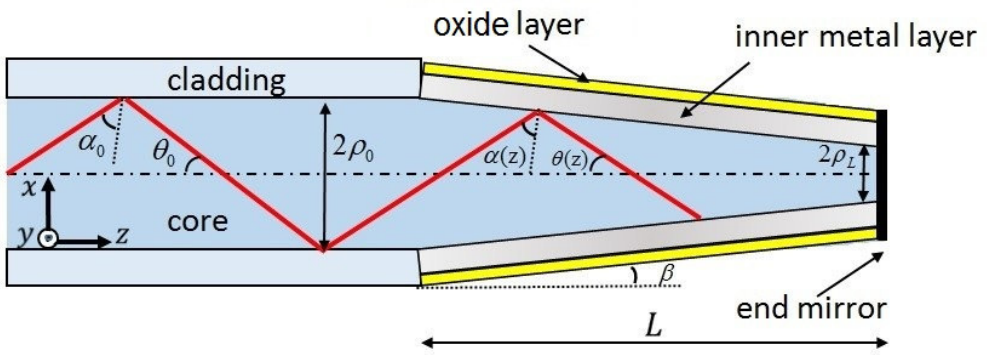

Figure 5.14 - Schematic illustration of the SPR fiber optrode under analysis. The top and bottom of the probe are polished to the same angle. The cladding of the optical fiber tip has been removed in the sensing region and replaced by a metallic film covered with an oxide overlayer.

In this analysis, it was considered a multimode silica fiber with 100 μm core diameter with numerical aperture of 0.24, tip end diameter 60 μm and sensing region L = 1 cm. Accordingly, the number of reflections estimated is N_{ref}=60. The refractive indices for the thin film materials were obtained from experimental data available in the literature [163-166]. Concerning the metallic layer, we have found in a previous study that silver is the most adequate one [196].

Figure 5.15 shows the spectrum of the light returning from the sensing head for different thicknesses of the silver layer and, when combined with the spectral curves obtained when the oxide layer is included, it turns out the best thickness for the silver layer is 80 nm, so this value was set for the analysis that provided the results delivered in the following.

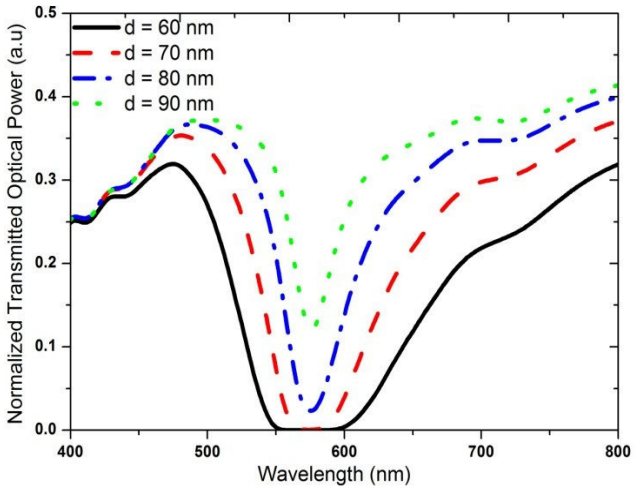

Figure 5.15 - Spectra of the normalized returned optical power for a fiber optic SPR structure with a single silver layer for several thicknesses (refractive index of the external medium: 1.33).

For the outer oxide layer, three different oxide materials were compared, titanium dioxide (TiO_2), silicon dioxide (SiO_2) and aluminum oxide (Al_2O_3). It is known that the introduction of this layer modifies substantially the characteristics of the SPR resonance, most notably the spectral region where it appears [190]. Figure 5.16 shows the location and shape evolution of the resonance for different thicknesses of the oxide layer. The SPR sensing head is assumed to be surrounded by a non-dispersive external medium with refractive index of n_s = 1.33.

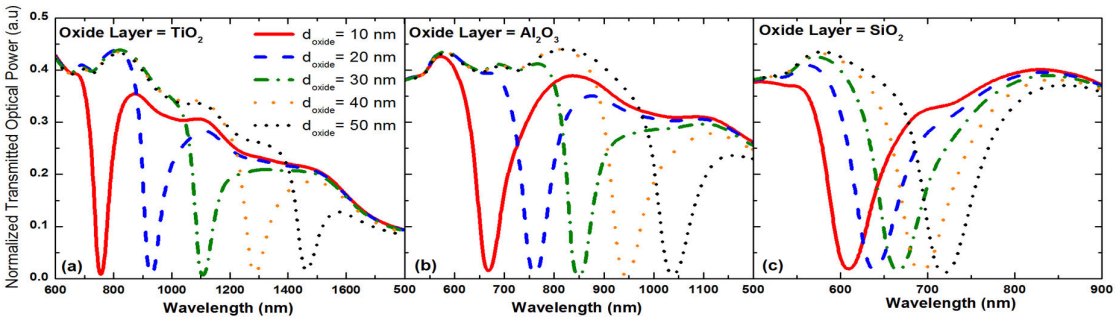

Figure 5.16 - Spectral behavior of the double layer fiber optic SPR structure for different thicknesses of the oxide layer (TiO_2, SiO_2 and Al_2O_3 oxide materials are associated with (a), (b) and (c), respectively; refractive index of the external medium: 1.33).

The data in this figure indicates the inclusion of a TiO_2 layer permits the largest displacement of the spectral response of the SPR resonance, making it possible to locate it within the 830, 1300 and 1550 nm telecommunication bands by adjusting the layer thickness within an interval technically feasible. Also, there are consequences in the width of the resonance, which consistently becomes larger when it moves to longer wavelengths, as is shown in figure 5.17 which displays the spectral width of the resonance versus the thickness of the oxide layer.

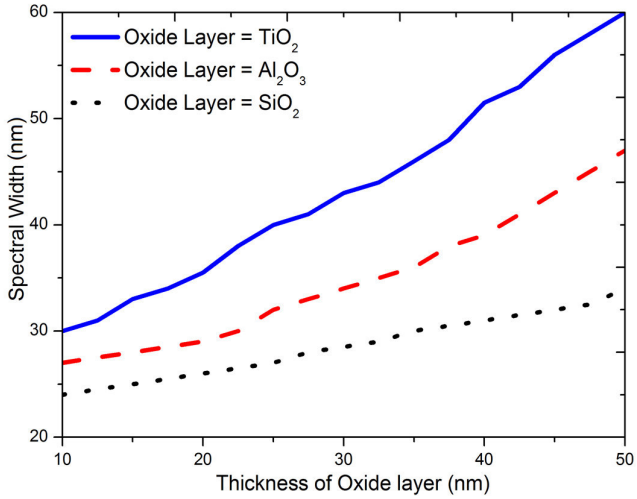

Figure 5.17 - Evolution of the spectral width of the SPR resonance (full width at the power level 6 dB above the minimum) as function of the thickness of the oxide layer. The refractive index of the external medium is considered to be 1.33.

To perform the study of phase interrogation of fiber optic based SPR sensing structures, a single oscillation angle of the light in the fiber, associated to a specific propagation mode, shall be considered (oscillation angle defined by the fiber axis and the light ray). The higher the numerical aperture of the fiber the larger this angle can be, meaning a smaller angle of incidence in the interface core-cladding of the fiber. In the fiber length where SPR occurs this condition favors the introduction of a larger phase difference $\Delta\phi_{p,s}$ between the TM and TE polarizations of the light in the reflection process, increasing the sensitivity to variations of the refractive index of the surrounding medium, n_s. As mentioned in the prior section, the phase shift introduced in each reflection was assumed constant, the average phase shift at the beginning of the taper is $\left(\delta\phi_{p,s}\right)_{\alpha_0} = (\phi_p - \phi_s)_{\alpha_0}$, with $\alpha_0 = 80^\circ$, and at the end of the taper $\left(\delta\phi_{p,s}\right)_{\alpha(L)} = (\phi_p - \phi_s)_{\alpha(L)}$, with $\alpha_L = 73$.

Figure 5.18 shows the normalized transmittance and the phase difference $\Delta\phi_{p,s}$ versus n_s for layouts with TiO_2 and Al_2O_3 layers of 15 nm and 30 nm, respectively, which enable to operate the sensor in the first telecommunications window (the data is shown for λ = 830 nm; from the data given in figure 5.16(c), this wavelength is not accessible by considering a SiO_2 layer). The analysis of the results shows the maximum of the refractive index phase sensitivity, $S_{n,\phi} = \delta(\Delta\phi_{p,s})/\delta n_s$, occurs close to n_s = 1.330, with a value of 5.72×10^4 degrees/RIU for the case of the titanium dioxide layer, while for the situation of aluminum oxide layer a slightly smaller value is obtained (5.57×10^4 degrees/RIU for n_s = 1.327). In both cases, maximum phase sensitivity is close to the SPR resonance, where the transmitted optical power is rather low. This means almost no light to detect, therefore decreasing substantially the signal-to-noise ratio. As such, a compromise is needed so that the phase sensitivity is degraded to a certain extent while the signal-noise-ratio in the detection process increases, therefore reaching a situation of maximum resolution in the measurement of n_s. Further analysis on this topic is delivered below.

For the sensing head to operate in the second (1300 nm) and third (1550 nm) telecommunications spectral windows, the observation of figure 5.16 indicates the need to consider an external layer of TiO_2 with thicknesses of 40 and 55 nm, respectively. The normalized transmittance and $\Delta\phi_{p,s}$ versus n_s are shown in figure 5.19. Regarding these results it turns out the maximum phase sensitivity has the value of 4.11×10^4 degrees/RIU (at n_s = 1.335) and 3.1×10^4 degrees/RIU (at n_s = 1.332) when the interrogation wavelengths are 1300 and 1550 nm, respectively.

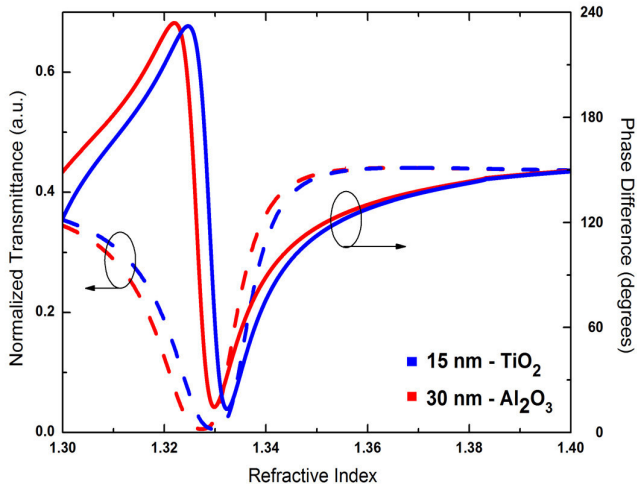

Figure 5.18 - Normalized transmittance and phase difference (between *p* and *s* polarizations) as function of the refractive index of the surrounding medium for an inner silver layer of 80 nm combined with a TiO_2 layer of 15 nm (solid curves) and a Al_2O_3 layer of 30 nm (dashed curves). These thicknesses were considered to allow operation wavelength around 830 nm.

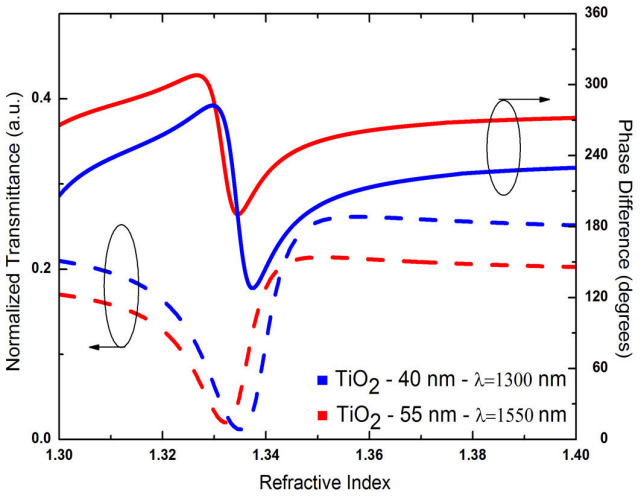

Figure 5.19 - Normalized transmittance and phase difference (between *p* and *s* polarizations) as function of the refractive index of the surrounding medium for an inner silver layer of 80 nm combined with a TiO_2 layer of 40 nm (solid curves) and a TiO_2 layer of 55 nm (dashed curves),associated with interrogation wavelengths of 1300 nm and 1550 nm, respectively.

As briefly outlined above, since maximum phase sensitivity occurs in a region close to the dip of the SPR resonance the available optical power level is rather low, which will degrade the signal-noise ratio to a point that such high sensitivity does not have impact in the final phase reading resolution. Therefore, it shall be considered to operate in a wavelength where there is enough transmitted optical power which, in principle, means it can be located in either side of the SPR

transmittance curve. To investigate this aspect, it was analyzed the achievable phase sensitivity for different levels of transmittance in both sides of the SPR resonance, for the case being selected the situation associated with figure 5.19, i.e. relative to an operating wavelength of 1300 nm. The results obtained are shown in figure 5.20.

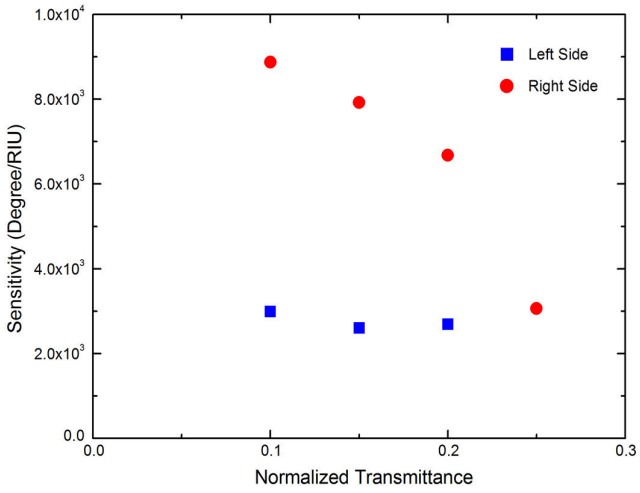

Figure 5.20 - Phase sensitivity versus normalized transmittance for a fiber optic SPR structure with an inner silver layer of 80 nm combined with a TiO_2 layer of 40 nm (interrogation wavelength of 1300 nm).

With the wavelength fixed, to access different transmittance levels means a different refractive index of the surrounding medium. As expected from the observation of figure 5.16(a), due to the asymmetry of the SPR resonance, its left side provides limited freedom to the choice of the operating pair (*transmittance, sensitivity*), indicating the preference to work out in the right side of the resonance. This statement is confirmed by the results shown in figure 5.20 which indicates, for example, that for a normalized transmittance level of 0.2, the right side of the SPR resonance permits a phase sensitivity of ~7×10^3 degrees/RIU, value that reduces to ~2.8×10^3 degrees/RIU when the left side is selected.

5.6 Conclusion

This Chapter addressed the study of optical fiber based SPR sensing structures incorporating a hybrid overlay, with an inner layer of metal and a dielectric outside layer. The metal considered was silver and the dielectrics were oxide materials, specifically titanium dioxide, silicon dioxide and aluminum oxide. The analysis of these structures developed focusing on the reading of the variations of the light phase difference between the p and s polarization states induced by variations of the refractive index of the surrounding medium. Another central element was the study of the dependence of the resonance wavelength on the characteristics of the oxide overlay,

which permits to tailor the operation wavelength to a spectral window more amenable to the optical fiber technology, most notably to the spectral region around 1550 nm due to its widespread utilization in optical communications.

Three different fiber configurations were considered, one associated with the standard fiber geometry and the other two with tapered and tip (optrode) layouts. In all cases was studied the phase sensitivity to variations of the external medium refractive index and analyzed the consequences of the spectral region of maximum phase sensitivity be located at the plasmonic resonance wavelength, meaning reduced levels of optical power which implies a degradation of the signal-to-noise ratio, therefore of the device phase sensitivity. It was outlined a strategy to attenuate this situation by selecting the operation wavelength in order to be located at the side of the spectral resonance, its precise position determined by a compromise between available optical power and phase sensitivity in order to obtain the maximum readout resolution.

As already indicated in previous chapter, the results presented here were obtained from a theoretical/computational analysis, not including experimental validation. Some clues of how to acquire such validation will be delivered in Chapter 7.

6

Grating Assisted Optical Fiber Sensing Structures Supported by Plasmonics

Summary: *This Chapter deals with the integration of fiber gratings with standard fiber optic SPR sensing technology to bring it to the singlemode domain, therefore turning it compatible with the vast field of fiber optic communication systems with its large portfolio of advanced and cost effective components and devices. In particular, emphasis is allocated on the theoretical analysis of long period grating (LPG) assisted optical fiber sensing structures supported by Plasmonics. It is concluded this (LPG + SPR) combination brings to the forefront the phase interrogation of SPR sensors and are outlined paths for the experimental investigation of interrogation techniques of this type, including advanced ones as the Pound-Drever-Hall interferometric interrogation approach.*

6.1 Introduction

In previous chapters were analyzed from a theoretical and computational point of view fiber optic sensing structures supported by the phenomenon of plasmonic resonance where the fiber cladding is removed to perform the deposition of the metallic thin film. Several configurations were investigated, starting with the basic one in which the cladding is removed but the core geometry is kept, and proceeding to potentially more favorable structures associated with fiber tapering and its particular but rather important case of the optrode (reflective) layout. Single metal layer, double metal layers and the hybrid (metal and dielectric) pattern were the subject of study. These structures require fibers with large cores to support light rays with oscillation angles (modes) large enough to induce plasmonic resonance with a fairly high Q-factor, which means they are not compatible with the optical fiber technology developed for optical communications which stands on singlemode propagation. This is certainly a relevant limitation for the application of fiber optic based SPR sensors because they require components and devices specific for this application with the inherent cost increase, contrary to would happen if the fiber singlemode approach become compatible with SPR sensing so, in such case, the remarkably large portfolio of fiber optic components, optical sources, optical detectors and optical systems developed within the realm of optical fiber communications would become readily available when addressing the development of SPR based optical fiber sensors.

As a matter of fact, it is possible to turn compatible these two worlds by the introduction of a connection element and for optical fibers it exists, the fiber grating, with its two main materializations, the Fiber Bragg Grating (FBG) and the Long Period Grating (LPG). The combination (FBG + SPR) in optical fibers have been the target of several studies looking to the development of fiber optic sensors operating within the domain of fiber optic single mode technology. The same cannot be stated when addressing the combination (LPG + SPR), which actually has the potential to support the development of high performance fiber sensors mostly when phase interrogation is applied. The circumstance this interrogation approach is rarely considered in SPR based fiber optic sensing may explain the reduced focus on LPGs within this context.

This Chapter presents some clues of how such combination (LPG + SPR) can be addressed to reach workable fiber optic sensing devices. It is also proposed its coupling to an highly sensitive interferometric technique that may progress SPR optical sensing to new measurement performance levels. The Chapter is organized in the following way. It starts with a short review of fiber gratings and proceeds to another one where it is reported some of the developments related with the application of the combination (FBG + SPR) in SPR sensing. Then, it is outlined how can be applied the combination (LPG + SPR) to achieve singlemode supported fiber optic SPR sensors

and results are delivered coming out from a theoretically analysis. Finally, it is proposed how this combination can be coupled to interferometric interrogation to achieve high performance SPR sensing based in singlemode optical fibers.

6.2 Fiber Gratings

A fiber grating is an optical diffraction grating and corresponds to a periodic modulation of the refractive index in the fiber core that satisfies a phase matching condition between a guided mode and other modes that can be core modes, cladding modes or radiation modes. Fiber gratings allow the transfer of power between modes of an optical fiber. Figure 6.1 represents an optical diffraction grating and its effect upon a light wave incident on the grating at an angle θ_1. The effect of the grating in the light wave can be described by the familiar grating equation [197]:

$$\mathrm{n}\sin\theta_2 = n\sin\theta_1 + m\frac{\lambda}{\Lambda} \tag{6.1}$$

where θ_1 is the angle of the diffracted wave, m determines the diffraction order and Λ is the grating periodicity.

Fiber gratings can be broadly classified into two types: Bragg Gratings (also called Reflection and Short-Period Gratings), in which coupling occurs between modes traveling in opposite directions; and Transmission Gratings (also called Long-Period Gratings), in which the coupling is between modes traveling in the same direction.

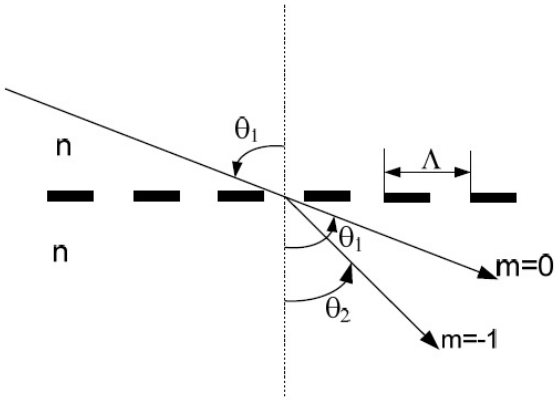

Figure 6.2 - The diffraction of a light wave by a grating.

6.2.1 Fiber Bragg Gratings

Figure 6.2 illustrates the general reflection layout for a fiber grating. In the case of a Bragg grating, a mode with an incidence angle of θ_1 is reflected into the same mode but traveling in the opposite direction with an angle of θ_2 = -θ_1.

Since the mode propagation constant β is simply defined by $\beta = \frac{2\pi}{\lambda} n_{eff}$, where $n_{eff} = n_{co} sin\theta$, the equation (6.1) can be rewritten for guided modes as [198, 199]:

$$\beta_2 = \beta_1 + m\frac{2\pi}{\Lambda} \tag{6.2}$$

where $\beta_1$and β_2 are the constants of the propagating modes. In fiber gratings usually dominates the first order diffraction, m=-1. This condition is illustrated in figure 6.2 in the β axis diagram.

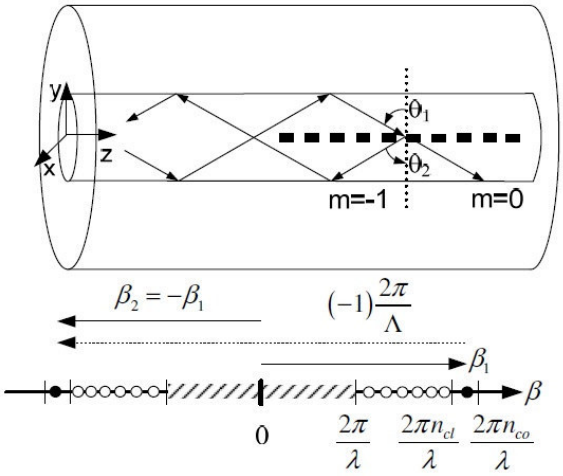

Figure 6.2 - The diffraction of a light wave by a grating. Ray-optics illustration of core-mode Bragg reflection by a fiber Bragg grating and the β axis diagram demonstrating the grating coupling condition for m=-1 [199].

In this figure, the solid circles represent bound core modes, the open circles represent cladding modes and the region filled with dots represents the continuum of radiation modes. A negative β value describes a mode that propagates in the –z direction. By using equation (6.2) and the fact that in this case β< 0, it is obtained the resonant wavelength for the reflection of a mode of index $n_{eff,1}$ into a mode of index $n_{eff,2}$ as given by:

$$\lambda = (n_{eff,1} + n_{eff,2})\Lambda \tag{6.3}$$

If the two modes are identical, the familiar result for the Bragg reflection would be obtained as:

$$\lambda_B = 2n_{eff}\Lambda \tag{6.4}$$

The principle of operation for these gratings is illustrated in figure 6.3.

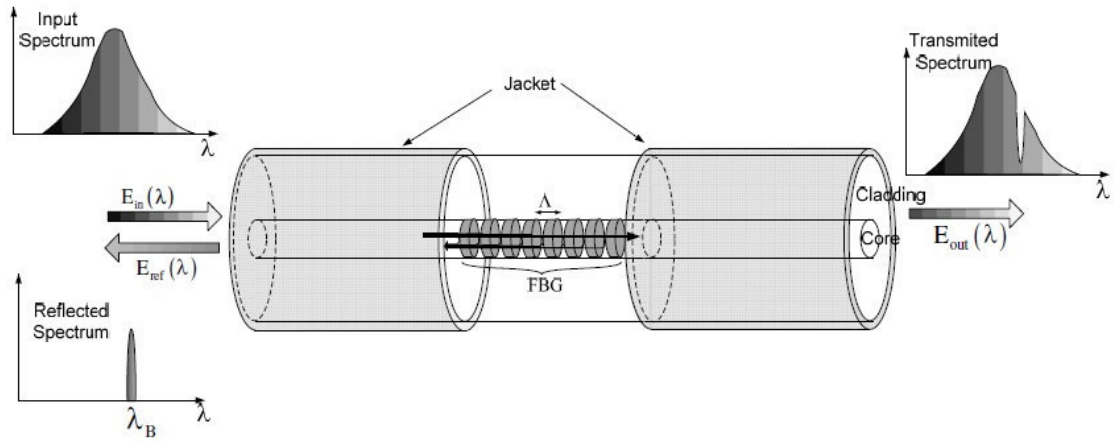

Figure 6.3 - FBG working principle.

In this type of grating, the light in the fundamental guided mode is perturbed by the presence of the periodic refractive index modulation in the fiber core and is reflected for wavelengths that satisfy equation (6.4). The typical response of a FBG is shown figure 6.4.

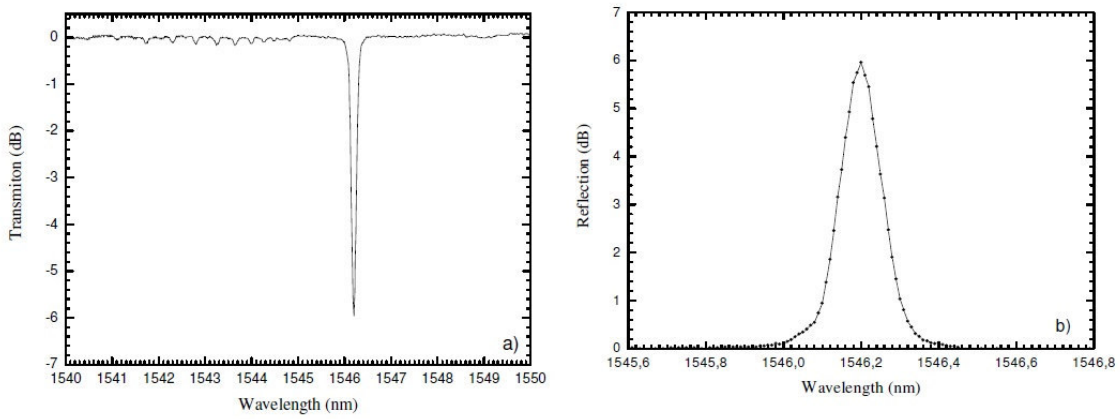

Figure 6.4 - Spectra of a typical FBG (data obtained at INESC TEC).

Figure 6.4(a) represents the transmission spectrum of a FBG where it can be seen the wavelength that satisfies the condition of phase matching, associated to a loss dip in the transmission spectrum. Figure 6.4(b) represents the reflection spectrum of the same FBG.

6.2.2 Long-Period Fiber Gratings

Figure 6.5 illustrates the diffraction by a long-period grating of a mode with a bounce angle of θ_1 into a co-propagating mode with a bounce angle of θ_2. In this illustration, the first mode is a core mode whereas the second is a cladding mode. Since here $\beta_2>0$, the equation (6.1) predicts the resonant wavelength for a long-period grating as

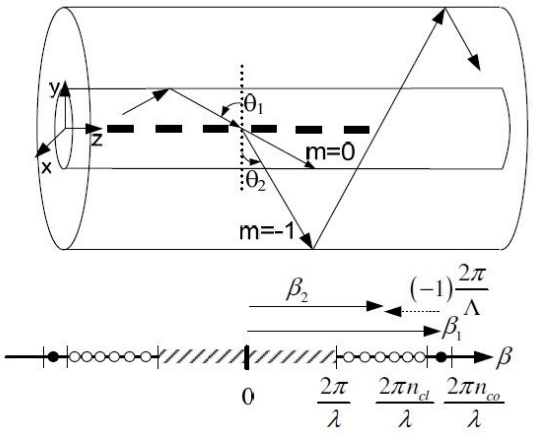

Figure 6.5 - Ray-optics illustration of cladding-mode coupling by a long-period grating and the β axis diagram demonstrating the grating coupling condition for m=-1 [199].

$$\lambda = (n_{eff,1} - n_{eff,2})\Lambda \tag{6.5}$$

Analyzing the equations (6.4) and (6.5), it can be seen that for copropagating coupling, at a given wavelength, a much longer grating period L is required than for counter-propagating coupling. figure 6.6 illustrates the principle of operation of long period gratings proposed by Vengsarkar et al. [198].

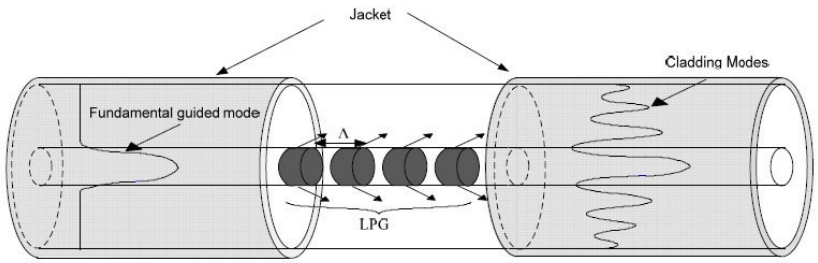

Figure 6.6 - Coupling of the fundamental guided mode to cladding modes in a long-period grating.

Light in the fundamental guided mode is perturbed by the presence of the grating in the fiber core. The difference between the propagation constant of the guided mode and the phase-matching vector of the grating equals the propagation constant of one or more cladding modes at appropriate wavelengths, which correspond to a specific cladding mode (order m) [199]. Phase-matching is a necessary, but not sufficient, condition for coupling between the core-guided and the cladding-guided modes. Cladding-modes exist, at least, in a three-layer cylindrical waveguide and share similarities with the modes present in multi-mode fibers (MMF) which supports hundreds of modes. For significant coupling to occur between the core-guided mode and a cladding-guided mode there must also be an overlap between the mode profiles. This requirement explains why, over large wavelength ranges, coupling occurs only to a finite number of distinct

cladding modes. The phase matching condition between the fundamental mode and the forward propagating cladding modes given by equation (6.5) can be rewritten as [198]:

$$\lambda_{res}^{m} = \left[n_{eff,co}(\lambda) - n_{eff,cl}^{m}(\lambda)\right]\Lambda \tag{6.6}$$

where λ_{res}^{m} is the resonance wavelength of the m^{th} cladding mode, n_{co} is the effective refractive index of the core mode and $n_{eff,cl}^{m}$ is the effective refractive index of the m^{th} cladding mode.

The light coupled into cladding-guided modes is, most typically, absorbed in the fiber buffer or radiates away from the fiber. Thus, this type of fiber grating acts as a wavelength selective transmission filter. The wavelength transmission response of a typical LPFG is shown figure 6.7.

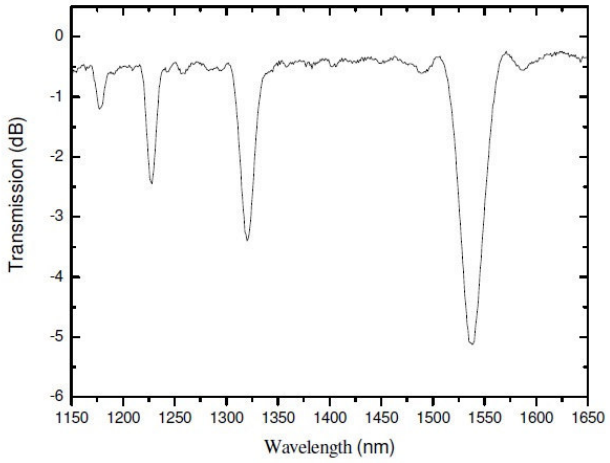

Figure 6.7 - Transmission spectrum of a typical LPG (data obtained at INESC TEC).

The wavelength dependence of the effective refractive indices in equation (6.6) is due to material and waveguide dispersion. Material dispersion can be assumed to have the same overall effect on n_{co} and $n_{eff,cl}^{m}(\lambda)$. Thus, when the difference is taken, it is the waveguide dispersion that is the dominant contributor to the grating spectrum [200]. From equation (6.6), it can be shown that:

$$\frac{d\lambda_{res}}{d\Lambda} = \frac{n_{eff,co}(\lambda) - n_{eff,cl}^{m}(\lambda)}{1 - \Lambda\left[\frac{dn_{eff,co}(\lambda)}{d\lambda} - \frac{dn_{eff,cl}^{m}(\lambda)}{d\lambda}\right]} \tag{6.7}$$

A particular grating period can cause the mode-coupling at the wavelength that would be predicted. The first step is the calculation of the effective refractive indices of the fundamental core mode and of the various resonant cladding modes of the fiber at a specific wavelength. A set of periodicities, L, is obtained that will meet the matching condition given by equation (6.6). This step is repeated for several wavelengths and the resulting plot of coupling wavelength versus grating period is shown in figure 6.8. The plot in figure 6.8 describes the process of mode coupling to azimuthally symmetric modes with uniform index perturbations perpendicular to the direction

of propagation. It is clear from the plot that as the higher order cladding modes are encountered (moving from right to left on the plot), the slope of the resonant line changes from a positive value to a negative value at a particular mode.

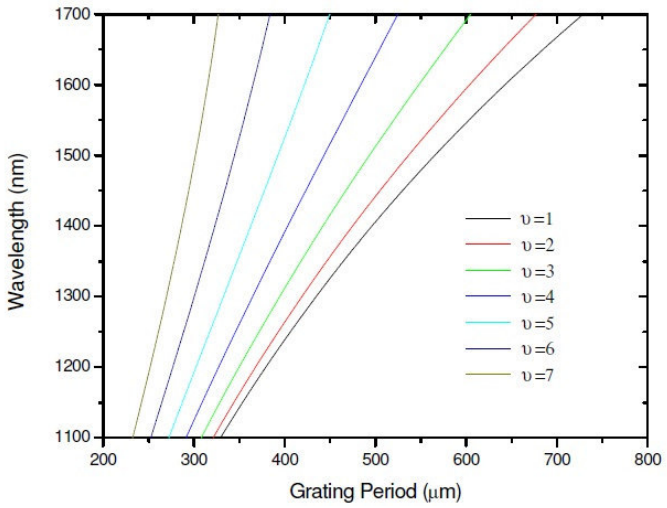

Figure 6.8 - Theoretical determination of the relationship between grating periodicity and wavelength where guided-to-cladding mode coupling takes place.

From this figure it comes out: (i) for a given grating period, the LPG can couple simultaneously the fundamental mode into many other modes at different resonant wavelengths; (ii) for a particular resonant wavelength, it can be selected a specific grating period to make the LPG to couple the fundamental mode into a specific fiber cladding mode; (iii) the higher the order of the coupled fiber mode, the shorter the grating period needed to obtain the occurrence of the mode coupling; (iv) the slope $d\lambda_{res}/d\Lambda$, given by equation (6.7), increases gradually from the lower-order mode to the higher order mode.

For the work reported in this Chapter, LPGs are more prominent than FBGs. Therefore, it is worthwhile to deliver some more information concerning these devices. To start with, about applications many have been demonstrated in the last decade, mostly concentrated on the development of long-period grating-based fiber devices for use in optical communications and fiber optic sensor systems. In optical communication systems, long-period gratings are applied as gain equalizing filters, wavelength selective devices, band-pass and band rejection filters [198, 201, 202] and wavelength tunable add/drop multiplexers [203]. In the field of sensing systems, long-period gratings are applied as structural bend sensors [204], temperature sensors [205-208], axial strain sensors [209], refractive index sensors [210-212] and biochemical optical sensors [213-215].

As an historical note, the first long period grating inscribed successfully in an optical fiber was described in 1996 by Vengsarkar et al. [216] for band-rejection filters and, in the same year, Bhatia et al. [217] presented the first application of long period gratings for sensing. At that time there was also presented the first theoretical studies on LPGs. The first theoretical model to determine the cladding modes was presented in 1996 by Bhatia [218] and is based on a two-layer model that neglects the effect of the core in the calculation of the cladding modes. In 1997 Erdogan presented a model that includes the effect of the core in the calculation of the cladding modes [219]. This model is known as the three – layer model. In these two models, the LPG was assumed to be fabricated by using UV laser radiation, resulting in cladding modes with symmetric distribution. The development of other techniques for the manufacture of LPGs (electric arc, CO_2, etc.) led to coupling to asymmetric cladding modes because these techniques produces a change in the refractive index of the core that is non-uniform across the fiber cross section. This new situation is not described by the two previous models. In 2003, Anemogiannis et al. [220] presented a theoretical model that already covers this situation and their implementation is more complex but has the advantage of solving the problems of asymmetric modes.

For long period gratings the analysis above outlined indicates the periodic modulation of the refractive index in the fiber core shall be situated typically in the range from 100 μm to 1000 μm along a fiber length of few centimeters. This modulation can be induced in the fiber using different processes: UV laser irradiation, electric-arc discharge, periodic etching, CO_2 laser irradiation and mechanical processes are the most common techniques. Due to such broad range of techniques, LPGs can been written virtually in all kinds of fiber, namely, in standard singlemode telecommunications fibers [198], in two-mode or few-mode fibers [221], in polarization maintaining fibers [222], in D-fibers [213], in non-photosensitive fibers [223], in multimode fibers [224], in specially designed fibers: dispersion shifted [198], dispersion compensating [225], depressed inner cladding [226], dual core [227] progressive three layered [228], in hybrid fibers containing silica and polymers [229] or metal coatings [230], in a microstructured polymer fiber [231] and in photonic crystal fibers [232], in pure-silica-core fiber [212] and other doped fibers [233].

As mentioned at the end of Section 1, in optical fiber sensing the combination of LPGs with the SPR phenomenon has been scarcely explored, and indeed it has rather interesting characteristics: one of them is the utilization of single mode optical fibers without the need to remove the cladding in order to access the core and to cover it with the metal layer to induce the plasmonic resonance light behavior. Therefore, the geometry of the single mode optical fiber is maintained, meaning full compatibility of such devices with standard optical fiber technology that shows a huge portfolio due to the optical communications demand. A second one is the amenability to change

the refractive index range where the sensor device is effective just by considering a grating with a different periodicity, so the light that propagates in the fiber core is coupled to a different cladding mode, meaning a different oscillation angle in the cladding, therefore different interaction behavior with the electronic cloud of the metallic layer, with the consequence that the SPR phenomenon will occur for different values of the refractive index of the external medium. A third one is the intrinsic compatibility of the (SPR + LPG) combination with interferometric interrogation, implying the possibility to reach rather high sensitivities to variations of the refractive index of the external medium. The (SPR + LPG) fiber layout explored in this work is schematically shown in figure 6.9, which effectively implements a fiber interferometer with SPR modulation.

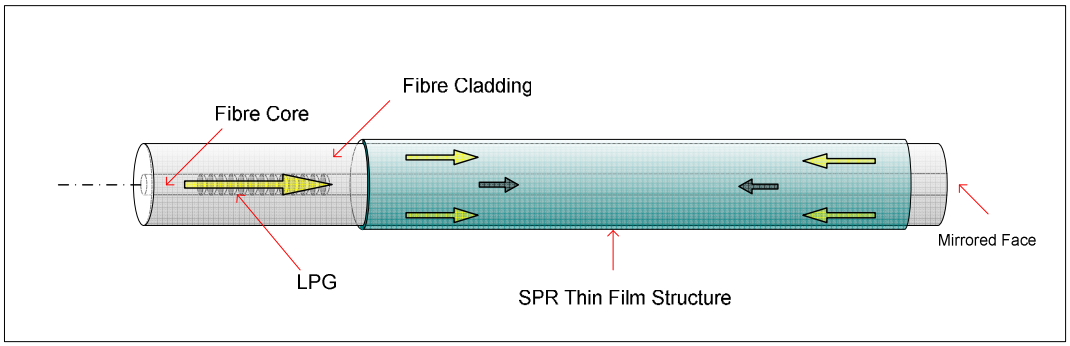

Figure 6.9. Fiber interferometer based on a LPG and SPR modulation.

The fibre interferometer relies on the interference of the light that propagates in the fibre core and the light that is coupled to a cladding mode by the LPG. The end of the fibre is mirrored, resulting in a Michelson modal configuration. The fibre is coated with material layers to have plasmonic resonance under excitation of the light in the cladding mode. When the refractive index of the surrounding medium changes the same happens with the resonance characteristics, with impact on the intensity and phase of the light in the cladding mode. These phase changes translate into interferometric phase variations and their recovery permits sensitive refractive index measurement.

Later in the Chapter this sensing approach will be detailed, but for the while it is relevant to deliver few notes on fiber optic SPR sensing assisted by fiber Bragg Gratings.

6.3 FBG Assisted SPR Based Optical Fiber Sensors

Several structures for optical fiber sensing supported in the SPRphenomenon assisted by fiber Bragg gratings have been reported in the literature. One of them was proposed in 1999 by Ctyroky

et al. [234]. It consists on a guided mode coupled to a surface plasmon-polariton as can be seen in figure 6.10.

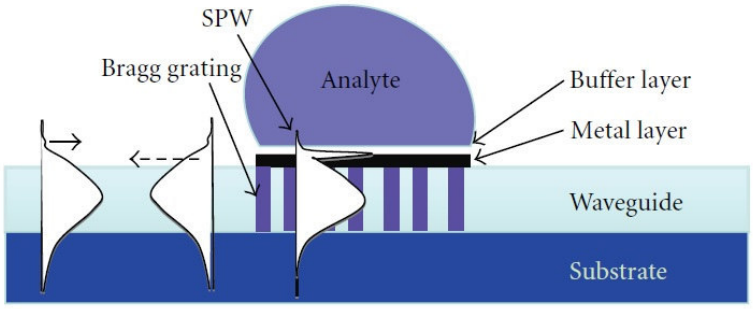

Figure 6.10 - Surface Plasmon resonance sensing structure with a fiber Bragg grating [234].

A Surface Plasmonic Wave (SPW) oscillates in the fiber core (or in the waveguide layer of the planar structure). Its effective refractive index is only slightly different from the effective refractive index of the guided mode supported by the structure without the metal layer. This is because most of the energy is associated with the guided mode and only slightly weighted by the plasmon-polariton's effective index. This interaction means that the hybrid mode is sensitive to any change in the effective index of the plasmon which depends on the refractive index of the surrounding layer, the measurement target parameter.

In 2006, Nemova et al. [235] suggested an improved configuration by the use of the so called "pure" SPP as opposed to the hybrid mode. Contrary to SPW, in this "pure" SPP almost all the energy is concentrated at the metal-dielectric interface. The "pure" SPP decays exponentially away from the metal surface, including a waveguide layer of the sensor structure. The difference between the effective refractive index of the guided mode and the effective refractive index of the "pure" SPP is thus large and requires a special scheme to excite the "pure" SPP. This is done with a grating, which allows the wave-vector matching condition to be met. The advantage of using the grating is that it decouples the coupling scheme from the second important parameter - the overlap integral between the guided exciting mode and the "pure" SPP. Since almost all energy of the "pure" SPP is concentrated at the metal-dielectric interface, this scheme is extremely sensitive to small changes in the refractive index of the sensed medium. The value of the change in the effective refractive index of the "pure" SPP caused by the variation in the refractive index of the sensed medium depends on the parameters of the structure. For the particular case of a hollow core layout, illustrated in figure 6.11, where a Bragg grating is imprinted in its waveguide layer, a full theoretical modelmay be found in [61].

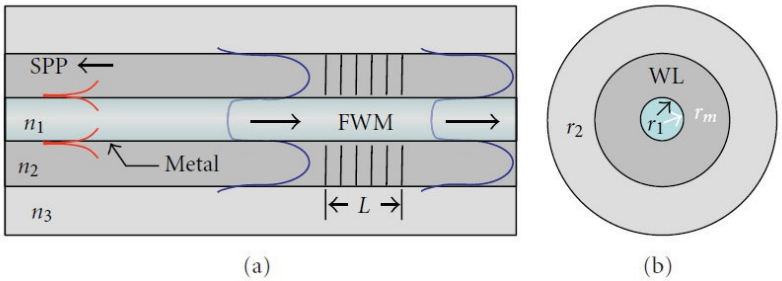

Figure 6.11 - (a) Hollow core sensing structure with Bragg grating. (b) Cross section of the structure [61].

Other planar structures with Bragg gratings imprinted into the waveguide layer or the use of a corrugated Bragg grating engraved on the top of the metal layer have also been considered [236, 237]. In these structures, shown in figure 6.12, the Bragg grating excites a counter-propagating SPP with characteristics that depend on the sensed medium. This modulates the guided mode transmitted through the Bragg grating, which can be used to recover the sensing information. The sensitivity of the structure, characterized by the shift in the wavelength of the grating transmission dip versus the refractive index of sensed medium, was found to reach values of ~250 nm/RIU when under optimized conditions.

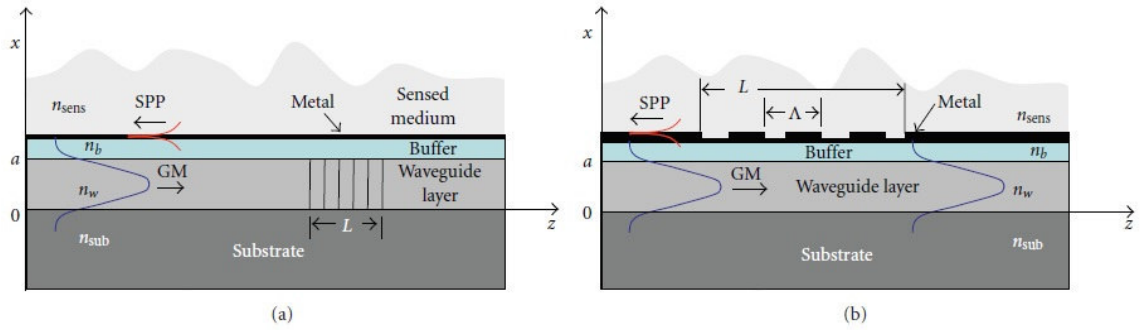

Figure 6.12 - Planar SPP sensor with (a) Bragg grating imprinted into the waveguide layer [236] and (b) Bragg grating engraved on the top of the metal layer [237].

To increase further the sensitivity of these sensing structures the Bragg grating may be replaced by a long period grating, as shown in figure 6.13. Now, the guided mode propagating in the waveguide layer of the structure excites a co-propagating SPP. Similarly to the FBG case, the LPG may be imprinted into the waveguide layer or engraved on the top of the metal layer, and the light transmitted through the LPG has encoded the measurand information.

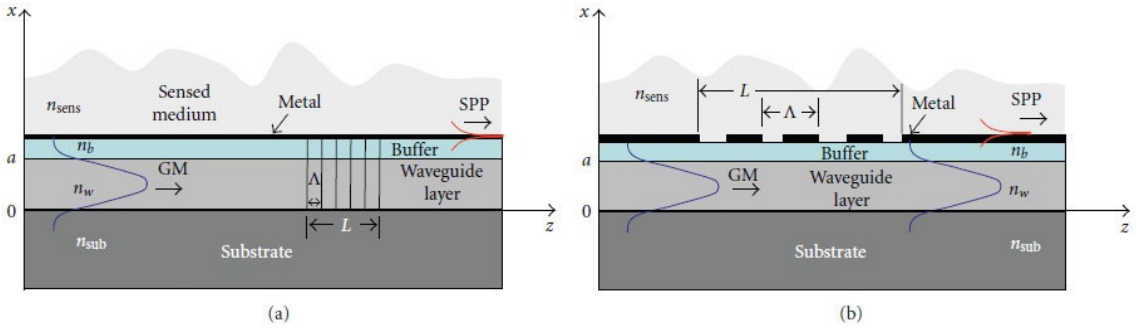

Figure 6.13 - Planar SPP sensor with (a) LPG imprinted into the waveguide layer and (b) LPG engraved on the top of the metal layer.

Rather remarkably these sensing structures may enable refractive index sensitivities which reach ~1100 nm/RIU. The reason for this enhancement relative to the FBG case can be understood by comparing the LPG and FBG modulation periods. The larger grating period of the LPG is connected with the difference between the propagation constants of the guided and SPP modes. On the other hand, the shorter period of the Bragg grating required to excite the counter-propagating SPP equals the sum of the propagation constants of the guided and SPP modes, since the SPP and the guided modes propagate in opposite directions. Any small change in the refractive index of the surrounding medium (n_{sens}) induces a larger fractional change in the LPG-based sensor as it changes the propagation constant of the SPP mode, that is, if δ_n is the change in the SPP's effective refractive index for a change in n_{sens}, then the fractional change in the mismatch is

$$\frac{\delta n}{(n^p - n^g)} \tag{6.8}$$

where n^p and n^g are the effective indexes of the SPP and guided modes, respectively. In the counter propagating scheme with the Bragg grating, a small change in the propagation constant of the SPP has a smaller fractional influence on the sum of the propagation constants of the SPP and the guided mode as

$$\frac{\delta n}{(n^p + n^g)} \tag{6.9}$$

The ratio of the sensitivities of the LPG and the SPG configurations is therefore

$$\mathrm{r} \approx \frac{n^p + n^g}{n^p - n^g} \tag{6.10}$$

In equation (6.10), the ratio *r* is greater than unity, indicating an enhanced sensitivity for the LPG (co-propagating) compared to the FBG-based sensor (counter-propagating).

6.4 LPG Assisted SPR Based Optical Fiber Sensors

As outlined at the end of Section 6.2, the consideration of fiber optic sensors associated with LPG assisted plasmonic resonance is an interesting approach, yet scarcely explored. The reason for this may be its coupling to interferometric (phase) interrogation, which is by far the less explored of the interrogation techniques when addressing SPR sensors, and yet it is the one that has the potential to provide the highest sensitivities. Owing to the focus of this work in the phase interrogation of fiber optic SPR sensors, the combination (SPR + LPG) was naturally addressed as described in the following.

The basic feature of the LPG assisted fiber optic SPR sensing is that the grating couples light which propagates in the fiber core to a cladding mode with a certain oscillation angle, interacting in each reflection at the cladding-metal interface in a condition of plasmonic resonance. An effective configuration consists in assuming TM light and operation in reflection, so the radiation propagates twice through the sensing region, with the LPG coupling light to the cladding and recoupling back to the core. In this way it accumulates a phase difference to the light fraction that always propagated in the core which provides the reference beam of the interferometric layout. The recovery of the interferometric phase shall allow obtaining the component introduced by the plasmonic resonance, therefore with information on the refractive index of the surrounding medium. An approach of this type, illustrated in figure 6.9, is quite promising considering it is fully compatible with single-mode fiber-optic technology while not compromising the performance of SPR measurement since, in the sensing region, the light is allowed to propagate with oscillation angles close to the critical angle where the phase shift introduced by the SPR phenomenon is maximum, i.e. in a situation of maximum sensitivity [238].

To design a structure of this type first it is necessary to analyze how a LPG can be efficiently operated within the context of this application. As shown in figure 6.14, when the LPG couples light from the core to the cladding this means after the LPG the light propagates in a multimode waveguide with diameter that equals the fiber diameter (125 μm for standard telecommunication fibers). It is well known from basic fiber optic theory that for a step-index profile the number of propagating modes is

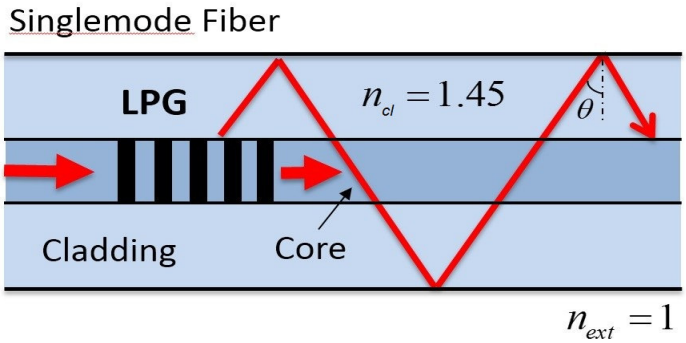

Figure 6.14 – LPG induced coupling of the core mode to a cladding mode associated with the oscillation angle θ.

$$Number\ of\ Modes = \frac{V^2}{2} \tag{6.11}$$

with the V parameter given by

$$\mathrm{V} = \frac{2\pi a}{\lambda_0}\sqrt{(n_{cl}^2 - n_s^2)} \tag{6.12}$$

where a is the fiber radius, λ_o the wavelength of light in vacuum and n_{cl}, n_s are the refractive indexes of the cladding and of the fiber surrounding medium, respectively. For 2a=125 μm, n_{cl} = 1.450, n_s= 1 and λ_o = 1550 nm, it comes out V = 266, with the number of modes equaling 35378.

The mode *m*, associated with the ray oscillation angle θ_m, has a propagation constant β_m, given by [239]:

$$\beta_m = k sin\theta_m = \frac{2\pi n_{cl}}{\lambda_0} sin\theta_m \tag{6.13}$$

On the other hand, the propagation constant needs to be in the interval

$$\beta_m \in [n_s k_0, n_{cl} k_0];\ k_0 = \frac{2\pi}{\lambda_0} \tag{6.14}$$

The ray more oblique has the smaller value of β_m, associated with the smaller value for the angle θ_m, i.e., the situation of the critical angle. Therefore, the highest order mode, the one more favorable for SPR operation, has:

$$\beta_{m_{max}} = n_{ext} k_0 = \frac{2\pi}{\lambda_0} \tag{6.15}$$

So, ideally the LPG should induce coupling between the most internal mode (with propagation essentially along the fiber axis, $\theta_1 \approx 90^{\circ}, \beta_1 \approx n_{cl} k_0$) and the mode with $\beta_{m_{max}}$, the most external one.

For a LPG induce coupling between two modes with propagation constants β_A and β_B, from equation (6.6) the grating periodicity, Λ, must satisfy the condition:

$$\lambda_0 = \frac{1}{k_0}(\beta_A - \beta_B)\Lambda \tag{6.16}$$

In the present case, $\beta_A = \beta_1 = n_{cl}k_0$ and $\beta_B = \beta_{m_{max}} = n_s k_0$, therefore

$$\Lambda = \frac{\lambda_0}{n_{clad} - n_{ext}} \tag{6.17}$$

For $\lambda_0 = 1550\ nm, n_{cl} = 1.450, n_s = 1$, it results $\Lambda = 3.3\ \mu m$. This is a rather small value, eventually not possible to fabricate a LPG with a refractive index modulation with such periodicity. Admitting it is feasible a value $\Lambda = 300\ \mu m$, it turns out to be possible to couple light to mode *m* with:

$$n_m = n_{cl} - \frac{\lambda_0}{\Lambda} = 1.450 - \frac{1.55 \times 10^{-6}}{300} = 1.445 \Rightarrow \beta_m = 1.445 \times \frac{2\pi}{1.55 \times 10^{-6}} = 5.854 \times 10^6\ m^{-1}$$

The angle θ_m is

$$\theta_m = \arcsin\left[\beta_m \frac{\lambda_0}{2\pi n_{cl}}\right] = \arcsin[0.99644] = 85.1^{\circ} \tag{6.18}$$

which is far from the critical angle $\theta_c = \arcsin\left[\frac{n_{air}}{n_{cl}}\right] = 43.6^{\circ}$, therefore it is rather difficult to induce plasmonic resonance with an acceptable Q-factor. As a matter of fact the situation is alleviated in most situations because for biochemical sensing the external medium is aqueous, meaning a refractive index close to 1.33.

This analysis indicates that to have effective LPG assisted SPR sensing operating at 1550 nm and with an aqueous environment an external mode needs to be excited by the LPG. To achieve this with LPGs showing a refractive index modulation amenable to standard fabrication techniques a double metal + oxide layer needs to be considered.

From the results delivered in previous chapters it can be drawn the conclusion that the combination of an internal layer of Ag and an oxide layer of TiO_2 permits high performance SPR sensing. Therefore, it was decided to apply this combination in the context of the analysis of LPG assisted fiber optic SPR sensors.

Following this line, for a grating periodicity of Λ = 300 μm the study performed permitted to conclude the best sensing performance compatible with operation at 1550 nm and an environmental with refractive index n_s = 1.33 is associated with layers of thicknesses of 70 nm (for the internal layer of Ag) and 60 nm for the oxide layer of TiO_2. For the same operating conditions but now assuming a grating periodicity of Λ = 500 μm, these thickness values change to 70 nm and 66 nm, respectively. For both cases the shape of the SPR resonance is shown in figure 6.15.

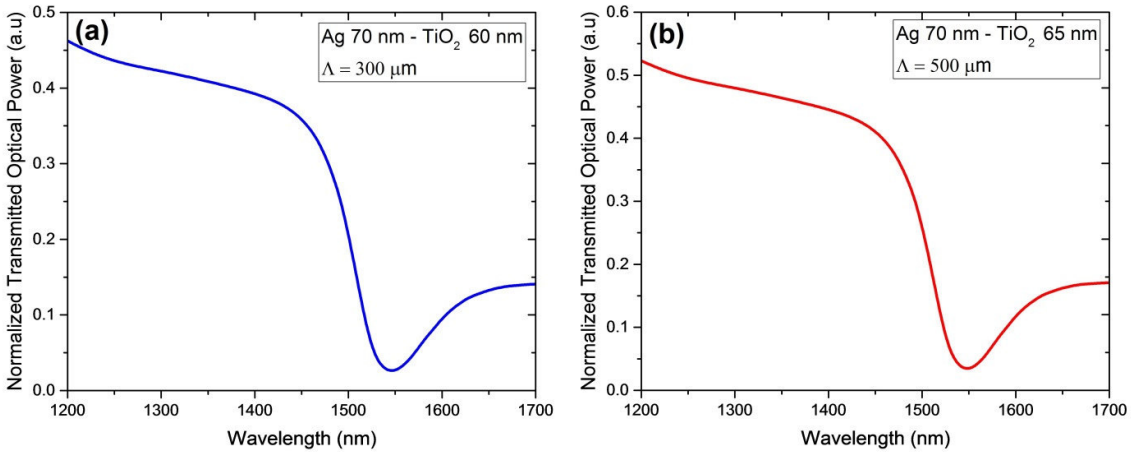

Figure 6.15 - Spectrum of the normalized transmitted optical power for the Ag-TiO_2 sensing structure for different grating periodicity (a) $\Lambda = 300\ \mu m$ and (b) $\Lambda = 500\ \mu m$ (when surrounding medium having a refractive index of 1.333).

The observation of these curves clearly indicates the left side at smaller wavelengths is better defined than the right one at longer wavelengths, indicating an asymmetry of the resonance Q- factor when evaluated from the perspective of each side. This indicates operation at the left side is more favorable when the structure is configured as a sensor device and intensity interrogation is adapted.

If the focus is phase (interferometric) interrogation, the best performance occurs at the resonance wavelength. When this wavelength is fixed (1550 nm for the case) and the surrounding refractive index changes, then the phase difference between the TE and TM polarizations also changes, as illustrated in figure 6.16-a for both LPG modulating periods, from where derives the phase sensitivity given at figure 6.16-b. It can be observed the phase difference between the two polarizations becomes lower when the grating periodicity increases, i.e., by using a smaller grating period the excited cladding mode is of higher order, so the penetration of the evanescent wave in the external medium becomes deeper, therefore increasing the device refractive index sensitivity.

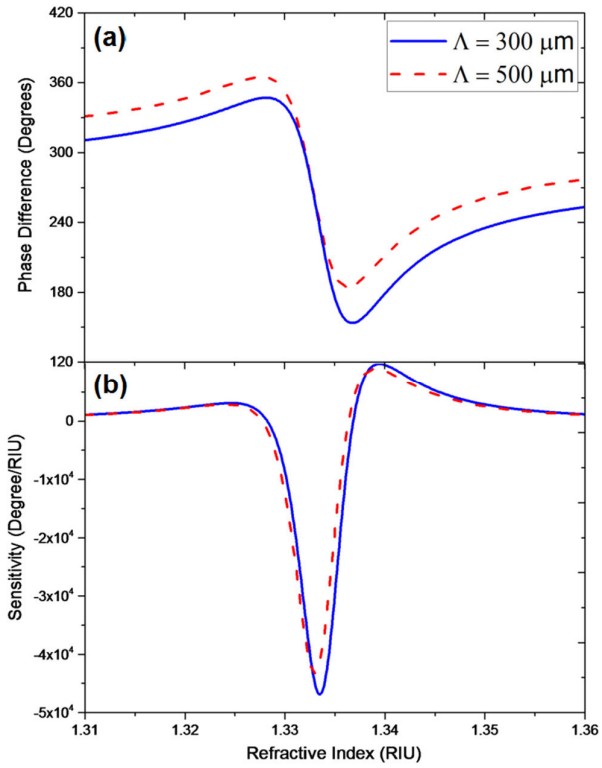

Figure 6.16 – (a) Phase difference (between *p* and *s* polarizations) and (b) phase sensitivity as function of the refractive index of the surrounding medium for different grating periodicities Λ = 300 μm and Λ = 500 μm. The interrogation wavelength is 1550 nm.

As pointed out in previous chapters, the sensor operation at resonance may bring reduced signal-to-noise ratio due to the foreseeable low levels of optical power. Following the strategy outlined before, this drawback can to some extent be attenuated by moving slightly the working wavelength from the resonance. Doing so, the phase sensitivity is somehow degraded, but the sensor resolution may improve because it also depends on the system signal-to-noise ratio.

6.5 Paths for Experimental Research

The work reported in this thesis is grounded on theoretical and computational analysis of fiber optic SPR based sensing structures with particular emphasis on the study of the performance associated with phase interrogation. As mentioned before, within the R&D strategy of the INESC TEC optical sensing team, there are research paths more oriented to the theoretical analysis of the behavior and performance of sensor devices and others more focused on experimental validation and characterization, these two perspectives requiring a constant cross-fertilization. An important example of this orientation is the study of the multiplexing of fiber optic SPR sensors where both components interacted looking for the best configuration, generating a valuable

output that deserved publication in a prestigious international journal[1]. Targetting the work reported in this thesis its experimental component did not proceed in parallel and will be tackled in the near future. Some paths for its development are outlined here, again focusing on phase interrogation of the SPR sensing structures. First, a general approach is outlined, applicable for any type of fiber optic SPR sensing device. Then, it is proposed an experimental arrangement oriented to LPG-assisted SPR based fiber optic sensors compatible with extreme resolutions in the measurement of refractive index variations of the surrounding.

6.5.1 A General Technique for Phase Interrogation of SPR Fiber Sensors

The experimental study of the SPR sensing elements presented in this work can be done by application of techniques developed along the years for the interrogation of polarimetric fiber sensing interferometers illuminated by monochromatic light [240]. Following these approaches, laser light is injected into the fiber at an angle such that it is excited the selected core mode. At the input of the sensing head, a fiber polarizer element shall be included in order to have light in the TE and TM polarizations, recombined at the output of the measurement region by means of a second polarizer. This will generate an interferometric signal with a phase proportional to the optical path difference accumulated by the propagation of the TE and TM polarizations, therefore including the phase variations of the light in the TM polarization induced by changes of the surrounding refractive index.

To recover the phase of this signal, a robust and sensitive technique involves adding a sine wave component to the interferometric phase, which can be generated by sine wave modulation of the wavelength of the laser light. After photodetection and incorporation of signal processing, which includes a feedback loop to the laser source to tune the DC value of the light wavelength, the information on the quasi-static phase of the polarimetric sensing interferometer, therefore on the refractive index of the external medium, can be obtained from the feedback signal [241]. This approach is compatible with a DC phase resolution of the order of 1 mrad, which from the results presented in this thesis means refractive index measurement resolutions of the order 10^{-6} shall be possible.

[1] L. Coelho, H. Moayed, J. M. M. de Almeida, J. L. Santos, D. Viegas, *Multiplexing of Surface Plasmon Resonance Sensing Devices on Etched Single Mode Fiber*, Journal of Lightwave Technology Journal of Lightwave Technology, 33, 432 – 438, 2014.

6.5.2 High Performance Phase Interrogation of LPG Assisted SPR Fiber Sensors

The interrogation of the modal interferometer associated with the operation mode of a LPG assisted fiber optic SPR based sensing element illustrated in figure 6.9 can be achieved using the general approach outlined in the previous section. However it is objective of INESC TEC optical sensing group to research the application in this context of powerful techniques that have been researched for gravitational wave detection with optical interferometry [242]. In general, they are based on the exploitation of the Pound-Drever-Hall (PDH) frequency looking technique that permits frequency noise performance compatible with pico-strain resolution [243, 244]. This is an extremely powerful technique for both static and dynamic phase recovery in optical interferometers. The configuration proposed to be studied is shown in figure 6.17.

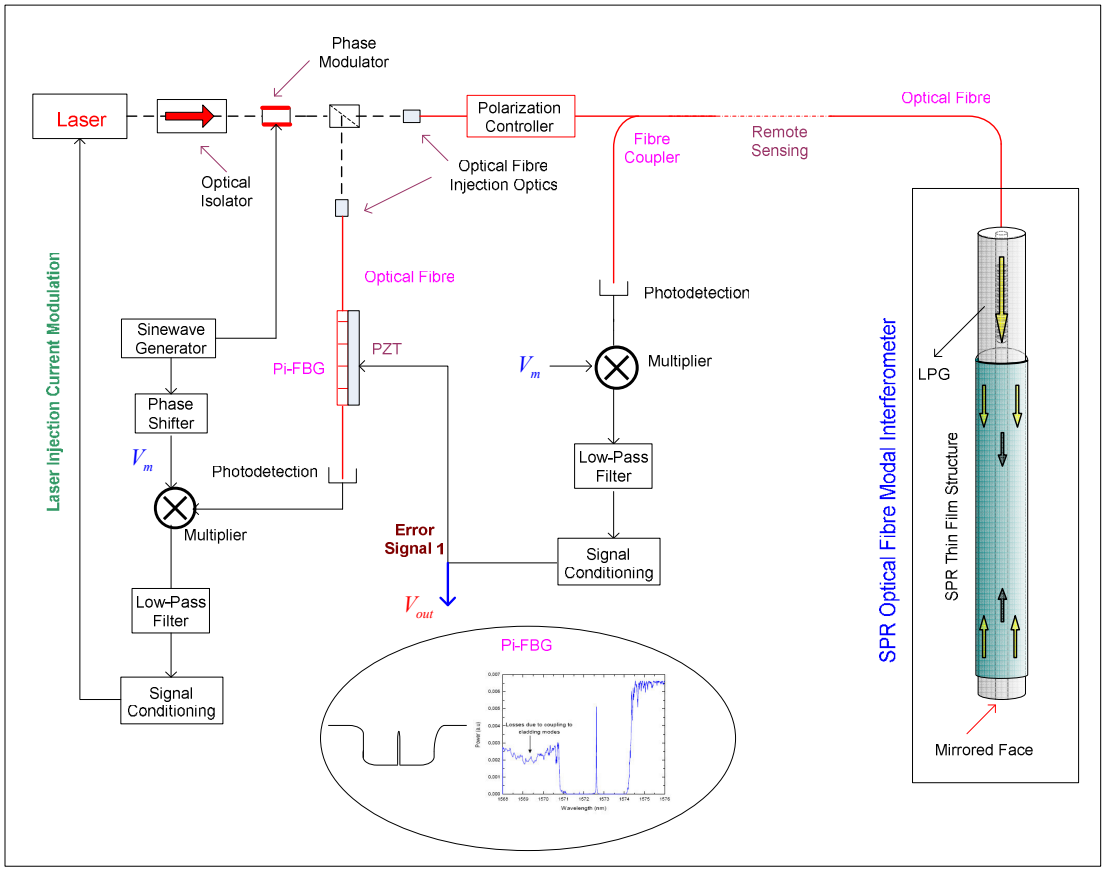

Figure 6.17 - Optical fibre SPR interferometric sensing configuration with PHD signal processing

The sine wave phase modulation of the laser light injected into the optical fiber system, when coupled to the transfer function of the sensing interferometer, generates a complex electrical spectrum at the photodetection output. After proper mixing and signal conditioning, an error signal is generated that is applied to a piezoelectric where a fiber optic filter is fixed. It is proposed

this filter to be a chirp pi-shifted fibre Bragg grating with a very narrow transmission window (in figure 6.17 it is shown a filter of this type fabricated in-house). A fraction of the light from the laser goes through this filter, and a second error signal is generated to lock the laser wavelength to the filter transmission line. Considering this line is also tuned by the first feedback loop to the sensing interferometer, the laser is also locked to this interferometer. This double loop control configuration shall permit to reduce the laser free-running frequency noise, which becomes now determined by the stability of the fibre transmission filter. Maximum readout sensitivity is obtained with adequate tuning of the electrical phase shifter. In the full bandwidth operation, the system output signal can be derived from any one of the error signals.

We propose to study in detail this demodulation technique and apply it to phase readout of the sensing interferometer. This phase will be affected by the temperature and by the external medium refractive index, which is the measurand of interest. Considering the Plasmon excitation is polarization sensitive, manipulation of the polarization of the input light shall permit to achieve maximum and minimum sensitivities to refractive index, while the temperature sensitivity shall be essentially constant. Therefore, this behaviour shall permit to measure the sensing head temperature and, therefore, to correct its effects on the recovered phase, an essential procedure when the objective is to have a highly sensitive refractive index measurement.

6.6 Conclusion

This chapter addressed the topic associated with the combination of fiber gratings with standard fiber optic SPR sensing technology to bring it to the singlemode domain, therefore turning it compatible with the vast field of fiber optic communication systems with its large portfolio of advanced and cost effective components and devices. Concerning fiber Bragg gratings, a short review was presented on developments reported in the literature showing how these structures can upgrade the global performance of fiber SPR sensors, in particular to enlarge the range of implementation possibilities for these sensors. The focus of the chapter was, however, to show how long period gratings can be efficiently integrated in fiber optic SPR sensing structures enabling novel configurations with intrinsic high performance when addressing the monitoring of the refractive index of the surrounding medium. The analysis performed permitted to conclude these LPG assisted SPR based fiber sensors are essentially interferometric in nature, therefore requiring phase reading to recover the measurand information. This is to say the combination (LPG + SPR) restricts the group of available interrogation techniques of SPR sensors to a single one, the phase interrogation approach. The immediate consequence is that the domain of LPG assisted SPR sensing is associated with high performance even when standard technics of interferometric phase readout are considered. This topic is addressed in the Chapter in the

context of the notes delivered about how the experimental investigation of these sensing structures could proceed, in particular it is proposed to research the applicability of the advanced Pound-Drever-Hall interferometric interrogation technique, looking to reach new resolution levels when targeting the measurement of refractive index and from it a large range of chemical and biochemical entities.

7

Conclusions and Future Work

The central objective of this thesis was the study of a number of fiber optic configurations showing sensing functionalities supported by the phenomenon of plasmonic resonance. It proceeded along the theoretical and computational components looking to understand their operation principles and to derive their main characteristics, owing also to guide the experimental investigation and to tailor the properties of a specific sensing device to a particular application.

The thesis was organized in seven chapters. **Chapter 1** delivered an historical overview about the phenomenon of plasmonic resonance in the optical domain and how it was configured to achieve sensing functionalities, first in bulk optics platforms and later associated with the utilization of optical fibers. Also, an effort was undertaken to contextualize this sensing approach within the actual dynamics of Plasmonics which is continuously opening new horizons in science and in technology. **Chapter 2** presented the physical concepts behind the phenomenon of plasmonics, particularly surface plasmonic resonance, and the conditions for their existence on dielectric-metal-dielectric slabs. The propagation of an electromagnetic field into a multilayer structure was also discussed, which later permitted to model surface plasmonic resonance based sensors. **Chapter 3** delivered a worked review of the different techniques reported to interrogate plasmonic based sensors, addressing in particular the performance level that can be achieved with each of the interrogation approaches, which include angular interrogation, spectral interrogation, intensity interrogation and phase interrogation. **Chapter 4** developed the study of SPR based optical fiber sensing configurations integrating a single metal or a bimetallic layer. With the focus on phase interrogation, it was analyzed the performance associated with the utilization of different metals, namely silver, gold, copper, and aluminum when the tapered and the tip (optrode) optical fiber geometric layouts were addressed. **Chapter 5** presents a theoretical investigation of optical fiber surface plasmonic resonance sensors incorporating an internal metallic layer of silver covered with an oxide layer. The objective was to study how to shift the resonance condition to longer wavelengths, more suited to benefit from a broad range of optical fiber technologies developed along the years within the context of optical fiber communications systems. Different oxide materials like titanium dioxide, silicon dioxide and aluminum oxide were considered aiming to achieve enhanced sensitivity to refractive index variations of the external medium, particularly when addressing phase interrogation. **Chapter 6** dealt with the integration of fiber gratings with standard fiber optic SPR sensing technology to bring it to the singlemode domain, therefore turning it compatible with the fiber optic communication world with its large portfolio of advanced and cost effective components and devices. In particular, emphasis was allocated on the theoretical analysis of long period grating (LPG) assisted optical fiber sensing structures supported by Plasmonics. It is concluded this (LPG + SPR) combination brings to the forefront the phase interrogation of SPR sensors and, consequently, were outlined paths for the

experimental investigation of interrogation techniques of this type, including advanced ones as the Pound-Drever-Hall interferometric interrogation approach.

Behind its intrinsic value, this research activity fits the strategic objectives of the optical sensing group of INESC TEC which, years ago, defined a R&D axis in plasmonics based fiber optic sensing. Understandably, the theoretical analysis and performance evaluation of devices situated along such axis are an important component of such strategy, for reasons that range from guiding their experimental investigation to the tailored design of a sensing device projected to a specific application. This means an always present component of future work is the continuous interaction with the experimental counterpart of the group R&D activity in plasmonics based fiber sensing, most in particular on the planned activity to test the performance of phase reading techniques applied to the phase interrogation of LPG assisted fiber optic sensing supported by plasmonics.

Besides this future work component, others are programmed more oriented to the theoretical investigation of fiber optic sensing supported by plasmonics. Some of them are:

- The theoretical studies performed used a model which is a hybrid of geometric optics (ray propagation) and wave optics (application of Fresnel equations in the interface where plasmons are excited). It is known this method works effectively when the waveguide propagation is far away the singlemode regime. When it is approached a full wave optics theory needs to be applied, which implies the consideration of other analytical tools and methodologies.

- The configurations analyzed in the work reported in this thesis deals with relatively simple fiber geometric layouts, situation that changes when the focus is oriented to photonic crystal fibers. So, a natural topic of research is the extension of the models and methodologies presented here to the more complex geometric reality associated with this type of fibers.

- A further expansion of the activity proposed in the previous entry is connected with the metamaterials domain where, by adequate geometric modulation of a particular material with spatial scales well below the optical wavelength, the refractive index of this structured material as seen by the light can be tailored within a large range of values. In this way artificial materials with enhanced properties for plasmonic interaction may be fabricated, which opens vast horizons in what concerns plasmonic supported optical sensing. This is a rather unexplored and huge domain requiring a multi-level approach, one of them associated with the theoretical evaluation of the properties of sensing structures of this nature.

- In Chapter 6 it was proposed the advanced *Pound-Drever-Hall* interrogation technique to read with extreme sensitivity the interferometric phase of the LPG-assisted SPR supported fiber optic modal interferometer. The evaluation of how "extreme" the readout sensitivity can be and the identification of the factors that determine its value is an evident topic of research.

These are just some themes that justify a thoroughly theoretical investigation, in complement to the laboratorial research, owing the objective of *INESC TEC – Center of Applied Photonics* to develop the subject of plasmonics based fiber optic sensing, supported also by the evidence of the relevance this field will have in the near future.

Annex

Symbols & Abbreviations

SPR	Surface Plasmon Resonance	RIU	Refractive index unit
ε_0	Free-space permittivity	θ_{cr}	Critical angle
μ	Magnetic permeability	S_n	Sensitivity
E	Electric field	χ	Quality parameter
H	Magnetic field	k_{SP}	Propagation constant of SP
β	Propagation constant	θ_{res}	Resonance angle
TM	Transverse Magnetic	λ_{res}	Resonance wavelength
TE	Transverse Electric	ρ_i	Radius of the core
SPP	Surface Plasmon Polaritons	ρ_0	Radius of the core in sensing region
$l_{SPP,m}$	skin depths into metal	L	Sensing region
$l_{SPP,d}$	skin depths into dielectric	NA	Numerical aperture
ATR	Attenuated total reflection	θ_0	Angle of incident
k_x	Wavevector of the incident light	$S_{n,\phi}$	Phase sensitivity
Λ	Grating period	λ	Interrogation wavelength
δ_k	Phase in the k^{th} layer	d_1	Thickness of inner layer
d_k	Thickness of the k^{th} layer	d_2	Thickness of outer layer
η_k	Optical admittance	FBG	Fiber Bragg Grating
r_s	Reflection coefficient – s wave	LPG	Long Period Grating
r_p	Reflection coefficient – P wave	n_{eff}	Effective refractive index
θ	Incident angle	MMF	Multi-mode fibers
$N_{ref}(\theta)$	Total number of reflections	λ_{res}^m	Resonance wavelength of the m^{th} cladding mode

References

[1] R.W. Wood, *On a remarkable case of uneven distribution of light in a diffraction grating spectrum.* Philosophical Magazine, 1902. 4(19-24): p. 396-402.

[2] L. Rayleigh, *Note on the remarkable case of diffraction spectra described by Prof. Wood.* Philosophical Magazine, 1907. 14(79-84): p. 60-65.

[3] A. Hessel, and A.A. Oliner, *A New Theory of Woods Anomalies on Optical Gratings.* Applied Optics, 1965. 4(10): p. 1275-&.

[4] R.W. Wood, *Anomalous diffraction gratings.* Physical Review, 1935. 48(12): p. 928-936.

[5] R.W. Wood, *Diffraction gratings with controlled groove form and abnormal distribution of intensity.* Philosophical Magazine, 1912. 23(133-8): p. 310-317.

[6] C.H. Palmer, *Parallel Diffraction Grating Anomalies.* Journal of the Optical Society of America, 1952. 42(4): p. 269-276.

[7] C.H. Palmer, *Diffraction Grating Anomalies .2. Coarse Gratings.* Journal of the Optical Society of America, 1956. 46(1): p. 50-53.

[8] Ritchie, R.H., *Plasma Losses by Fast Electrons in Thin Films.* Physical Review, 1957. 106(5): p. 874-881.

[9] C.J. Powell, and J.B. Swan, *Effect of Oxidation on the Characteristic Loss Spectra of Aluminum and Magnesium.* Physical Review, 1960. 118(3): p. 640-643.

[10] D. Bohm and D. Pines, *A Collective Description of Electron Interactions .1. Magnetic Interactions.* Physical Review, 1951. 82(5): p. 625-634.

[11] D. Pines and D. Bohm, *A Collective Description of Electron Interactions .2. Collective Vs Individual Particle Aspects of the Interactions.* Physical Review, 1952. 85(2): p. 338-353.

[12] D. Bohm and D. Pines, *A Collective Description of Electron Interactions .3. Coulomb Interactions in a Degenerate Electron Gas.* Physical Review, 1953. 92(3): p. 609-625.

[13] E. Burstein, et al., *Surface Polaritons - Propagating Electromagnetic Modes at Interfaces.* Journal of Vacuum Science & Technology, 1974. 11(6): p. 1004-1019.

[14] E. Kretschm and H. Raether, *Radiative Decay of Non Radiative Surface Plasmons Excited by Light.* Zeitschrift Fur Naturforschung Part a-Astrophysik Physik Und Physikalische Chemie, 1968. A 23(12): p. 2135-&.

[15] E. Kretschm, *Determination of Optical Constants of Metals by Excitation of Surface Plasmons.* Zeitschrift Fur Physik, 1971. 241(4): p. 313-&.

[16] A. Otto, *Excitation of Nonradiative Surface Plasma Waves in Silver by Method of Frustrated Total Reflection.* Zeitschrift Fur Physik, 1968. 216(4): p. 398-&.

[17] H. Raether, *Surface-Plasmons on Smooth and Rough Surfaces and on Gratings.* Springer Tracts in Modern Physics, 1988. 111: p. 1-133.

[18] Boardman, A.D., *Electromagnetic surface modes.* John Wiley & Sons, New York, 1982.

[19] D.W. Lubbers and N. Opitz, The pCO2-/pO2-optode: a new probe for measurement of pCO2 or pO in fluids and gases. Zeitschrift Fur Naturforschung C-a Journal of Biosciences, 1975. 30(7-8): p. 532-533.

[20] I. Pockrand, et al., *Surface-Plasmon Spectroscopy of Organic Monolayer Assemblies.* Surface Science, 1978. 74(1): p. 237-244.

[21] B. Liedberg, I. Lundstrom, and E. Stenberg, *Principles of Biosensing with an Extended Coupling Matrix and Surface-Plasmon Resonance.* Sensors and Actuators B-Chemical, 1993. 11(1-3): p. 63-72.

[22] M.T. Flanagan and R.H. Pantell, *Surface-Plasmon Resonance and Immunosensors.* Electronics Letters, 1984. 20(23): p. 968-970.

[23] C. Nylander, B. Liedberg, and T. Lind, *Gas-Detection by Means of Surface-Plasmon Resonance.* Sensors and Actuators, 1982. 3(1): p. 79-88.

[24] O.S. Wolfbeis, *Optical Sensing Based on Analyte Recognition by Enzymes, Carriers and Molecular-Interactions.* Analytica Chimica Acta, 1991. 250(1): p. 181-201.

[25] A. Brecht and G. Gauglitz, *Optical Probes and Transducers.* Biosensors & Bioelectronics, 1995. 10(9-10): p. 923-936.

[26] J.G. Gordon and S. Ernst, *Surface-Plasmons as a Probe of the Electrochemical Interface.* Surface Science, 1980. 101(1-3): p. 499-506.

[27] B. Liedberg, C. Nylander, and I. Lundstrom, *Surface-Plasmon Resonance for Gas-Detection and Biosensing.* Sensors and Actuators, 1983. 4(2): p. 299-304.

[28] B. Liedberg, C. Nylander, and I. Lundstrom, *Biosensing with Surface-Plasmon Resonance - How It All Started.* Biosensors & Bioelectronics, 1995. 10(8): p. R1-R9.

[29] E.S. Forzani, et al., *Detection of arsenic in groundwater using a surface plasmon resonance sensor.* Sensors and Actuators B-Chemical, 2007. 123(1): p. 82-88.

[30] H. Tran, et al., *Surface plasmon resonance detection of ricin and horticultural ricin variants in environmental samples.* Toxicon, 2008. 52(4): p. 582-588.

[31] B.N., Feltis, et al., *A hand-held surface plasmon resonance biosensor for the detection of ricin and other biological agents.* Biosensors & Bioelectronics, 2008. 23(7): p. 1131-1136.

[32] M. Seifert, S. Haindl, and B. Hock, *Development of an enzyme linked receptor assay (ELRA) for estrogens and xenoestrogens.* Analytica Chimica Acta, 1999. 386(3): p. 191-199.

[33] B. Hock, M. Seifert, and K. Kramer, *Engineering receptors and antibodies for biosensors.* Biosensors & Bioelectronics, 2002. 17(3): p. 239-249.

[34] C. Mouvet, et al., *Determination of simazine in water samples by waveguide surface plasmon resonance.* Analytica Chimica Acta, 1997. 338(1-2): p. 109-117.

[35] E. Mauriz, et al., *Determination of carbaryl in natural water samples by a surface plasmon resonance flow-through immunosensor.* Biosensors & Bioelectronics, 2006. 21(11): p. 2129-2136.

[36] E. Mauriz, et al., *Real-time detection of chlorpyrifos at part per trillion levels in ground, surface and drinking water samples by a portable surface plasmon resonance immunosensor.* Analytica Chimica Acta, 2006. 561(1-2): p. 40-47.

[37] E. Mauriz, et al., *Determination of environmental organic pollutants with a portable optical immunosensor.* Talanta, 2006. 69(2): p. 359-364.

[38] C. Boulart, et al., *A novel, low-cost, high performance dissolved methane sensor for aqueous environments.* Optics Express, 2008. 16(17): p. 12607-12617.

[39] T. Kang, et al., *Fabrication of reusable sensor for detection of Cu2+ in an aqueous solution using a self-assembled monolayer with surface plasmon resonance spectroscopy.* Chemical Communications, 2005(29): p. 3721-3723.

[40] T.M. Chinowsky, et al., *Portable 24-analyte surface plasmon resonance instruments for rapid, versatile biodetection (vol 22, pg 9, 2007).* Biosensors & Bioelectronics, 2007. 23(1): p. 149-149.

[41] V. Koubova, et al., *Detection of foodborne pathogens using surface plasmon resonance biosensors.* Sensors and Actuators B-Chemical, 2001. 74(1-3): p. 100-105.

[42] S.J. Kim, et al., *Novel miniature SPR immunosensor equipped with all-in-one multi-microchannel sensor chip for detecting low-molecular-weight analytes.* Biosensors & Bioelectronics, 2007. 23(5): p. 701-707.

[43] M. Palumbo, et al., *Surface plasmon resonance sensing of liquids using polyelectrolyte thin films.* Sensors and Actuators B-Chemical, 2003. 91(1-3): p. 291-297.

[44] E. Maciak, Z. Opilski, and T. Pustelny, *Effect of humidity on nh3 gas sensitivity of nafion/wo3 sensing structure of spr sensor.* Molecular and Quantum Acoustics, 2001. 26: p. 205-2015.

[45] D. Kitenge, et al., *Nanostructured Silver Films for Surface Plasmon Resonance-Based Gas Sensors.* Ieee Sensors Journal, 2009. 9(12): p. 1797-1801.

[46] A.S. El-Basaty, et al., *Surface plasmon sensor for NO_2 gas.* Surface and Interface Analysis, 2008. 40(13): p. 1623-1626.

[47] P. Tobiska, et al., *An integrated optic hydrogen sensor based on SPR on palladium.* Sensors and Actuators B-Chemical, 2001. 74(1-3): p. 168-172.

[48] X. Bevenot, et al., *Surface plasmon resonance hydrogen sensor using an optical fibre.* Measurement Science & Technology, 2002. 13(1): p. 118-124.

[49] J.L. Hu, et al., *Smart and Reversible Surface Plasmon Resonance Responses to Various Atmospheres for Silver Nanoparticles Loaded in Mesoporous SiO2.* Journal of Physical Chemistry C, 2009. 113(44): p. 19039-19045.

[50] H. Nanto, et al. *Odor sensor utilizing surface plasmon resonance for environmental monitoring*. 2004.

[51] N.M. Aguirre, et al., *Development of a surface plasmon resonance n-dodecane vapor sensor.* Sensors, 2007. 7(9): p. 1954-1961.

[52] J. Homola, *Surface plasmon resonance sensors for detection of chemical and biological species.* Chemical Reviews, 2008. 108(2): p. 462-493.

[53] A. Leinse, et al. *The life marker chip for the Exomars mission*. in *Information Photonics (IP), 2011 ICO International Conference on*. 2011.

[54] J. Dakin, and B. Culshaw, *Optical fiber sensors: applications, analysis, and future trends*. 1997: Artech House Publishers.

[55] R.C. Jorgenson and S.S. Yee, *A fiber-optic chemical sensor based on surface plasmon resonance.* Sensors and Actuators B: Chemical, 1993. 12(3): p. 213-220.

[56] A.J.C. Tubb, et al., *Single-mode optical fibre surface plasma wave chemical sensor.* Sensors and Actuators B: Chemical, 1997. 41(1–3): p. 71-79.
[57] J. Villatoro, D. Monzón-Hernández, and E. Mejía, *Fabrication and modeling of uniform-waist single-mode tapered optical fiber sensors.* Applied Optics, 2003. 42(13): p. 2278-2283.
[58] J. Homola and R. Slavik *Fibre-optic sensor based on surface plasmon resonance*. Electronics Letters, 1996. 32, 480-482.
[59] R. Kashyap and G. Nemova, *Surface Plasmon Resonance-Based Fiber and Planar Waveguide Sensors.* Journal of Sensors, 2009. 2009: p. 9.
[60] B.D. Gupta and A.K. Sharma, *Sensitivity evaluation of a multi-layered surface plasmon resonance-based fiber optic sensor: a theoretical study.* Sensors and Actuators B-Chemical, 2005. 107(1): p. 40-46.
[61] G. Nemova and R. Kashyap, *Modeling of plasmon-polariton refractive-index hollow core fiber sensors assisted by a fiber Bragg grating.* Lightwave Technology, Journal of, 2006. 24(10): p. 3789-3796.
[62] M. Skorobogatiy and A. Kabashin, *Plasmon excitation by the Gaussian-like core mode of a photonic crystal waveguide.* Optics Express, 2006. 14(18): p. 8419-8424.
[63] P.J.A. Sazio, et al., *Microstructured optical fibers as high-pressure microfluidic reactors.* Science, 2006. 311(5767): p. 1583-1586.
[64] M. Hautakorpi, M. Mattinen, and H. Ludvigsen, *Surface-plasmon-resonance sensor based on three-hole microstructured optical fiber.* Optics Express, 2008. 16(12): p. 8427-8432.
[65] Y.T Zhang, et al., *Wagon wheel fiber based multichannel plasmonic sensor.* Optics Express, 2011. 19(23): p. 22863-22873.
[66] I.R. Hooper, M. Rooth, and J.R. Sambles, *Dual-channel differential surface plasmon ellipsometry for bio-chemical sensing.* Biosensors & Bioelectronics, 2009. 25(2): p. 411-417.
[67] T. Allsop, et al., *Generation of infared surface plasmon resonances with high refractive index sensitivity utilizing titled fiber Bragg grafings.* Applied Optics, 2007. 46(22): p. 5456-5460.
[68] N. Díaz-Herrera, et al., *Refractive index sensing of aqueous media based on plasmonic resonance in tapered optical fibres operating in the 1.5 μm region.* Sensors and Actuators B: Chemical, 2010. 146(1): p. 195-198.
[69] V. Singh, et al., *Integrated Optical Sensors.* Ieee Photonics Journal, 2012. 4(2): p. 638-641.
[70] Manickam, G., et al., *Protection and functionalisation of silver as an optical sensing platform for highly sensitive SPR based analysis.* Analyst, 2012. 137(22): p. 5265-71.
[71] E. Hutter, and J.H. Fendler, *Exploitation of localized surface plasmon resonance.* Advanced Materials, 2004. 16(19): p. 1685-1706.
[72] W. Fritzsche, and T.A. Taton, *Metal nanoparticles as labels for heterogeneous, chip-based DNA detection.* Nanotechnology, 2003. 14(12): p. R63-R73.
[73] S.M. Nie and S.R. Emery, *Probing single molecules and single nanoparticles by surface-enhanced Raman scattering.* Science, 1997. 275(5303): p. 1102-1106.
[74] K. Kneipp, et al., *Single molecule detection using surface-enhanced Raman scattering (SERS).* Physical Review Letters, 1997. 78(9): p. 1667-1670.
[75] Z.Q. Tian, B. Ren, and D.Y. Wu, *Surface-enhanced Raman scattering: From noble to transition metals and from rough surfaces to ordered nanostructures.* Journal of Physical Chemistry B, 2002. 106(37): p. 9463-9483.
[76] A. Pucci, et al., *Surface enhanced infrared spectroscopy using gold nanoantennas.* Physica Status Solidi B-Basic Solid State Physics, 2010. 247(8): p. 2071-2074.
[77] C.D. Geddes, et al., *Metal-enhanced fluorescence (MEF) due to silver colloids on a planar surface: Potential applications of indocyanine green to in vivo imaging.* Journal of Physical Chemistry A, 2003. 107(18): p. 3443-3449.
[78] J.A. Sanchez-Gil, J.V. Garcia-Ramos, and E.R. Mendez, *Electromagnetic mechanism in surface-enhanced Raman scattering from Gaussian-correlated randomly rough metal substrates.* Optics Express, 2002. 10(17): p. 879-886.
[79] E. Prodan, et al., *A hybridization model for the plasmon response of complex nanostructures.* Science, 2003. 302(5644): p. 419-422.
[80] C.E. Talley, et al., *Surface-enhanced Raman scattering from individual Au nanoparticles and nanoparticle dimer substrates.* Nano Letters, 2005. 5(8): p. 1569-1574.
[81] P.K. Jain and M.A. El-Sayed, *Plasmonic coupling in noble metal nanostructures.* Chemical Physics Letters, 2010. 487(4-6): p. 153-164.
[82] K. Yoshida, et al., *Quantitative evaluation of electromagnetic enhancement in surface-enhanced resonance Raman scattering from plasmonic properties and morphologies of individual Ag nanostructures.* Physical Review B, 2010. 81(11).

[83] J. Grand, et al., *Role of localized surface plasmons in surface-enhanced Raman scattering of shape-controlled metallic particles in regular arrays.* Physical Review B, 2005. 72(3).
[84] H.Y. Chu, et al., *A high sensitive fiber SERS probe based on silver nanorod arrays.* Optics Express, 2007. 15(19): p. 12230-12239.
[85] J. Homola, *Electromagnetic Theory of Surface Plasmons*, in *Surface Plasmon Resonance Based Sensors*, J. Homola, Editor. 2006, Springer Berlin Heidelberg. p. 3-44.
[86] P.P. Markowicz, et al., *Phase-sensitive time-modulated surface plasmon resonance polarimetry for wide dynamic range biosensing.* Optics Express, 2007. 15(4): p. 1745-1754.
[87] J.N. Anker, et al., *Biosensing with plasmonic nanosensors.* Nature Materials, 2008. 7(6): p. 442-453.
[88] K.R., Li, et al., *Surface plasmon amplification by stimulated emission in nanolenses.* Physical Review B, 2005. 71(11).
[89] A.J. Haes, and R.P. Van Duyne, *A unified view of propagating and localized surface plasmon resonance biosensors.* Analytical and Bioanalytical Chemistry, 2004. 379(7-8): p. 920-930.
[90] S. Lal, S. Link, and N.J. Halas, *Nano-optics from sensing to waveguiding.* Nature Photonics, 2007. 1(11): p. 641-648.
[91] R. Karlsson, *SPR for molecular interaction analysis: a review of emerging application areas.* Journal of Molecular Recognition, 2004. 17(3): p. 151-161.
[92] E. Popov, B. Bozkov, and M. Neviere, *The inverted surface plasmon resonance: Phenomenological explanation.* Journal of Modern Optics, 1996. 43(6): p. 1101-1110.
[93] A. Otto, *Excitation of nonradiative surface plasma waves in silver by the method of frustrated total reflection.* European Physical Journal A, 1968. 216(4): p. 398-410.
[94] J. Homola, H.B. Lu, and S.S. Yee, *Dual-channel surface plasmon resonance sensor with spectral discrimination of sensing channels using dielectric overlayer.* Electronics Letters, 1999. 35(13): p. 1105-1106.
[95] G.G. Nenninger, et al., *Reference-compensated biosensing using a dual-channel surface plasmon resonance sensor system based on a planar lightpipe configuration.* Sensors and Actuators B-Chemical, 1998. 51(1-3): p. 38-45.
[96] A. Snyder, and J. Love, *Optical waveguide theory*. 1983: Springer.
[97] O. Esteban, et al., *Simple model of compound waveguide structures used as fiber-optic sensors.* Optics and Lasers in Engineering, 2000. 33(3): p. 219-230.
[98] P. Yeh, *Optical waves in layered media*. 1988: Wiley New York.
[99] M. Kanso, S. Cuenot, and G. Louarn, *Sensitivity of optical fiber sensor based on surface plasmon resonance: Modeling and experiments.* Plasmonics, 2008. 3(2-3): p. 49-57.
[100] A.K. Sharma, and B.D. Gupta, *On the sensitivity and signal to noise ratio of a step-index fiber optic surface plasmon resonance sensor with bimetallic layers.* Optics Communications, 2005. 245(1-6): p. 159-169.
[101] P. Mulvaney, *Surface plasmon spectroscopy of nanosized metal particles.* Langmuir, 1996. 12(3): p. 788-800.
[102] W. Tropf, M. Thomas, and T. Harris, *Optical properties of crystals and glasses*, in *Handbook of Optics*. 1995.
[103] B.D. Gupta, A. Sharma, and S.D. Singh, Int. J. Optoelectron, 1993. 8: p. 409.
[104] C. Hu, and D. Liu, *High-performance Grating Coupled Surface Plasmon Resonance Sensor Based on Al-Au Bimetallic Layer.* Mod. Appl. Sci., 2010. 4(6): p. 8.
[105] A.K. Sharma, and B.D. Gupta, *On the performance of different bimetallic combinations in surface plasmon resonance based fiber optic sensors.* Journal of Applied Physics, 2007. 101(9).
[106] N. Díaz-Herrera, et al., *Fibre-optic SPR sensor with a FBG interrogation scheme for readout enhancement.* Sensors and Actuators B: Chemical, 2010. 144(1): p. 226-231.
[107] S. Lofas, et al., *Bioanalysis with Surface-Plasmon Resonance.* Sensors and Actuators B-Chemical, 1991. 5(1-4): p. 79-84.
[108] E.C. Nice, and B. Catimel, *Instrumental biosensors: new perspectives for the analysis of biomolecular interactions.* Bioessays, 1999. 21(4): p. 339-352.
[109] C. Thirstrup, et al., *Diffractive optical coupling element for surface plasmon resonance sensors.* Sensors and Actuators B-Chemical, 2004. 100(3): p. 298-308.
[110] H.C. Pedersen, and C. Thirstrup, *Design of near-field holographic optical elements by grating matching.* Applied Optics, 2004. 43(6): p. 1209-1215.
[111] H.C. Pedersen, et al., *Integrated holographic grating chip for surface plasmon resonance sensing.* Optical Engineering, 2004. 43(11): p. 2505-2510.
[112] D.G. Hong, et al., *Development of an immunosensor with angular interrogation-based SPR spectroscopy.* Measurement Science & Technology, 2007. 18(5): p. 1367-1371.

[113] J. Homola, I. Koudela, and S.S. Yee, *Surface plasmon resonance sensors based on diffraction gratings and prism couplers: sensitivity comparison.* Sensors and Actuators B-Chemical, 1999. 54(1-2): p. 16-24.
[114] J. Homola, et al., *Spectral surface plasmon resonance biosensor for detection of staphylococcal enterotoxin B in milk.* International Journal of Food Microbiology, 2002. 75(1-2): p. 61-69.
[115] G.G. Nenninger, M. Piliarik, and J. Homola, *Data analysis for optical sensors based on spectroscopy of surface plasmons.* Measurement Science & Technology, 2002. 13(12): p. 2038-2046.
[116] J. Homola, et al., *A novel multichannel surface plasmon resonance biosensor.* Sensors and Actuators B-Chemical, 2001. 76(1-3): p. 403-410.
[117] J. Dostalek, H. Vaisocherova, and J. Homola, *Multichannel surface plasmon resonance biosensor with wavelength division multiplexing.* Sensors and Actuators B-Chemical, 2005. 108(1-2): p. 758-764.
[118] R.C. Jorgenson and S.S. Yee, *A Fiberoptic Chemical Sensor-Based on Surface-Plasmon Resonance.* Sensors and Actuators B-Chemical, 1993. 12(3): p. 213-220.
[119] L.A. Obando, et al., *Manufacture of robust surface plasmon resonance fiber optic based dip-probes.* Sensors and Actuators B-Chemical, 2004. 100(3): p. 439-449.
[120] M. Iga, A. Seki, and K. Watanabe, *Hetero-core structured fiber optic surface plasmon resonance sensor with silver film.* Sensors and Actuators B-Chemical, 2004. 101(3): p. 368-372.
[121] X. Zhao, et al., *Improvement of the sensitivity of the surface plasmon resonance sensors based on multi-layer modulation techniques.* Optics Communications, 2015. 335(0): p. 32-36.
[122] M.J. Jory, et al., *A Surface-Plasmon-Based Optical Sensor Using Acoustooptics.* Measurement Science & Technology, 1995. 6(8): p. 1193-1200.
[123] B. Sepulveda, et al., *Highly sensitive detection of biomolecules with the magneto-optic surface-plasmon-resonance sensor.* Optics Letters, 2006. 31(8): p. 1085-1087.
[124] C.E. Jordan, et al., *Surface plasmon resonance imaging measurements of DNA hybridization adsorption and streptavidin/DNA multilayer formation at chemically modified gold surfaces.* Analytical Chemistry, 1997. 69(24): p. 4939-4947.
[125] C.E. Jordan and R.M. Corn, *Surface plasmon resonance imaging measurements of electrostatic biopolymer adsorption onto chemically modified gold surfaces.* Analytical Chemistry, 1997. 69(7): p. 1449-1456.
[126] B.P. Nelson, et al., *Near-infrared surface plasmon resonance measurements of ultrathin films. 1. Angle shift and SPR imaging experiments.* Analytical Chemistry, 1999. 71(18): p. 3928-3934.
[127] B.P. Nelson, et al., *Surface plasmon resonance imaging measurements of DNA and RNA hybridization adsorption onto DNA microarrays.* Analytical Chemistry, 2001. 73(1): p. 1-7.
[128] E. Fu, J. Foley, and P. Yager, *Wavelength-tunable surface plasmon resonance microscope.* Review of Scientific Instruments, 2003. 74(6): p. 3182-3184.
[129] E. Fu, et al., *Characterization of a wavelength-tunable surface plasmon resonance microscope.* Review of Scientific Instruments, 2004. 75(7): p. 2300-2304.
[130] A.W. Wark, H.J. Lee, and R.M. Corn, *Long-range surface plasmon resonance imaging for bioaffinity sensors.* Analytical Chemistry, 2005. 77(13): p. 3904-3907.
[131] A. Zybin, et al., *Double-wavelength technique for surface plasmon resonance measurements: Basic concept and applications for single sensors and two-dimensional sensor arrays.* Analytical Chemistry, 2005. 77(8): p. 2393-2399.
[132] J.S. Shumaker-Parry and C.T. Campbell, *Quantitative methods for spatially resolved adsorption/desorption measurements in real time by surface plasmon resonance microscopy.* Analytical Chemistry, 2004. 76(4): p. 907-917.
[133] J.S. Shumaker-Parry, R. Aebersold, and C.T. Campbell, *Parallel, quantitative measurement of protein binding to a 120-element double-stranded DNA array in real time using surface plasmon resonance microscopy.* Analytical Chemistry, 2004. 76(7): p. 2071-2082.
[134] C.T. Campbell and G. Kim, *SPR microscopy and its applications to high-throughput analyses of biomolecular binding events and their kinetics.* Biomaterials, 2007. 28(15): p. 2380-2392.
[135] M. Piliarik, J. Katainen, and J. Homola, *Novel polarization control for high-throughput surface plasmon resonance sensors.* Optical Sensing Technology and Applications, 2007. 6585.
[136] M. Piliarik, H. Vaisocherova, and J. Homola, *A new surface plasmon resonance sensor for high-throughput screening applications.* Biosensors & Bioelectronics, 2005. 20(10): p. 2104-2110.
[137] M. Piliarik, H. Vaisocherova, and J. Homola, *Towards parallelized surface plasmon resonance sensor platform for sensitive detection of oligonucleotides.* Sensors and Actuators B-Chemical, 2007. 121(1): p. 187-193.
[138] P.I. Nikitin, et al., *Surface plasmon resonance interferometry for biological and chemical sensing.* Sensors and Actuators B-Chemical, 1999. 54(1-2): p. 43-50.

[139] P.I. Nikitin, et al., *Surface plasmon resonance interferometry for micro-array biosensing.* Sensors and Actuators a-Physical, 2000. 85(1-3): p. 189-193.
[140] A.G. Notcovich, V. Zhuk, and S.G. Lipson, *Surface plasmon resonance phase imaging.* Applied Physics Letters, 2000. 76(13): p. 1665-1667.
[141] C.M. Wu, et al., *High-sensitivity sensor based on surface plasmon resonance and heterodyne interferometry.* Sensors and Actuators B-Chemical, 2003. 92(1-2): p. 133-136.
[142] E. Alieva, and V.N. Konopsky, *Biosensor based on surface plasmon interferometry independent on variations of liquid's refraction index.* Sensors and Actuators B-Chemical, 2004. 99(1): p. 90-97.
[143] R. Naraoka and K. Kajikawa, *Phase detection of surface plasmon resonance using rotating analyzer method.* Sensors and Actuators B-Chemical, 2005. 107(2): p. 952-956.
[144] H.P. Ho, W.W. Lam, and S.Y. Wu, *Surface plasmon resonance sensor based on the measurement of differential phase.* Review of Scientific Instruments, 2002. 73(10): p. 3534-3539.
[145] S.Y. Wu, et al., *Highly sensitive differential phase-sensitive surface plasmon resonance biosensor based on the Mach-Zehnder configuration.* Optics Letters, 2004. 29(20): p. 2378-2380.
[146] H.P. Ho, et al., *Real-time optical biosensor based on differential phase measurement of surface plasmon resonance.* Biosensors & Bioelectronics, 2005. 20(10): p. 2177-2180.
[147] H.P. Ho, et al., *Phase-sensitive surface plasmon resonance biosensor using the photoelastic modulation technique.* Sensors and Actuators B-Chemical, 2006. 114(1): p. 80-84.
[148] W. Yuan, et al., *Surface plasmon resonance biosensor incorporated in a Michelson interferometer with enhanced sensitivity.* Ieee Sensors Journal, 2007. 7(1-2): p. 70-73.
[149] Y.C. Li, et al., *Differential-phase surface plasmon resonance biosensor.* Analytical Chemistry, 2008. 80(14): p. 5590-5595.
[150] Y. Xinglong, et al., *Immunosensor based on optical heterodyne phase detection.* Sensors and Actuators B: Chemical, 2001. 76(1–3): p. 199-202.
[151] H.P. Chiang, J.L. Lin, and Z.W. Chen, *High sensitivity surface plasmon resonance sensor based on phase interrogation at optimal incident wavelengths.* Applied Physics Letters, 2006. 88(14).
[152] S.P. Ng, et al., *White-light spectral interferometry for surface plasmon resonance sensing applications.* Optics Express, 2011. 19(5): p. 4521-4527.
[153] T.T. Ehler, and L.J. Noe, *Surface Plasmon Studies of Thin Silver/Gold Bimetallic Films.* Langmuir, 1995. 11(10): p. 4177-4179.
[154] S.A. Zynio, et al., *Bimetallic layers increase sensitivity of affinity sensors based on surface plasmon resonance.* Sensors, 2002. 2(2): p. 62-70.
[155] M. Mitsushio, K. Miyashita, and M. Higo, *Sensor properties and surface characterization of the metal-deposited SPR optical fiber sensors with Au, Ag, Cu, and Al.* Sensors and Actuators A: Physical, 2006. 125(2): p. 296-303.
[156] R. Slavik, J. Homola, and J. Ctyroky, *Miniaturization of fiber optic surface plasmon resonance sensor.* Sensors and Actuators B-Chemical, 1998. 51(1-3): p. 311-315.
[157] B.D. Gupta and C.D. Singh, *Evanescent-absorption coefficient for diffuse source illumination: uniform- and tapered-fiber sensors.* Appl. Opt., 1994. 33(13): p. 2737-2742.
[158] B. Grunwald, and G. Holst, *Fibre optic refractive index microsensor based on white-light SPR excitation.* Sensors and Actuators a-Physical, 2004. 113(2): p. 174-180.
[159] Y.C. Kim, et al., *Tapered fiber optic surface plasmon resonance sensor for analyses of vapor and liquid phases.* Optics Letters, 2005. 30(17): p. 2218-2220.
[160] M. Niggemann, et al., *Remote sensing of tetrachloroethene with a micro-fibre optical gas sensor based on surface plasmon resonance spectroscopy.* Sensors and Actuators B: Chemical, 1996. 34(1–3): p. 328-333.
[161] L.A. Obando, and K.S. Booksh, *Tuning Dynamic Range and Sensitivity of White-Light, Multimode, Fiber-Optic Surface Plasmon Resonance Sensors.* Analytical Chemistry, 1999. 71(22): p. 5116-5122.
[162] Y. Yuan, et al., *Theoretical investigations for surface plasmon resonance based optical fiber tip sensor.* Sensors and Actuators B: Chemical, 2013. 188(0): p. 757-760.
[163] P. Winsemius, et al., *Temperature dependence of the optical properties of Au, Ag and Cu.* Journal of Physics F: Metal Physics, 1976. 6(8): p. 1583.
[164] J.R. Devore, *Refractive Indices of Rutile and Sphalerite.* Journal of the Optical Society of America, 1951. 41(6): p. 416-417.
[165] E.D. Palik, *Handbook of optical constants of solids*. 1985, Orlando: Academic Press.
[166] I.H. Malitson, *Interspecimen Comparison of the Refractive Index of Fused Silica.* Journal of the Optical Society of America, 1965. 55(10): p. 1205-1208.
[167] O. Frazao, et al., *Optical flowmeter using a modal interferometer based on a single nonadiabatic fiber taper.* Optics Letters, 2007. 32(14): p. 1974-1976.

[168] Z.B. Tian, et al., *Refractive index sensing with Mach-Zehnder interferometer based on concatenating two single-mode fiber tapers.* Ieee Photonics Technology Letters, 2008. 20(5-8): p. 626-628.
[169] T.A. Birks, *Twist-Induced Tuning in Tapered Fiber Couplers.* Applied Optics, 1989. 28(19): p. 4226-4233.
[170] F.J. Arregui, I.R. Matias, and M. Lopez-Amo, *Optical fiber strain gauge based on a tapered single-mode fiber.* Sensors and Actuators a-Physical, 2000. 79(2): p. 90-96.
[171] K.Q. Kieu, and M. Mansuripur, *Biconical fiber taper sensors.* Ieee Photonics Technology Letters, 2006. 18(21-24): p. 2239-2241.
[172] S. Patane, et al., *Polarization-maintaining near-field optical probes.* Journal of Microscopy-Oxford, 2008. 229(2): p. 377-383.
[173] G.J. Pendock, H.S. Mackenzie, and F.P. Payne, *Dye-Lasers Using Tapered Optical Fibers.* Applied Optics, 1993. 32(27): p. 5236-5242.
[174] A.J. Fielding, and C.C. Davis, *Tapered single-mode optical fiber evanescent coupling.* Ieee Photonics Technology Letters, 2002. 14(1): p. 53-55.
[175] M.J. Humphrey, et al., *Calculation of optimal fiber radius and whispering-gallery mode spectra for a fiber-coupled microsphere.* Optics Communications, 2007. 271(1): p. 124-131.
[176] J.M. Ward, P. Feron, and S.N. Chormaic, *A taper-fused microspherical laser source.* Ieee Photonics Technology Letters, 2008. 20(5-8): p. 392-394.
[177] T.A. Birks, W.J. Wadsworth, and P.S. Russell, *Supercontinuum generation in tapered fibers.* Optics Letters, 2000. 25(19): p. 1415-1417.
[178] J. Villatoro, D. Monzon-Hernandez, and E. Mejia, *Fabrication and modeling of uniform-waist single-mode tapered optical fiber sensors.* Applied Optics, 2003. 42(13): p. 2278-2283.
[179] O. Esteban, et al., *Surface plasmon resonance sensors based on uniform-waist tapered fibers in a reflective configuration.* Applied Optics, 2006. 45(28): p. 7294-7298.
[180] B.D. Gupta and C.D. Singh, *Evanescent-Absorption Coefficient for Diffuse Source Illumination - Uniform-Fiber and Tapered-Fiber Sensors.* Applied Optics, 1994. 33(13): p. 2737-2742.
[181] R. Jha, R.K. Verma, and B.D. Gupta, *Surface Plasmon Resonance-Based Tapered Fiber Optic Sensor: Sensitivity Enhancement by Introducing a Teflon Layer Between Core and Metal Layer.* Plasmonics, 2008. 3(4): p. 151-156.
[182] A. Ankiewicz, C. Pask, and A.W. Snyder, *Slowly Varying Optical Fibers.* Journal of the Optical Society of America, 1982. 72(2): p. 198-203.
[183] J.L. Santos and F. Farahi, *Handbook of Optical Sensors*. 2014: CRC Press.
[184] J., Janata, *Principles of Chemical Sensing*. 2009: Springer.
[185] F.S. Ligler and C.R. Taitt, *Optical Biosensors: Today and Tomorrow*. 2011.
[186] J.G. Webster and H. Eren, *Measurement, Instrumentation and Sensors Handbook*. 2014.
[187] Y. Q. Yuan, et al., *Theoretical investigations for surface plasmon resonance based optical fiber tip sensor.* Sensors and Actuators B-Chemical, 2013. 188: p. 757-760.
[188] S. Enoch and N. Bonod, *Plasmonics: from basics to advanced topics*. 2012: Springer.
[189] A.K. Sharma, R. Jha, and B.D. Gupta, *Fiber-Optic Sensors Based on Surface Plasmon Resonance: A Comprehensive Review.* Sensors Journal, IEEE, 2007. 7(8): p. 1118-1129.
[190] P. Bhatia and B.D. Gupta, *Surface-plasmon-resonance-based fiber-optic refractive index sensor: sensitivity enhancement.* Applied Optics, 2011. 50(14): p. 2032-2036.
[191] S. Patskovsky, et al., *Near-infrared surface plasmon resonance sensing on a silicon platform.* Sensors and Actuators B: Chemical, 2004. 97(2): p. 409-414.
[192] A. Dıez, M. Andres, and J. Cruz, *In-line fiber-optic sensors based on the excitation of surface plasma modes in metal-coated tapered fibers.* Sensors and Actuators B: Chemical, 2001. 73(2): p. 95-99.
[193] T. Allsop, et al., *Generation of infrared surface plasmon resonances with high refractive index sensitivity utilizing tilted fiber Bragg gratings.* Applied optics, 2007. 46(22): p. 5456-5460.
[194] R.C. Jorgenson and S.S. Yee, *Control of the Dynamic-Range and Sensitivity of a Surface-Plasmon Resonance Based Fiber Optic Sensor.* Sensors and Actuators a-Physical, 1994. 43(1-3): p. 44-48.
[195] J. Ctyroky, J. Homola, and M. Skalsky, *Tuning of spectral operation range of a waveguide surface plasmon resonance sensor.* Electronics Letters, 1997. 33(14): p. 1246-1248.
[196] H. Moayyed, et al., *Analysis of Phase Interrogated SPR Fiber Optic Sensors With Bimetallic Layers.* Ieee Sensors Journal, 2014. 14(10): p. 3662-3668.
[197] M. Born, and E. Wolf, *Principles of Optics*. 2003.
[198] A.M. Vengsarkar, et al., *Long-period fiber gratings as band-rejection filters.* Journal of Lightwave Technology, 1996. 14(1): p. 58-65.
[199] T. Erdogan, *Fiber grating spectra.* Journal of Lightwave Technology, 1997. 15(8): p. 1277-1294.

[200] T.W. MacDougall, et al., *Generalized expression for the growth of long period gratings.* Ieee Photonics Technology Letters, 1998. 10(10): p. 1449-1451.
[201] Y.N. Zhu, et al., *EDFA gain flattening using phase-shifted long-period grating.* Microwave and Optical Technology Letters, 2003. 37(2): p. 153-157.
[202] O. Deparis, et al., *Bandpass filters based on pi-shifted long-period fiber gratings for actively mode-locked erbium fiber lasers.* Optics Letters, 2001. 26(16): p. 1239-1241.
[203] X.W. Dong, et al., *Add/drop channel filter based on two parallel long-period fiber gratings coupler.* Optik, 2009. 120(16): p. 855-859.
[204] H.J. Patrick, C.C. Chang, and S.T. Vohra, *Long period fibre gratings for structural bend sensing.* Electronics Letters, 1998. 34(18): p. 1773-1775.
[205] F.J. O'Flaherty, et al., *Temperature characterisation of long-period gratings for sensor applications.* Microwave and Optical Technology Letters, 2004. 42(5): p. 402-405.
[206] G. Ghosh, *Temperature Dispersion of Refractive-Indexes in Some Silicate Fiber Glasses.* Ieee Photonics Technology Letters, 1994. 6(3): p. 431-433.
[207] M. Chomat, et al., *Temperature sensitivity of long-period gratings inscribed with a CO2 laser in optical fiber with graded-index cladding.* Sensors and Actuators B-Chemical, 2006. 119(2): p. 642-650.
[208] A. van Brakel and P.L. Swart, *Temperature-compensated optical fiber Michelson refractometer.* Optical Engineering, 2005. 44(2).
[209] V. Bhatia, et al., *Simultaneous strain and temperature measurement with long-period gratings.* Optics Letters, 1997. 22(9): p. 648-650.
[210] J. Yang, et al., *Long-period grating refractive index sensor with a modified cladding structure for large operational range and high sensitivity.* Applied Optics, 2006. 45(24): p. 6142-6147.
[211] J.H. Chong, et al., *Measurements of refractive index sensitivity using long-period grating refractometer.* Optics Communications, 2004. 229(1-6): p. 65-69.
[212] G.M. Rego, J.L. Santos, and H.M. Salgado, *Refractive index measurement with long-period gratings arc-induced in pure-silica-core fibres.* Optics Communications, 2006. 259(2): p. 598-602.
[213] X. Chen, et al., *Optical chemsensors utilizing long-period fiber gratings UV-Inscribed in D-Fiber with enhanced sensitivity through cladding etching.* Ieee Photonics Technology Letters, 2004. 16(5): p. 1352-1354.
[214] A. Trouillet, E. Marin, and C. Veillas, *Fibre gratings for hydrogen sensing.* Measurement Science & Technology, 2006. 17(5): p. 1124-1128.
[215] R. Falciai, A.G. Mignani, and A. Vannini, *Long period gratings as solution concentration sensors.* Sensors and Actuators B-Chemical, 2001. 74(1-3): p. 74-77.
[216] A.M. Vengsarkar, *Long-period fiber gratings shape optical spectra.* Laser Focus World, 1996. 32(6): p. 243-+.
[217] V. Bhatia and A.M. Vengsarkar, *Optical fiber long-period grating sensors.* Optics Letters, 1996. 21(9): p. 692-694.
[218] V. Bhatia, et al., *Comparison of optical fiber long-period and Bragg grating sensors.* Smart Structures and Materials 1996: Smart Sensing, Processing, and Instrumentation, 1996. 2718: p. 110-121.
[219] T. Erdogan, *Cladding-mode resonances in short- and long-period fiber grating filters.* Journal of the Optical Society of America a-Optics Image Science and Vision, 1997. 14(8): p. 1760-1773.
[220] E. Anemogiannis, E.N. Glytsis, and T.K. Gaylord, *Transmission characteristics of long-period fiber gratings having arbitrary azimuthal/radial refractive index variations.* Journal of Lightwave Technology, 2003. 21(1): p. 218-227.
[221] C.D. Poole, H.M. Presby, and J.P. Meester, *2-Mode Fiber Spatial-Mode Converter Using Periodic Core Deformation.* Electronics Letters, 1994. 30(17): p. 1437-1438.
[222] H. Kyung Jun, et al., *Simultaneous measurement of strain and temperature incorporating a long-period fiber grating inscribed on a polarization-maintaining fiber.* Photonics Technology Letters, IEEE, 2004. 16(9): p. 2114-2116.
[223] G. Rego, et al., *High-temperature stability of long-period fiber gratings produced using an electric arc.* Journal of Lightwave Technology, 2001. 19(10): p. 1574-1579.
[224] S.T. Lee, et al., *Long period gratings in multimode optical fibers: application in chemical sensing.* Optics Communications, 2003. 224(4-6): p. 237-241.
[225] T.J. Eom, et al., *Optical pulse multiplication and temporal coding using true time delay achieved by long-period fiber gratings in dispersion compensating fiber.* Optics Express, 2004. 12(26): p. 6410-6420.
[226] L. Dong, L. Reekie, and J.L. Cruz, *Long period gratings formed in depressed cladding fibres.* Electronics Letters, 1997. 33(22): p. 1897-1898.

[227] G. Humbert, et al., *Long period grating filters fabricated with electric arc in dual concentric core fibers.* Optics Communications, 2003. 225(1-3): p. 47-53.
[228] I. Allsop, D.J. Webb, and I. Bennion, *Investigations of the spectral sensitivity of long period gratings fabricated in three-layered optical fiber.* Journal of Lightwave Technology, 2003. 21(1): p. 264-268.
[229] A.A. Abramov, et al., *Electrically tunable efficient broad-band fiber filter.* Ieee Photonics Technology Letters, 1999. 11(4): p. 445-447.
[230] D.M. Costantini, et al., *Tunable loss filter based on metal-coated long-period fiber grating.* Ieee Photonics Technology Letters, 1999. 11(11): p. 1458-1460.
[231] M.A. van Eijkelenborg, W. Padden, and J.A. Besley, *Mechanically induced long-period gratings in microstructured polymer fibre.* Optics Communications, 2004. 236(1-3): p. 75-78.
[232] P. Steinvurzel, et al., *Long period grating resonances in photonic bandgap fiber.* Opt Express, 2006. 14(7): p. 3007-14.
[233] P. Caldas, et al., *Characterization of the response of a dual resonance of an arc-induced long-period grating to various physical parameters.* Applied Optics, 2010. 49(16): p. 2994-2999.
[234] J. Ctyroky, et al., *Modelling of the surface plasmon resonance waveguide sensor with Bragg grating.* Optical and Quantum Electronics, 1999. 31(9-10): p. 927-941.
[235] G. Nemova and R. Kashyap, *Fiber-Bragg-grating-assisted surface plasmon-polariton sensor.* Optics Letters, 2006. 31(14): p. 2118-2120.
[236] G. Nemova and R. Kashyap, *Theoretical model of a planar integrated refractive index sensor based on surface plasmon-polariton excitation.* Optics Communications, 2007. 275(1): p. 76-82.
[237] G. Nemova, and R. Kashyap, *A compact integrated planar-waveguide refractive-index sensor based on a corrugated metal grating.* Journal of Lightwave Technology, 2007. 25(8): p. 2244-2250.
[238] Y.J. He, Y.L. Lo, and J.F. Huang, *Optical-fiber surface-plasmon-resonance sensor employing long-period fiber gratings in multiplexing.* Journal of the Optical Society of America B-Optical Physics, 2006. 23(5): p. 801-811.
[239] A. Al-Azzawi, *Fiber optics: principles and practices*. 2016: CRC Press.
[240] B. Culshaw, *Interferometric optical fibre sensors.* Journal of Optical Sensors, 1986. 1: p. 237-252.
[241] C.J. Misas, et al., *Interrogation of low-finesse Fabry-Perot cavities based on modulation of the transfer function of a wavelength division multiplexer.* Lightwave Technology, Journal of, 2001. 19(5): p. 673-681.
[242] Y. Chen, et al., *Interferometers for displacement-noise-free gravitational-wave detection.* Physical review letters, 2006. 97(15): p. 151103.
[243] E.D. Black, *An introduction to Pound–Drever–Hall laser frequency stabilization.* American Journal of Physics, 2001. 69(1): p. 79-87.
[244] J.H. Chow, et al., *Demonstration of a passive subpicostrain fiber strain sensor.* Optics letters, 2005. 30(15): p. 1923-1925.